PLANETS AROUND LOW-MASS STARS (PALMS). IV. THE OUTER ARCHITECTURE OF M DWARF PLANETARY SYSTEMS[*]

BRENDAN P. BOWLER[1,2,5,6], MICHAEL C. LIU[2], EVGENYA L. SHKOLNIK[3], AND MOTOHIDE TAMURA[4]

[1] California Institute of Technology, Division of Geological and Planetary Sciences, 1200 East California Boulevard,
Pasadena, CA 91101, USA; bpbowler@caltech.edu
[2] Institute for Astronomy, University of Hawai'i, 2680 Woodlawn Drive, Honolulu, HI 96822, USA
[3] Lowell Observatory, 1400 West Mars Hill Road, Flagstaff, AZ 86001, USA
[4] National Astronomical Observatory of Japan, 2-21-1 Osawa, Mitaka, Tokyo 181-8588, Japan

ABSTRACT

We present results from a high-contrast adaptive optics imaging search for giant planets and brown dwarfs ($\gtrsim 1$ $M_{\rm Jup}$) around 122 newly identified nearby ($\lesssim 40$ pc) young M dwarfs. Half of our targets are younger than 135 Myr and 90% are younger than the Hyades (620 Myr). After removing 44 close stellar binaries (implying a stellar companion fraction of $>35.4\% \pm 4.3\%$ within 100 AU), 27 of which are new or spatially resolved for the first time, our remaining sample of 78 single M dwarfs makes this the largest imaging search for planets around young low-mass stars (0.1–0.6 $M_\odot$) to date. Our H- and K-band coronagraphic observations with Keck/NIRC2 and Subaru/HiCIAO achieve typical contrasts of 12–14 mag and 9–13 mag at $1''$, respectively, which correspond to limiting planet masses of 0.5–10 $M_{\rm Jup}$ at 5–33 AU for 85% of our sample. We discovered four young brown dwarf companions: 1RXS J235133.3+312720 B (32 ± 6 $M_{\rm Jup}$; L0$^{+2}_{-1}$; 120 ± 20 AU), GJ 3629 B (64$^{+30}_{-23}$ $M_{\rm Jup}$; M7.5 ± 0.5; 6.5 ± 0.5 AU), 1RXS J034231.8+121622 B (35 ± 8 $M_{\rm Jup}$; L0 ± 1; 19.8 ± 0.9 AU), and 2MASS J15594729+4403595 B (43 ± 9 $M_{\rm Jup}$; M8.0 ± 0.5; 190 ± 20 AU). Over 150 candidate planets were identified; we obtained follow-up imaging for 56% of these but all are consistent with background stars. Our null detection of planets enables strong statistical constraints on the occurrence rate of long-period giant planets around single M dwarfs. We infer an upper limit (at the 95% confidence level) of 10.3% and 16.0% for 1–13 $M_{\rm Jup}$ planets between 10–100 AU for hot-start and cold-start (Fortney) evolutionary models, respectively. Fewer than 6.0% (9.9%) of M dwarfs harbor massive gas giants in the 5–13 $M_{\rm Jup}$ range like those orbiting HR 8799 and β Pictoris between 10–100 AU for a hot-start (cold-start) formation scenario. The frequency of brown dwarf (13–75 $M_{\rm Jup}$) companions to single M dwarfs between 10–100 AU is 2.8$^{+2.4}_{-1.5}$%. Altogether we find that giant planets, especially massive ones, are rare in the outskirts of M dwarf planetary systems. Although the first directly imaged planets were found around massive stars, there is currently no statistical evidence for a trend of giant planet frequency with stellar host mass at large separations as predicted by the disk instability model of giant planet formation.

Key words: binaries: visual – brown dwarfs – planetary systems – stars: individual (2MASS J15594729+4403595, GJ 3629, 1RXS J034231.8+121622) – stars: low-mass

Supporting material: machine-readable table

1. INTRODUCTION

M dwarfs with masses between 0.1–0.6 $M_\odot$ constitute the peak of the initial mass function and vastly outnumber all earlier-type stars put together. In the solar neighborhood, they make up ≈75% of stars (Henry et al. 2006; Kirkpatrick et al. 2012), which is a good estimate for their galactic-wide rate (Bochanski et al. 2010), and there is some evidence that M dwarfs represent even larger fractions of stellar populations in evolved galaxies (van Dokkum & Conroy 2010; Conroy & van Dokkum 2012). Their abundance and relatively low close binary fractions (≈30%; Fischer & Marcy 1992; Delfosse et al. 2004; Janson et al. 2012;

Dieterich et al. 2012) mean that low-mass stars may also be the most common sites of planet formation (Lada 2006).

At small separations ($\lesssim 2$ AU) where radial velocity and transit techniques are most sensitive, the frequency of giant planets between ∼1–10 $M_{\rm Jup}$ has been found to be relatively low around single M dwarfs (2.5% ± 0.9%) compared to high-mass A-type stars (11% ± 2%; Johnson et al. 2010). This well-established trend between planet occurrence rate and stellar host mass (Butler et al. 2004, 2006; Endl et al. 2006; Johnson et al. 2007; Lovis & Mayor 2007; Cumming et al. 2008; Bowler et al. 2010; Bonfils et al. 2013; Gaidos et al. 2013) lends support to the core accretion plus migration model of planet formation (Pollack et al. 1996; Alibert et al. 2005), which predicts fewer gas giants around M dwarfs as a result of lengthened timescales for planetesimal growth (Laughlin et al. 2004; Ida & Lin 2005; Kennedy & Kenyon 2008).

On the other hand, recent radial velocity and transit surveys are showing that Earth- to Neptune-sized planets not only exist in this stellar mass regime (e.g., Udry et al. 2007; Mayor et al. 2009; Charbonneau et al. 2009; Muirhead et al. 2012) but appear to be quite common (Bonfils et al. 2013; Berta et al. 2013). In particular, Swift et al. (2013) and Dressing &

Charbonneau (2013) find that the average rate of small planets from *Kepler* is about one per star for periods shorter than 50 days, implying a vast galaxy-wide presence of rocky planets (Morton & Swift 2014). This in turn has generated increasing interest in the habitability of planets around M dwarfs since the nearest examples of habitable Earths may orbit low-mass stars (e.g., Joshi et al. 1997; Cantrell et al. 2013; Quintana et al. 2014).

Far less is known about planets at moderate separations of $\sim$2–10 AU. Although microlensing probes the full range of planetary masses in this region (Gould & Loeb 1992), the masses and metallicities of the host stars are usually poorly constrained with this technique and so are of limited value for statistical constraints. The lensing signal from the star itself becomes very weak beyond projected separations of $\sim$10 AU (Han 2006, 2009), leading to an ambiguity between isolated planetary-mass objects and bound planets on wide orbits (Sumi et al. 2011). Nevertheless, initial statistical results point to a large reservoir of planets orbiting M dwarfs at moderate separations. Gould et al. (2010) find that the frequency of planets in the ice giant to gas giant range ($\gtrsim 0.05$ $M_{\rm Jup}$) is a factor of 8 time larger than those from Doppler studies at small separations. In a follow-up study, Cassan et al. (2012) measure a frequency of 17^{+6}_{-9}% (52^{+22}_{-29}%) for 0.3–10 $M_{\rm Jup}$ (10–30 $M_\oplus$) planets between 0.5–10 AU. Across the entire range of sensitivity (10 $M_\oplus$–10 $M_{\rm Jup}$, 0.5–10 AU), these occurrence rates imply that M dwarfs harbor on average $1.6^{+0.7}_{-0.9}$ planets per star. This result was recently bolstered by Clanton & Gaudi (2014), who found that the total number of 1–10^4 $M_\oplus$ planets with periods of 1–10^4 days is 1.9 ± 0.5 by combining statistical results from radial velocity and microlensing surveys.

Another form of planet population statistical analysis in this intermediate-separation regime comes from combining long-baseline radial velocity monitoring with adaptive optics (AO) imaging. Montet et al. (2014) apply this method to old M dwarfs in the field and find a frequency of 6.5% $\pm$ 3% for 1–13 $M_{\rm Jup}$ planets within 20 AU, which is consistent with microlensing results over the same region.

Beyond $\sim$10 AU, direct imaging is the best way to study the outer architecture of planetary systems. Following the discoveries of planets orbiting the A-type stars HR 8799, Fomalhaut, and β Pic (Marois et al. 2008, 2010b; Kalas et al. 2008; Lagrange et al. 2010), high-mass stars have received the most attention in direct imaging planet searches (Ehrenreich et al. 2010; Janson et al. 2011; Vigan et al. 2012; Rameau et al. 2013a; Nielsen et al. 2013). Yet despite their prevalence in the galaxy, imaging surveys have mostly neglected low-mass stars, so little is known about the demographics of gas giants on wide orbits around M dwarfs. This is largely due to a dearth of known nearby young M dwarfs, a population that has been substantially enlarged over the past few years (Shkolnik et al. 2009, 2012; Schlieder et al. 2012c; Malo et al. 2013, 2014a; Rodriguez et al. 2013). Low-mass stars are also optically faint and typically result in poorer AO performance than their brighter, earlier-type counterparts. Furthermore, few of the surveys that have incorporated M dwarfs expressly vetted close binaries from their statistical analyses, which is crucial if the results are to be compared with radial velocity planet searches of single stars. A handful of surveys sensitive to 1–10 $M_{\rm Jup}$ companions have targeted single, young, M0–M5 stars: Biller et al. (2007) observed 12 targets with Very Large Telescope (VLT)/MMT Simultaneous Differential Imaging (SDI), Lafrenière et al. (2007a) imaged 16 stars with Gemini-North/NIRI, Chauvin et al.

(2010) imaged 16 single M dwarfs with VLT/NaCo, Delorme et al. (2012) targeted 12 stars with VLT/NaCo in L' band, and Biller et al. (2013) observed 35 single M dwarfs with Gemini-South/NICI.[7]

The aim of the Planets Around Low-Mass Stars (PALMS) survey is to find young giant planets and brown dwarfs for spectroscopic characterization and to measure the frequency of gas giants orbiting M dwarfs beyond 10 AU. In Bowler et al. (2012b) and Bowler et al. (2012a), we discovered two new brown dwarf companions to young M dwarfs in our sample.[8] In this paper, we present two additional substellar companion discoveries and the statistical analysis of our entire sample. Below we describe our target selection, observations, processing pipeline, discoveries, survey statistical analysis, and implications for giant planet formation around low-mass stars.

2. TARGET SELECTION

Our targets are selected primarily for their youth and proximity in order to achieve the highest sensitivity to giant planets at small separations. Previously known visual binaries with physical separations $\lesssim$100 AU have been excluded since moderate-separation ($\sim$5–100 AU) binaries disperse protoplanetary disks on rapid timescales (Duchêne 2010; Kraus et al. 2012), limiting the raw ingredients of planet formation and diminishing the region of dynamically stable orbits in these systems. In addition, we have specifically designed our survey to compare with statistical results from radial velocity programs, which generally discard close binaries from their samples. We have also prioritized targets not previously observed in direct imaging surveys to minimize target selection biases and increase the chances of new discoveries.

Among our 122 targets, 69 originate from a recent search for nearby young M dwarfs by Shkolnik et al. (2009) and Shkolnik et al. (2012). Motivated by the dearth of known low-mass members of young moving groups (YMGs), Shkolnik et al. (2009) identified 144 X-ray active M dwarfs with distances $\lesssim$30 pc and ages of $\sim$10–300 Myr. In a follow-up study, Shkolnik et al. (2012) obtained parallaxes for about half of these systems and found several dozen probable kinematic members of YMCs. Targets from Shkolnik et al. (2009) have been vetted for close spectroscopic binaries with few-day periods (Shkolnik et al. 2010), which also produce activity as a result of rotationally enhanced dynamo activity caused by tidal locking (e.g., Torres et al. 2002; Kraus et al. 2011).

Another 42 targets in our sample are drawn from an ongoing, complementary search for nearby young M dwarfs using *Galaxy Evolution Explorer* (*GALEX*) data (Shkolnik et al. 2011; E. L. Shkolnik et al., in preparation). Among these, 10 systems have been kinematically tied to YMGs by Malo et al. (2013), Lépine & Simon (2009), and Riedel et al. (2014) and two new candidate members are identified in this work (LHS 2613 and NLTT 48651). Seven other systems (LHS1864 AB, NLTT 26359, LHS 2672, G 202-48, GJ 3997 AB; LP 447-38 AB; LHS 3321) either show Hα absorption or have red $NUV-W1$

---

[7] Other imaging programs that have also observed single young M dwarfs with ground-based adaptive optics or the *Hubble Space Telescope* have primarily been sensitive to brown dwarfs at wide separations, rarely reaching 1–5 $M_{\rm Jup}$ limits at small separations of $\sim$10 AU (McCarthy & Zuckerman 2004; Lowrance et al. 2005; Daemgen et al. 2007; Allen & Reid 2008).

[8] As part of a complementary imaging survey targeting a much larger sample of young M dwarfs with shorter exposures, we have also discovered the young L-type companion 2MASS J01225093−2439505 B which has a mass at the deuterium-burning limit (Bowler et al. 2013).
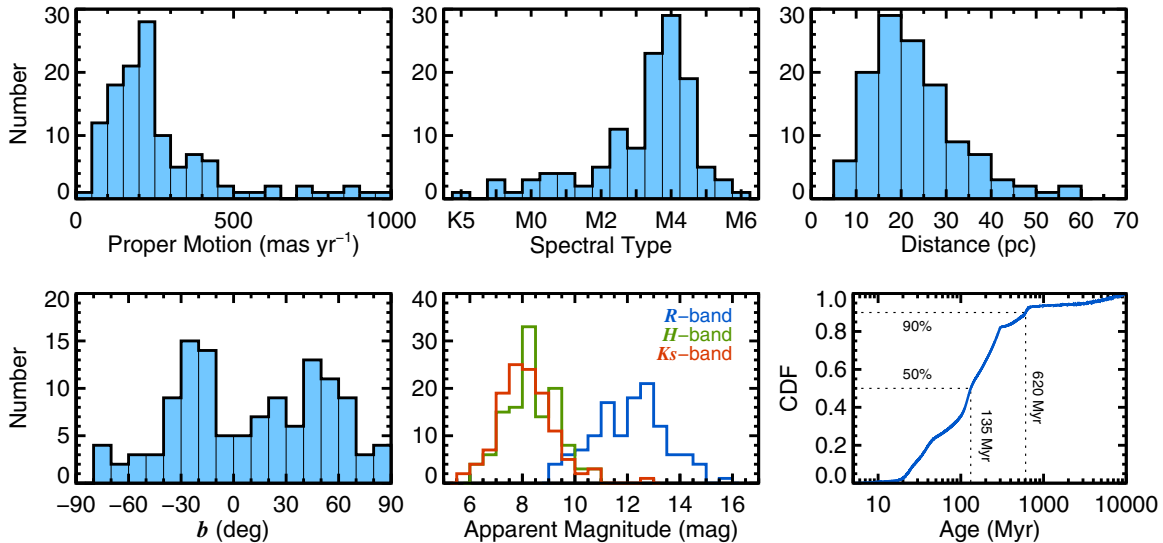
Figure 1. Summary of our target sample. The proper motions of our targets are high enough ($\gtrsim 50$ mas yr^{-1}) to distinguish comoving companions from background objects on short timescales (~ 1 yr). Spectral types peak at M4 and range from K5 to M6. Most of the distances to our targets are between 10–40 pc, and we have prioritized high galactic latitudes to avoid fields with high background stellar densities. Nearly all targets are bright enough for NGS observations either at Subrau or Keck ($R < 15$ mag). A single target, NLTT 13844, was observed with LGS-AO. The bottom right panel shows the cumulative distribution of ages for our sample. 50% are younger than 135 Myr and 90% of our targets are younger than 620 Myr.

colors (>13 mag) compared to YMG members (Rodriguez et al. 2013). These targets appear to be old inactive field stars that passed early NUV selection cuts, so we adopt minimum ages from the activity-lifetime relations of West et al. (2008). One system, 2MASS J04220833–2849053 AB, has its age constrained from the detection of Li I λ6708 absorption by Torres et al. (2006; see Appendix C). Similarly, the age of 2MASS J15594729+4403595 is constrained from signatures of low gravity in the spectrum of its substellar companion (Section 5.1.4). The remaining 21 of these 42 targets show photometric and spectroscopic indications of youth similar to known YMG members. A detailed analysis of their ages, including a discussion of high-resolution optical spectroscopy for these targets, will be presented in a forthcoming paper (E. L. Shkolnik et al., in preparation). For this work we adopt conservative age ranges of 10–300 Myr similar to Shkolnik et al. (2009) for the 21 targets without age estimates in the literature.

Finally, 11 targets are compiled from the literature from recent searches for M dwarf members of YMGs. Six originate from Schlieder et al. (2012a, 2012b, 2012c), while another five are from Looper et al. (2010b, TWA 30A), Riedel et al. (2011, AP Col), Scholz et al. (2005a, L 449-1 AB), Lépine & Simon (2009, TYC 7443-1102-1), and Lowrance et al. (2005, GJ 354.1 B).

Where available, age estimates and YMG memberships have been taken from the literature. Altogether, 46 targets (38% of our total sample) are associated with YMGs. Ages for YMG members (or likely members) are listed in Table 1.[9] Five systems are kinematically linked to YMGs here for the first time: LHS 2613 (Argus), 1RXS J022735.8+471021 (AB Dor),

Table 1
Adopted Ages for Young Moving Group Members

Moving Group	No. of Targets	Age	Age Ref
TWA	1	8 ± 2 Myr	1, 2, 3, 4, 5
β Pic	8	23 ± 3 Myr	6, 7, 8, 9
Carina, Columba	5	30 ± 5 Myr	10
Tuc-Hor	3	35 ± 5 Myr	10, 11, 12, 13
Argus	6	40 ± 5 Myr	10, 14, 15
AB Doradus	10	120 ± 10 Myr	16, 17, 18, 19
Castor	3	400 ± 100 Myr	20, 21, 22, 23
Ursa Major	6	500 ± 100 Myr	24, 25, 26
Hyades	4	620 ± 30 Myr	27, 28, 29, 30

References. (1) Webb et al. 1999; (2) Navascués 2006; (3) Mamajek 2005; (4) Torres et al. 2006; (5) Weinberger et al. 2013; (6) Yee & Jensen 2010; (7) Binks & Jeffries 2014; (8) Malo et al. 2014b; (9) Mamajek & Bell 2014; (10) Torres et al. 2008; (11) Torres et al. 2000; (12) Zuckerman et al. 2001; (13) Kraus et al. 2014; (14) Torres et al. 2003; (15) Silva et al. 2013; (16) Zuckerman et al. 2004; (17) Ortega et al. 2007; (18) Luhman et al. 2005; (19) Barenfeld et al. 2013; (20) Barrado y Navascués 1998; (21) Torres & Ribas 2002; (22) Ribas 2003; (23) Mamajek 2012; (24) Eggen 1983; (25) Soderblom & Mayor 1993; (26) King et al. 2003; (27) Perryman et al. 1998; (28) Eggen 1998; (29) Lebreton et al. 2001; (30) Degennaro et al. 2009.

NLTT 48651 (AB Dor), GJ 354.1 B (Carina), and G 227-22 (UMa).

Figure 1 and Table 2 summarize the properties of our sample. Proper motions mostly originate from the UCAC4 database (Zacharias et al. 2013) and generally fall between 100–500 mas yr^{-1}, which is high enough so that background stars can be distinguished from bona fide comoving companions on timescales of about one year. Spectral types are compiled from the literature and range from K5 to M6 (≈ 0.2–$0.6\ M_\odot$), with most of the sample falling between M3 and M5. 69 targets (57% of the sample) have parallactic distances. For the rest, we have either adopted photometric distances (42 targets) or kinematic distances based on YMG memberships (11 targets) from the literature (see Table 2 for details). 97 targets (80% of

---

[9] Recently the ages of several of the youngest moving groups have been called into question from Li depletion boundary measurements. For example, Binks & Jeffries (2014) find an older age of 21 ± 4 for the β Pic YMG from its Li-depletion boundary compared to its isochronal age of ≈ 12 Myr. These results are bolstered by recent studies by Malo et al. (2014b) and Mamajek & Bell (2014). Similarly, Kraus et al. (2014) infer a Li-depletion age of ≈ 40 Myr for the Tuc-Hor moving group, which is roughly 10 Myr older than its age from isochrone fitting. Here we adopt the more recently determined and internally consistent ages of 23 ± 3 Myr for the β Pic MG and 35 ± 5 Myr for Tuc-Hor.

Table 2
Target Sample

Name	α_{J2000}	δ_{J2000}	$\mu_\alpha\cos\delta$ (mas yr^{-1})	μ_δ (mas yr^{-1})	PM Ref	SpT (±0.5)	SpT Ref	Distance (pc)	Method	Dist Ref	YMG[a]	Age (Myr)	Age Ref
G 217-32 AB	00 07 42.64	60 22 54.3	342.0 ± 8.0	−29.0 ± 8.0	Z13	M4.5	L13	14.6 ± 0.4	π	D14	. . .	35–300	Sh09
1RXS J001557.5−163659 AB	00 15 58.08	−16 36 57.9	−110.2 ± 2.2	35.0 ± 2.2	Z13	M4.0	Ri06	18.0 ± 0.4	π	Sh12	. . .	35–300	Sh09
GJ 3030 AB	00 21 57.81	49 12 38.0	221.4 ± 10.8	−32.7 ± 12.6	Z13	M2.4	Sh09	25 ± 9	Phot	Sh12	Carina?	30 ± 5	Sh12
NLTT 1875	00 35 04.88	59 53 08.0	223.4 ± 2.1	−3.4 ± 1.5	Z13	M4.3	Sh09	38.3 ± 2.2	π	D14	. . .	100–500	B14
G 132-50 Aab	01 03 40.14	40 51 28.9	126.7 ± 0.7	−167.2 ± 0.8	Z13	M0.0	L13	29.9 ± 2.2	π	vL07	AB Dor	120 ± 10	Sh12
G 172-56	01 29 12.57	48 19 35.5	214.0 ± 8.0	−22.0 ± 8.0	Z13	M5.4	S09	18 ± 3	Phot	Sh12	. . .	60–300	Sh09
G 272-43	01 33 58.00	−17 38 23.5	44.4 ± 2.1	−185.1 ± 3.5	Z13	M3.5	Ri06	16 ± 7	Phot	L11	. . .	10–300	Sh15
G 271-110	01 36 55.30	−06 47 36.4	172.6 ± 8.0	−84.2 ± 8.0	Z13	M4.0	Ri06	24.0 ± 0.4[b]	π	Sh12	βPic	23 ± 3	M13
TYC 1752-63-1	01 37 23.23	26 57 12.0	120.2 ± 0.9	−126.5 ± 1.4	Z13	K7	Sc10	37 ± 1	Kin	M13	AB Dor?	120 ± 10	Sc10
G 272-115	01 53 11.33	−21 05 43.3	271.4 ± 8.0	72.5 ± 8.0	Z13	M1.5	Ri06	16 ± 7	Phot	L11	. . .	10–300	Sh15
NLTT 6549 AB	01 58 13.61	48 44 19.7	213.0 ± 8.0	−41.0 ± 8.0	Z13	M1.5	Sh09	44 ± 18	Phot	Sh12	Hyades?	620 ± 30	Sh12
GJ 3136	02 08 53.60	49 26 56.6	231.9 ± 10.8	−284.5 ± 12.5	Z13	M4.0	L13	15 ± 6	Phot	Sh12	AB Dor?	120 ± 10	Sh12
LP 353-51	02 23 26.64	22 44 06.9	96.1 ± 2.7	−114.2 ± 1.0	Z13	M0.5	L13	28.7 ± 2.5	π	vL07	βPic	23 ± 3	Sc10
1RXS J022735.8+471021	02 27 37.26	47 10 04.5	119.0 ± 8.0	−183.0 ± 8.0	Z13	M4.6	Sh09	27.4 ± 1.7	π	D14	AB Dor	120 ± 10	B14
1RXS J023138.7+445640	02 31 39.27	44 56 38.8	94.4 ± 5.4	−47.3 ± 3.7	Z13	M4.4	Sh09	16 ± 4	Phot	Sh12	. . .	40–300	Sh09
G 75-35	02 41 15.11	−04 32 17.7	352.3 ± 8.0	−58.8 ± 8.0	Z13	M4.0	Ri06	16 ± 7	Phot	L11	. . .	10–300	Sh15
2MASS J03033668−2535329 AB	03 03 36.69	−25 35 32.9	213.2 ± 8.0	94.5 ± 8.0	Z13	M0.0	Ri06	38.6 ± 4.2	π	vL07	. . .	10–300	Sh15
LP 247-13	03 15 37.83	37 24 14.3	209.0 ± 8.0	−97.0 ± 8.0	Z13	M2.7	Sh09	34.4 ± 0.6	π	Sh12	Hyades	620 ± 30	R11, Sh12
1RXS J034231.8+121622 AB	03 42 31.80	12 16 22.6	196.8 ± 2.2	−16.3 ± 3.8	Z13	M4.0	Ri06	23.9 ± 1.1	π	D14	. . .	60–300	S09
G 160-54 ABC	04 13 45.86	−05 09 04.9	182.0 ± 8.0	−112.5 ± 8.0	Z13	[M4][c]	L11	21 ± 9	Phot	L11	. . .	10–300	Sh15
2MASS J04220833−2849053 AB	04 22 08.33	−28 49 05.4	−80.6 ± 1.3	−86.2 ± 1.9	Z13	K7.0	Ri06	28 ± 12	Phot	L11	. . .	50–200	B14, Sh15
GJ 3287	04 27 41.30	59 35 16.7	119.0 ± 8.0	−200.0 ± 8.0	Z13	M3.8	Sh09	22.5 ± 1.2	π	D14	. . .	35–300	Sh09
LP 834-32	04 35 36.19	−25 27 34.7	82.8 ± 10.3	−179.7 ± 12.4	Z13	M3.5	Ri06	15 ± 1	Kin	M13	AB Dor?	120 ± 10	M13
NLTT 13844	04 45 05.62	43 24 34.2	388.0 ± 8.0	−638.0 ± 8.0	Z13	M4.6	Sh09	21.0 ± 0.5	π	D14	. . .	60–300	Sh09
2MASS J04472312−2750358	04 47 23.13	−27 50 35.8	82.0 ± 15.9	156.0 ± 16.7	Z13	K7.0	Ri06	20 ± 3	Phot	Sh12	. . .	400–1200	Sh09
G 81-34 AB	04 49 29.47	48 28 45.9	180.0 ± 8.0	−195.0 ± 8.0	Z13	M4.0	Sh09	21.2 ± 0.9	π	D14	. . .	35–300	Sh09
1RXS J045101.0+312734	04 51 01.38	31 27 23.9	198.0 ± 8.0	−41.0 ± 8.0	Z13	M3.7	Sh09	13 ± 4	Phot	Sh12	. . .	35–300	Sh09
L 449-1 AB	05 17 22.93	−35 21 54.5	−234.2 ± 12.1	−162.6 ± 9.5	Ri14	M4.0	Ri06	11.85 ± 0.19	π	Ri14	UMa?	500 ± 100	Ri14
1RXS J055446.0+105559	05 54 45.74	10 55 57.1	−134.0 ± 8.0	−67.0 ± 8.0	Z13	M3.0	L13	25.4 ± 1.9	π	Sh12	. . .	20–150	Sh09
GJ 3371 A	05 59 37.75	58 35 35.1	15.7 ± 2.1	−256.5 ± 1.9	Z13	M1.0	L13	13.5 ± 0.3	π	vL07	Castor?	400 ± 100	Sh12
GJ 3372 B	05 59 55.69	58 34 15.6	5.9 ± 2.8	−255.3 ± 3.7	Z13	M4.2	Sh09	13.5 ± 0.3[b]	π	vL07	Castor?	400 ± 100	Sh12
AP Col	06 04 52.16	−34 33 36.1	21.4 ± 12.1	341.2 ± 9.4	Ri14	M5.0	Ri06	8.39 ± 0.07	π	Ri11	Argus	40 ± 5	Ri11
G 249-36	06 05 29.36	60 49 23.2	288.8 ± 5.0	−787.2 ± 5.0	Ro10	M4.9	Sh09	14.0 ± 0.4	π	D14	. . .	60–300	Sh09
2MASS J06131330−2742054 AB	06 13 13.31	−27 42 05.5	−13.1 ± 1.6	−0.3 ± 1.3	Z13	M3.5	Ri06	29.4 ± 0.9	π	Ri14	βPic	23 ± 3	M13, Ri14
2MASS J06180730+7506032	06 18 07.30	75 06 03.3	−41.9 ± 1.1	68.7 ± 2.4	Z13	M2.0	L13	18 ± 8	Phot	L11	. . .	10–300	Sh15
GJ 3395	06 31 01.16	50 02 48.6	−110.3 ± 1.0	−170.2 ± 0.6	Z13	M1.0	L13	28 ± 9	Phot	Sh12	. . .	20–150	Sh09
LHS 1864 AB	06 43 49.70	51 08 21.0	91.0 ± 5.1	−881.7 ± 5.1	Ro10	M3.5	L13	19.1 ± 1.7	π	vA95	. . .	3–10 × 10^3 [d]	B14, Sh15
G 108-36	06 51 59.01	03 12 55.3	−213.0 ± 8.0	−46.0 ± 8.0	Z13	M2.5	Sh09	22.2 ± 0.6	π	Sh12	. . .	20–150	Sh09
1RXS J073829.3+240014	07 38 29.52	24 00 08.8	−179.0 ± 8.0	−107.0 ± 8.0	Z13	M3.5	L13	18.9 ± 0.9	π	Sh12	. . .	20–300	Sh09
1RXS J091744.5+461229 AB	09 17 44.73	46 12 24.7	−129.1 ± 0.7	−19.3 ± 1.2	Z13	M2.5	L13	32 ± 9	Phot	Sh12	. . .	20–150	Sh09
GJ 354.1 B	09 32 48.27	26 59 44.3	−134.0 ± 8.0	−242.0 ± 8.0	Z13	M5.5	L05	17.8 ± 0.2[b]	π	vL07	Carina?	30 ± 5	B14, Sh15
PYC J09362+3731 AB	09 36 15.93	37 31 45.7	−102.7 ± 0.7	−89.6 ± 0.7	Z13	M0.5	L13	33.7 ± 2.8	π	vL07	. . .	10–10^4	Sc12c
G 161-71	09 44 54.22	−12 20 54.4	−331.1 ± 8.0	30.9 ± 8.0	Z13	M5.0	Ri06	8 ± 3	Phot	L11	Argus?	40 ± 5	M13
NLTT 22741 A	09 51 04.60	35 58 09.8	−100.8 ± 4.3	−154.7 ± 4.3	Z13	M4.5	Re06	29.8 ± 1.7	π	D14	. . .	100–200	RW06
GJ 3577 A	09 59 18.80	43 50 25.6	−104.0 ± 8.0	−222.0 ± 8.0	Ro10	M3.3	H97	24.9 ± 1.1	π	D14	. . .	25–300	Sh09
GJ 3578 B	09 59 20.94	43 50 25.9	−101.1 ± 4.8	−224.3 ± 4.8	Z13	M3.8	H97	24.9 ± 1.1[b]	π	D14	. . .	25–300[e]	Sh09

Table 2
(Continued)

Name	α_{J2000}	δ_{J2000}	$\mu_\alpha\cos\delta$ (mas yr^{-1})	μ_δ (mas yr^{-1})	PM Ref	SpT (±0.5)	SpT Ref	Distance (pc)	Method	Dist Ref	YMG[a]	Age (Myr)	Age Ref
G 196-3 A	10 04 21.49	50 23 13.6	-137.6 ± 3.0	-199.3 ± 5.1	Z13	M2.5	L13	24.4 ± 2.5	π	ZO14	...	10–150	K08, A13
GJ 2079 AB	10 14 19.19	21 04 29.8	-137.2 ± 0.5	-165.8 ± 0.5	Z13	M0.5	L13	23.1 ± 1.0	π	vL07	Carina?	30 ± 5	Sh12
GJ 3629 AB	10 51 20.60	36 07 25.6	-192.0 ± 1.0	-48.0 ± 6.0	Z05	M3.0	H97	32.3 ± 2.4	π	D14	...	25–300	Sh09
PYC J10571+0544 AB	10 57 11.39	05 44 54.7	-55.3 ± 1.9	-40.4 ± 2.5	Z13	M2.0	Sc12a	46 ± 11	Phot	L11	βPic?	23 ± 3	Sc12a
GJ 3639	11 03 10.00	36 39 08.5	-196.0 ± 8.0	27.0 ± 8.0	Z13	M3.5	H97	24.0 ± 0.9	π	D14	...	25–300	Sh09
NLTT 26114	11 03 21.25	13 37 57.1	-185.0 ± 8.0	68.0 ± 8.0	Z13	M4.0	L13	15.4 ± 0.7	π	Sh12	...	25–300	Sh09
NLTT 26359	11 07 27.73	-19 17 29.4	-238.6 ± 2.4	-48.7 ± 2.1	Z13	K5[f]	S86	18.7 ± 0.6	π	vL07	...	10–300	Sh15
G 119-62	11 11 52.15	33 32 11.1	-176.6 ± 6.6	127.1 ± 6.1	Z13	M4.0	L13	14.6 ± 2.7	π	vA95	...	25–300	Sh09
2MASS J11240434+3808108	11 24 04.35	38 08 10.9	121.7 ± 2.6	-12.4 ± 2.3	Z13	M4.5	Re07	20.3 ± 1.3[g]	Phot	B14	UMa?	500 ± 100	Sh12
TWA 30 A	11 32 18.32	-30 19 51.8	-87.8 ± 1.3	-25.2 ± 1.3	Z13	M5[f]	Lo10	42 ± 2	Kin	Lo10	TWA	8 ± 2	Lo10
G 10-52	11 48 35.49	07 41 40.4	137.0 ± 8.0	-164.0 ± 8.0	Z13	M3.5[f]	Sh09	20.7 ± 0.9	π	Sh12	...	25–300	Sh09
2MASS J12062214$-$1314559 AB	12 06 22.14	-13 14 56.0	73.0 ± 2.4	-61.3 ± 1.3	Z13	M3.5	Ri06	27 ± 10	Phot	J12	...	10–300	Sh15
LP 734-34	12 10 28.34	-13 10 23.5	242.8 ± 8.0	-342.7 ± 8.0	Z13	M4.5	Ri06	16 ± 4	Phot	L11	...	10–300	Sh15
G 13-33 AB	12 22 50.62	-04 04 46.2	-255.0 ± 8.0	-65.7 ± 8.0	Z13	M4.5	S05b	15 ± 3	Phot	Sh12	...	10–300	Sh15
LP 735-48 AB	12 26 44.13	-12 29 17.5	-164.4 ± 1.2	-82.7 ± 1.2	Z13	M3[h]	B14	24 ± 8[h]	Phot	B14	...	10–300	Sh15
GJ 3729 AB	12 29 02.90	41 43 49.7	-196.0 ± 8.0	-222.0 ± 8.0	Z13	M4.0	L13	17 ± 5	Phot	Sh12	Tuc-Hor?	35 ± 5	Sh12
2MASS J12383713$-$2703348 AB	12 38 37.13	-27 03 34.9	-185.1 ± 5.1	-185.2 ± 5.1	Ro10	M2.5	Ri06	25 ± 1	Kin	M13	AB Dor?	120 ± 10	M13
1RXS J124147.5+564506	12 41 47.37	56 45 13.8	111.8 ± 1.6	0.6 ± 1.5	Z13	M3.0	Ri06	30 ± 11	Phot	Sh12	UMa?	500 ± 100	Sh12
LHS 2613	12 42 49.96	41 53 47.0	-539.0 ± 8.0	34.0 ± 8.0	Z13	M4.0	L13	10.6 ± 1.3	π	vA95	Argus	40 ± 5	B14, Sh15
GJ 490 Bab	12 57 39.35	35 13 19.5	-281.8 ± 3.6	-147.0 ± 6.7	Z13	M4.5	L13	19.3 ± 1.1[b]	π	vL07	Tuc-Hor?	35 ± 5	Sh12
GJ 490 Aab	12 57 40.30	35 13 30.6	-264.0 ± 1.9	-150.6 ± 2.1	Z13	M1.0	L13	19.3 ± 1.1	π	vL07	Tuc-Hor?	35 ± 5	Sh12
LHS 2672	13 02 47.52	41 31 09.9	-550.0 ± 8.0	-165.0 ± 8.0	Z13	M3.5[f]	B98	17 ± 4	Phot	L11	...	$(3–10) \times 10^3$[d]	B14, Sh15
GJ 1167 A	13 09 34.95	28 59 06.6	-338.0 ± 8.0	-211.0 ± 8.0	Z13	M3.5	Ri06	11.5 ± 2.4	π	vA95	Carina?	30 ± 5	Sh12
LHS 2686	13 10 12.69	47 45 19.0	-643.0 ± 8.0	-621.0 ± 8.0	Z13	M4.5	Ri06	13.1 ± 0.4	π	D14	...	100–500[i]	B14, Sh15
2MASS J13233804$-$2554449	13 23 38.05	-25 54 45.0	-556.7 ± 8.0	-249.4 ± 8.0	Z13	M3.5	Ri06	24.0 ± 0.3	π	Ri10	...	10–300	Sh15
2MASS J13292408$-$1422122	13 29 24.08	-14 22 12.3	103.5 ± 5.4	-41.0 ± 5.4	Ro10	M3.5	Ri06	21 ± 5	Phot	Sh12	...	20–150	Sh09
NLTT 34410 AB	13 32 39.08	30 59 06.5	-197.0 ± 6.6	-82.8 ± 4.6	Z13	M4.5	S05b	20.5 ± 1.1	π	D14	...	10–300	Sh15
2MASS J14124864$-$1629561	14 12 48.64	-16 29 56.1	-110.2 ± 1.1	-95.2 ± 1.5	Z13	M3.0	Ri06	27 ± 6	Phot	L11	...	10–300	Sh15
GQ Vir	14 13 04.92	-12 01 26.3	-601.0 ± 8.0	-387.3 ± 8.0	Z13	M4.5	Ri06	10 ± 2	Phot	L11	...	10–300	Sh15
2MASS J14215503$-$3125537 AB	14 21 55.04	-31 25 53.7	-165.3 ± 2.3	-54.4 ± 2.3	Z13	M3.9	Sh09	40 ± 2	π	Sh12	...	35–300	Sh09
2MASS J14442809$-$0424078	14 44 28.10	-04 24 07.8	117.5 ± 5.0	-99.2 ± 5.0	Ro10	M2.0	Ri06	29 ± 10	Phot	Sh12	UMa?	500 ± 100	Sh12
G 166-49	14 51 10.44	31 06 40.7	-345.0 ± 8.0	-181.0 ± 8.0	Z13	M4.0	L13	12.5 ± 0.5	π	D14	...	10–300	Sh15
1RXS J150907.2+590422 A	15 09 08.08	59 04 25.8	98.8 ± 20.9	-55.9 ± 20.9	Ro08	M2.5	Ri06	33 ± 11	Phot	Sh12	...	20–150	Sh09
2MASS J15323737+4653048	15 32 37.38	46 53 04.9	-120.9 ± 0.8	-8.1 ± 1.6	Z13	M1.0	Ri06	33 ± 12	Phot	J12	...	10–300	Sh15
NLTT 40561	15 33 50.62	25 10 10.6	8.0 ± 8.0	-233.0 ± 8.0	Z13	M3.5	Sh09	29.1 ± 1.8	π	D14	...	25–300	Sh09
LHS 3122 AB	15 49 38.33	34 48 55.5	-663.0 ± 8.0	688.0 ± 8.0	Z13	M4.0	L13	17.0 ± 1.2	π	vA95	...	10–300	Sh15
2MASS J15594729+4403595 AB	15 59 47.29	44 03 59.5	-70.7 ± 0.9	-8.9 ± 0.6	Z13	M2.0	L13	27 ± 2	Phot	B14	...	50–200	B14
2MASS J16074132$-$1103073 AB	16 07 41.33	-11 03 07.4	-69.7 ± 6.0	-145.6 ± 6.0	Ro10	M4.0	Ri06	36 ± 2	Kin	M13	AB Dor?	120 ± 10	M13
G 202-48	16 25 24.59	54 18 14.9	442.7 ± 8.0	-166.6 ± 9.2	Z13	M2.0	L13	6.52 ± 0.04	π	vL07	...	$1.2–10 \times 10^3$[d]	B14, Sh15
GJ 3966 AB	16 35 27.41	35 00 57.7	143.0 ± 8.0	-142.0 ± 8.0	Z13	M4.0	L13	16.2 ± 0.7	π	D14	...	10–300	Sh15
GJ 3997 AB	17 15 50.10	19 00 00.1	-132.5 ± 1.7	13.5 ± 1.4	Z13	M0.5	L13	12 ± 3	Phot	L11	...	$(0.6–10) \times 10^3$[d]	B14, Sh15
LP 447-38 AB	17 18 22.84	18 08 56.8	-7.7 ± 5.7	-220.8 ± 4.0	Z13	M3.0	H97	26 ± 4	Phot	L11	...	$(3–10) \times 10^3$	B14, Sh15
GJ 669 B	17 19 52.98	26 30 02.6	-217.0 ± 8.0	354.0 ± 8.0	Z13	M4.5	L13	11.8 ± 0.7	π	Sh12	Hyades?	620 ± 30	Sh12
GJ 669 A	17 19 54.22	26 30 03.0	-207.9 ± 1.1	354.3 ± 1.2	Z13	M3.5	L13	11.7 ± 0.7	π	Sh12	Hyades?	620 ± 30	Sh12
LHS 3321	17 43 55.95	43 22 44.1	9.5 ± 8.0	-602.6 ± 8.0	Z13	M2.5	L13	9.48 ± 0.11	π	vL07	...	$(1.6–10) \times 10^3$	B14, Sh15
G 227-22	18 02 16.60	64 15 44.6	206.0 ± 8.0	-386.0 ± 8.0	Z13	M5.0	L13	8.5 ± 0.3	π	D14	UMa	500 ± 100	B14
LP 390-16	18 13 06.58	26 01 51.9	218.0 ± 8.0	-36.0 ± 8.0	Z13	M4.5	L13	17.2 ± 0.7	π	Sh12	...	40–300	Sh09
GJ 9652 A	19 14 39.26	19 19 02.6	-617.4 ± 8.0	434.8 ± 8.0	Z13	M3.5	L13	19.1 ± 1.1	π	vL07	...	60–300	Sh09
2MASS J19303829$-$1335083	19 30 38.30	-13 35 08.4	177.3 ± 11.3	331.4 ± 11.3	Ro10	M6.0	Sh09	27.7 ± 1.2	π	Sh12	...	90–300	Sh09

Table 2
(Continued)

Name	α_{J2000}	δ_{J2000}	$\mu_\alpha\cos\delta$ (mas yr^{-1})	μ_δ (mas yr^{-1})	PM Ref	SpT (±0.5)	SpT Ref	Distance (pc)	Method	Dist Ref	YMG[a]	Age (Myr)	Age Ref
1RXS J193528.9+374605	19 35 29.23	37 46 08.2	−134.1 ± 6.5	−98.7 ± 4.1	Z13	M3.5	L13	10 ± 4	Phot	Sh12	. . .	20–300	Sh09
2MASS J19435432−0546363	19 43 54.33	−05 46 36.4	57.4 ± 7.3	7.3 ± 8.4	Z13	M4.0	Ri06	32 ± 2	Kin	M13	Argus?	40 ± 5	M13
2MASS J19560294−3207186 AB	19 56 02.94	−32 07 18.7	35.2 ± 1.8	−59.9 ± 1.5	Z13	M4.0	Ri06	58 ± 3[b]	Kin	L09	β Pic?	23 ± 3	L09, K11
TYC 7443-1102-1	19 56 04.38	−32 07 37.6	31.9 ± 1.4	−65.1 ± 1.2	Z13	M0.0	L09	58 ± 3	Kin	L09	β Pic?	23 ± 3	L09, K11
2MASS J20003177+5921289 AB	20 00 31.77	59 21 29.0	74.4 ± 27.5	21.6 ± 42.5	Z13	M4.1	Sh09	20 ± 5	Phot	Sh12	Castor?	400 ± 100	Sh12
NLTT 48651	20 04 30.78	−23 42 01.9	122.9 ± 8.0	−339.3 ± 8.0	Z13	M4.5	S05b	10 ± 2	Phot	L11	AB Dor?	120 ± 10	B14, Sh15
2MASS J20100002−2801410 AB	20 10 00.03	−28 01 41.1	40.7 ± 3.0	−62.0 ± 1.7	Z13	M3.0	Ri06	45.1 ± 3.1	π	Ri14	β Pic	23 ± 3	M13, Ri14
2MASS J20284361−1128307	20 28 43.62	−11 28 30.8	166.4 ± 5.2	−93.3 ± 5.2	Ro10	M3.5	Ri06	18.8 ± 0.6	π	R14	Argus	40 ± 5	Sh15
TYC 523-573-1	20 39 54.60	06 20 11.8	89.3 ± 1.1	−98.4 ± 1.5	Z13	K7.5	L13	38.5[j]	Kin	Sc10	AB Dor?	120 ± 10	Sc10
NLTT 50066 AB	20 53 14.65	−02 21 21.9	186.8 ± 8.0	15.7 ± 8.0	Z13	M3.0	Ri06	37.9 ± 5.7	π	Sh12	. . .	20–300	Sh09
NLTT 50710	21 11 13.67	−22 48 17.3	−55.4 ± 8.0	−345.6 ± 8.0	Z13	M4.0	Ri06	21 ± 5	Phot	L11	. . .	10–300	Sh15
GJ 4186 B	21 16 03.79	29 51 46.0	219.9 ± 3.5	45.7 ± 2.6	Z13	M3.3	Sh09	19.3 ± 1.1	π	Sh12	. . .	25–300	Sh09
GJ 4185 Aab	21 16 05.76	29 51 51.1	206.0 ± 2.0	35.3 ± 2.2	Z13	M4.0	L13	19.5 ± 1.1	π	Sh12	. . .	25–300	Sh09
PYC J21376+0137 AB	21 37 40.19	01 37 13.7	80.3 ± 2.8	−59.4 ± 3.1	Z13	M4.5	L13	39 ± 4	Kin	Sc12b	β Pic?	23 ± 3	Sc12c
1RXS J221419.3+253411 AB	22 14 17.66	25 34 06.6	167.0 ± 8.0	−53.0 ± 8.0	Z13	M4.3	Sh09	28.7 ± 2.1	π	Sh12	Columba?	30 ± 5	Sh12
GJ 4274	22 23 06.97	−17 36 25.0	248.3 ± 8.0	−895.2 ± 8.0	Z13	M4.0	Ri06	7.26 ± 0.09	π	Ri14	. . .	100–500[k]	Sh15, Ri14
NLTT 54873	22 47 37.65	40 41 25.4	169.0 ± 8.0	96.0 ± 8.0	Z13	M4.0	Ri06	22 ± 5	Phot	Sh12	. . .	35–300	Sh09
2MASS J22581643−1104170	22 58 16.44	−11 04 17.1	106.8 ± 2.9	−5.9 ± 2.9	Z13	M2.7	Sh09	31.1 ± 2.9	π	Sh12	. . .	20–300	Sh09
GJ 4338 Bab	23 29 22.59	41 27 52.2	421.0 ± 10.9	−62.2 ± 12.7	Z13	M4.5	L13	14.7 ± 0.5	π	vA95	. . .	40–300	Sh09
GJ 4337 A	23 29 23.46	41 28 06.9	415.0 ± 8.0	−41.0 ± 8.0	Z13	M3.5	L13	14.9 ± 0.5	π	vA95	. . .	20–300	Sh09
GJ 1290	23 44 20.84	21 36 05.0	449.0 ± 8.0	73.0 ± 8.0	Z13	M3.4	Sh09	22.0 ± 2.2	π	vA95	. . .	25–300	Sh09
G 68-46	23 51 22.28	23 44 20.8	265.0 ± 8.0	−74.0 ± 8.0	Z13	M4.0	Ri06	21.0 ± 1.3	π	D14	. . .	35–300	Sh09
1RXS J235133.3+312720 AB	23 51 33.67	31 27 23.0	106.6 ± 1.7	−87.9 ± 3.8	Z13	M2.0	Sh09	50 ± 10	Phot	B12b	AB Dor?	120 ± 10	B12b, Sh12
1RXS J235452.2+383129	23 54 51.47	38 31 36.3	−130.0 ± 8.0	−86.0 ± 8.0	Z13	M4.0	L13	15.9 ± 0.7	π	D14	. . .	25–300	Sh09
G 158-8	23 55 55.13	−13 21 23.8	308.5 ± 8.0	21.2 ± 8.0	Z13	M2.5	Ri06	19 ± 4	Phot	L11	Argus?	40 ± 5	M13
GJ 4381 AB	23 57 49.89	38 37 46.9	−125.0 ± 8.0	−138.0 ± 8.0	Z13	M3.5	L13	21 ± 8	Phot	Sh12	UMa?	500 ± 100	Sh12
G 130-31	23 59 19.86	32 41 24.5	−174.0 ± 8.0	−241.0 ± 8.0	Z13	M5.6	Sh09	13 ± 3	Phot	Sh12	. . .	90–300	Sh09

Notes.

[a] Question marks imply some uncertainty about the young moving group (YMG) status. Usually one kinematic component (radial velocity or distance) is missing so *UVW* space velocities are ill-constrained along one dimension.

[b] Distances to the primary stars are adopted for the following companions: the *Hipparcos* parallax for EX Cet is used for G 271-110; the *Hipparcos* parallax for GJ 3371 A is used for GJ 3372 B; the parallactic distance to GJ 3577 A (Dittmann et al. 2013) is used for GJ 3578 B; the *Hipparcos* parallax for GJ 490 A is used for GJ 490 B; the *Hipparcos* parallax for DX Leo is used for GJ 354.1 B; the kinematic distance to TYC 7443-1102-1 (Lépine & Simon 2009) is used for 2MASS J19560294-3207186 AB.

[c] Spectral types are estimated from photometry (see associated reference) and have uncertainties of ±2 subclasses.

[d] Age based on the activity-lifetime relation from West et al. (2008).

[e] The age for GJ 3577 A from Shkolnik et al. (2009) is adopted for the companion GJ 3578 B.

[f] Spectral type uncertainties are ±1 subclass.

[g] This distance is the photometric distance to the M8.5 companion 2MASS J11240487+3808054 (Appendix C).

[h] Spectral type and distance are estimated using the *V–J* relations from Lépine et al. (2013). The uncertainty in spectral type is one subclass.

[i] The minimum ages of these stars are ZAMS since they lie on the main sequence in the {M_V, $V–K_S$} diagram.

[j] No distance uncertainty is provided in Schlieder et al. (2010).

[k] The position of GJ 4274 (LHS 3799) on the HR diagram (Riedel et al. 2014) implies a minimum age ZAMS age of ∼100 Myr.

References. (A13) Allers & Liu 2013; (B12a) Bowler et al. 2012b; (B14) this work; (B98) Buscombe 1998; (D14) Dittmann et al. 2013; (H97) Hawley et al. 1996, Reid et al. 1995; (J12) Janson et al. 2012; (K11) Kiss et al. 2010; (K08) Kirkpatrick et al. 2008; (M13) Malo et al. 2013; (L05) Lowrance et al. 2005; (Lo10) Looper et al. 2010b; (L09) Lépine & Simon 2009; (L11) Lépine & Gaidos 2011; (L13) Lépine et al. 2013; (L08) Law et al. 2008; (Re06) Reid & Walkowicz 2006; (Re07) Reid et al. 2007; (Ri06) Riaz et al. 2006; (Ri10) Riedel et al. 2010; (Ri11) Riedel et al. 2011; (Ri14) Riedel et al. 2014; (R11) Röser et al. 2011; (Ro08) PPMX Catalog (Röser et al. 2008); (Ro10) PPMXL Catalog (Roeser et al. 2010); (RW06) Reid & Walkowicz 2006; (S86) Stephenson 1986; (S05a) Scholz et al. 2005b; (S05b) Scholz et al. 2005a; (Sc10) Schlieder et al. 2010; (Sc12a) Schlieder et al. 2012a; (Sc12b) Schlieder et al. 2012c; (Sh09) Shkolnik et al. 2009; (Sh12) Shkolnik et al. 2012; (Sh15) E. L. Shkolnik et al. (in preparation); (vA95) van Altena et al. 1995; (vL07) van Leeuwen 2007, Perryman et al. 1997; (Z05) NOMAD (Zacharias et al. 2005); (Z13) UCAC4 (Zacharias et al. 2013); (ZO14) Zapatero Osorio et al. 2014.

the sample) are within 30 pc and 114 (93% of the sample) are within 40 pc.

When possible we avoided stars with low galactic latitudes where background contamination rates are high. Targets near the galactic plane were generally only observed if an RA gap existed in the target list for any particular night. This preference is reflected in the relative dearth of targets for $|b| \lesssim 20°$ in Figure 1. The distribution of R-band magnitudes ranges from $≈10$–15 mag and is roughly divided into two bins according to observability with NGS-AO at Subaru ($\lesssim 13$ mag) and Keck ($\lesssim 15$ mag). The cumulative age distribution of our sample is shown in Figure 1: 50% of stars are younger than 135 Myr and 90% are younger than 620 Myr.

3. OBSERVATIONS

3.1. Keck II/NIRC2 Adaptive Optics Imaging

We carried out our observations at the Keck II 10 m telescope with the facility near-infrared imaging camera NIRC2 using natural guide star adaptive optics (NGS-AO; Wizinowich et al. 2000) between 2010 August and 2013 August (Table 3). A single target, NLTT 13844 ($R \sim 14.8$ mag), was observed with laser guide star AO (LGS-AO; Wizinowich et al. 2006; van Dam et al. 2006). Most of our imaging was carried out with the narrow camera, which has a plate scale of 9.952 ± 0.002 mas pixel^{-1} (Yelda et al. 2010) and provides Nyquist sampling at the diffraction limit beyond ~ 1.2 μm. In this mode, the field of view (FOV) across the array's 1024×1024 pixels is $10''.2 \times 10''.2$. When conditions were good (seeing below $\sim 1''$) we used the Mauna Kea Observatory (MKO) H-band filter (Simons & Tokunaga 2002; Tokunaga & Vacca 2005) as a compromise between higher Strehl and increased sky background levels at longer wavelengths. When conditions were below average, we used the K_S filter to benefit from better AO correction.

We first obtained short, unsaturated images of each target to check for stellar multiplicity. Binary systems were generally skipped, although in a few cases close companions were only resolved in our second-epoch imaging. For single stars we typically obtained 40 minutes of total on-source integration time (usually 40 frames each with 60 s exposures and 1 coadd reading out with multiple correlated double sampling) in Angular Differential Imaging mode (ADI; Liu 2004; Marois et al. 2006) after centering the target behind the partly opaque ($\Delta H \sim 6$ mag) 600 mas diameter coronagraph. To avoid the lower-left quadrant of NIRC2, which suffers from elevated noise levels, we positioned the coronagraph at column 616 (the occulting spot is fixed in y at row 430). Raw images were first cleaned of bad pixels and cosmic rays then flat-fielded to remove pixel-to-pixel sensitivity variations.

This results in an inner working angle (IWA) of 300 mas and an outer working angle (OWA) between $≈4''$ (for complete spatial coverage) and $8''.5$ (for partial coverage). The NIRC2 coronagraph is particularly useful for image registration and photometric calibration since the star is visible behind the mask. Corrections for differential atmospheric refraction were applied during most of the observations to keep the star centered behind the coronagraph. To further monitor the quality of AO correction, we also obtained a set of unsaturated frames immediately before and after our ADI sequences.

The scheduling of our ADI observations were optimized to maximize rotation at small separations ($\sim 0''.5$) but minimize blurring at modest separations ($\sim 3''$). This compromise ensures that physical companions will have undergone enough rotation

on the detector to avoid strong self-subtraction during post-processing. This strategy also reduces sensitivity losses at several arcseconds caused by smearing when rotation rates are high, which can occur near transit for declinations near the observing site's latitude ($+20°$ for Mauna Kea; see Biller et al. 2008 for a detailed discussion of these effects). In practice it is difficult to strictly adhere to these constraints, but most of the FOV rotations are near the desired values of $\sim 15°$–$40°$.

Follow-up second-epoch observations were carried out in ADI mode, standard imaging mode with the telescope rotator on, and with the wide ($0''.04$ pixel^{-1}; $40''$ FOV) and narrow NIRC2 camera modes depending on the candidate being recovered. Integration times were generally much shorter than first-epoch exposures since it is often not necessary to achieve the same limiting depth to recover faint candidates.

For the NIRC2 narrow camera, we adopt the plate scale measurement of 9.952 ± 0.002 mas pixel^{-1} and orientation of $+0°.252 \pm 0°.009$ found by Yelda et al. (2010). Post-fit residuals for the NIRC2 narrow camera distortion solution made available by Keck Observatory are $≈0.6$ mas (B. Cameron, 2007, private communication).

3.2. Subaru/HiCIAO Adaptive Optics Imaging

Our NGS-AO observations at the 8.2 m Subaru Telescope were obtained with the AO188 adaptive optics system (Hayano et al. 2010) coupled with the High Contrast Instrument for the Subaru Next Generation Adaptive Optics (HiCIAO) imaging instrument (Hodapp et al. 2008; Suzuki et al. 2010; Table 3). Our observing strategy with HiCIAO was similar to that with NIRC2. ADI observations were carried out with the star centered behind the 300 mas diameter opaque Lyot coronagraph. The H (MKO) and K_S filters were used for our deep imaging with typical on-source integration times of 40 minutes (1 coadd $\times$ 60 s $\times$ 40 frames). Sets of short unsaturated frames were taken before, in the middle, and after each ADI sequence to monitor AO correction and photometrically calibrate our data. The atmospheric dispersion corrector for the AO188 (Egner et al. 2010) was employed to minimize drifting caused by changing airmass. With a plate scale of 9.723 ± 0.011 mas pixel^{-1} in the H band (Appendix A), the 2048×2048 pixel HAWAII-2RG detector corresponds to a FOV of $20''.5$. For our deep coronagraphic data the IWA is $0''.2$ and the OWA is $≈10''$ ($≈14''$) for full (partial) coverage. Dome flats and bias frames were obtained at the start and end of each observing run.

The raw HiCIAO images suffer from horizontal and vertical electronic readout structure imprinted in each image, which corresponds to 32 readout channels with different voltages (Suzuki et al. 2010; Brandt et al. 2013). To remove these random and changing bias stripes we use a procedure developed by the Subaru Strategic Exploration of Exoplanets and Disks (SEEDS; Tamura et al. 2006) team (R. Kandori 2011, private communication), which is based on measuring and subtracting these patterns in the science data itself. To further remove residual patterns, we subtract the median-combined horizontal and vertical profiles after masking out the science target in each image. Together these eliminate nearly all systematic features caused by the electronics. After bias subtraction, cosmic rays and bad pixels are removed and the images are divided by a normalized flat field.

Seeing was poor ($1''$–$2''$) during most of our HiCIAO observations. This significantly degraded the AO correction and the limiting contrasts for many of our targets. While we attempted to

Table 3
Summary of Coronagraphic Observations

Name	2MASS ID	UT Date (Y-M-D)	Instrument[a]	Filter	Cor. (mas)[b]	No. of Exp.	Exp. Time (minutes)[c]	Mode[d]	Rotation (°)	Strehl[e] (%)
GJ 3030 AB	J00215781+4912379	2011 Dec 27	HiCIAO	H	300	39	39.0	ADI	26.4	...
		2013 Aug 17	NIRC2/W	K_S	600	4	0.33	ADI	0.5	...
NLTT 1875	J00350487+5953079	2010 Aug 18	NIRC2/N	H	600	40	40.0	ADI	16.5	26
		2011 Aug 20	NIRC2/N	H	600	10	10.0	DI	...	...
G 132-50 Aab	J01034013+4051288	2011 Dec 28	HiCIAO	K_S	300	40	40.0	ADI	34.1	...
G 172-56	J01291257+4819354	2010 Aug 17	NIRC2/N	H	600	41	41.0	ADI	22.6	22
G 272-43	J01335800−1738235	2012 Jan 3	HiCIAO	K_S	300	40	40.0	ADI	19.5	...
G 271-110	J01365529−0647363	2010 Aug 18	NIRC2/N	H	600	36	36.0	ADI	17.5	32
		2012 Aug 23	NIRC2/N	K_S	600	20	20.0	DI	...	30
		2013 Feb 4	NIRC2/N	H	600	40	40.0	DI	...	4
TYC 1752-63-1	J01372322+2657119	2012 Aug 23	NIRC2/N	K_S	600	40	40.0	ADI	16.5	30
G 272-115	J01531133−2105433	2011 Dec 27	HiCIAO	H	300	40	40.0	ADI	14.1	...
NLTT 6549 AB	J01581361+4844197	2011 Jan 26	HiCIAO	H	300	42	42.0	ADI	18.1	...
		2011 Aug 20	NIRC2/N	H	600	40	40.0	ADI	22.6	35
GJ 3136	J02085359+4926565	2011 Jan 27	HiCIAO	K_S	300	40	40.0	ADI	17.6	...
LP 353-51	J02232663+2244069	2011 Dec 28	HiCIAO	K_S	300	40	40.0	ADI	12.2	...
1RXS J022735.8+471021	J02273726+4710045	2010 Aug 17	NIRC2/N	H	600	40	40.0	ADI	14.2	27
		2013 Feb 4	NIRC2/N	H	600	35	35.0	DI	...	11
1RXS J023138.7+445640	J02313926+4456387	2010 Aug 18	NIRC2/N	H	600	39	39.0	ADI	22.8	38
G 75-35	J02411510−0432177	2012 Jan 3	HiCIAO	H	300	40	40.0	ADI	17.7	...
2MASS J03033668−2535329 AB	J03033668−2535329	2011 Dec 28	HiCIAO	K_S	300	20	20.0	ADI	7.1	...
LP 247-13	J03153783+3724143	2011 Jan 26	HiCIAO	K_S	300	40	40.0	ADI	14.2	...
		2011 Aug 20	NIRC2/N	H	600	10	10.0	DI	...	38
		2011 Aug 20	NIRC2/N	K_S	600	6	3.0	DI	...	58
		2012 Jan 14	NIRC2/N	H	600	5	5.0	DI	...	...
		2012 Jan 14	NIRC2/N	K	600	5	5.0	DI	...	...
GJ 3287	J04274130+5935167	2013 Feb 4	NIRC2/N	K_S	600	40	40.0	ADI	15.9	41
LP 834-32	J04353618−2527347	2011 Dec 28	HiCIAO	K_S	300	40	40.0	ADI	16.0	...
NLTT 13844	J04450562+4324342	2012 Oct 8	NIRC2/N[f]	H	600	10	10.0	DI	...	17
		2013 Jan 17	NIRC2/N[f]	K	600	5	5.0	DI	...	...
1RXS J045101.0+312734	J04510138+3127238	2011 Jan 27	HiCIAO	K_S	300	40	40.0	ADI	13.9	...
		2011 Dec 28	HiCIAO	K_S	300	40	40.0	ADI	26.4	...
		2012 Jan 3	HiCIAO	K_S	300	20	20.0	ADI	3.60	...
L 449-1 AB	J05172292−3521545	2011 Dec 28	HiCIAO	K_S	300	27	27.0	ADI	8.5	...
1RXS J055446.0+105559	J05544574+1055570	2011 Jan 27	HiCIAO	K_S	300	40	40.0	ADI	5.0	...
		2013 Feb 4	NIRC2/N	K_S	600	40	40.0	ADI	17.5	46
GJ 3371 A	J05593774+5835351	2011 Dec 27	HiCIAO	H	300	74	37.0	ADI	18.9	...
GJ 3372 B	J05595569+5834155	2011 Mar 25	NIRC2/N	K_S	600	50	50.0	ADI	20.6	44
AP Col	J06045215−3433360	2011 Dec 27	HiCIAO	K_S	300	60	60.0	ADI	21.1	...
		2012 Jan 3	HiCIAO	H	300	40	40.0	ADI	13.6	...
		2012 Oct 8	NIRC2/W	H	1500	9	4.5	DI	...	...
G 249-36	J06052936+6049231	2011 Jan 27	HiCIAO	K_S	300	40	40.0	ADI	14.2	...
2MASS J06180730+7506032	J06180730+7506032	2012 Jan 3	HiCIAO	H	300	40	40.0	ADI	13.3	...
GJ 3395	J06310116+5002485	2011 Jan 26	HiCIAO	K_S	300	40	40.0	ADI	23.6	...
G 108-36	J06515901+0312553	2011 Jan 27	HiCIAO	K_S	300	40	40.0	ADI	13.9	...
		2012 Jan 3	HiCIAO	K_S	300	29	29.0	ADI	28.4	...
1RXS J073829.3+240014	J07382951+2400088	2010 Nov 27	NIRC2/N	H	600	42	42.0	ADI	7.6	30
		2011 Dec 27	HiCIAO	K_S	300	40	40.0	ADI	20.4	...
		2012 Jan 3	HiCIAO	K_S	300	40	40.0	ADI	5.7	...
		2013 Jan 17	NIRC2/N	K	600	8	8.0	DI	...	...
1RXS J091744.5+461229 AB	J09174473+4612246	2011 Dec 28	HiCIAO	K_S	300	40	40.0	ADI	18.4	...
GJ 354.1 B	J09324827+2659443	2013 May 2	NIRC2/N	K_S	600	40	40.0	ADI	19.5	32
PYC J09362+3731 AB	J09361593+3731456	2012 May 22	NIRC2/N	H	600	105	35.0	ADI	16.9	9
G 161-71	J09445422−1220544	2011 Nov 16	NIRC2/N	H	600	37	37.0	ADI	61.7	30
NLTT 22741 A	J09510459+3558098	2012 May 21	NIRC2/N	K_S	600	40	40.0	ADI	11.8	8
GJ 3577 A	J09591880+4350256	2013 Feb 4	NIRC2/N	K_S	600	40	40.0	ADI	26.3	30
GJ 3578 B	J09592093+4350258	2013 Feb 4	NIRC2/N	K_S	600	40	40.0	ADI	22.6	39
G 196-3 A	J10042148+5023135	2011 Jan 26	HiCIAO	K_S	300	40	40.0	ADI	10.7	...
GJ 2079 AB	J10141918+2104297	2011 Dec 28	HiCIAO	K_S	300	40	40.0	ADI	22.9	...
		2013 Feb 4	NIRC2	K_S	600	62	31.0	ADI	14.5	26
GJ 3629 AB	J10512059+3607255	2012 May 10	HiCIAO	H	300	20	20.0	ADI	17.5	...
GJ 3639	J11031000+3639085	2011 Jan 27	HiCIAO	K_S	300	40	40.0	ADI	38.3	...
NLTT 26114	J11032125+1337571	2012 Jan 14	NIRC2/N	K	600	32	32.0	ADI	15.3	...

Table 3
(Continued)

Name	2MASS ID	UT Date (Y-M-D)	Instrument[a]	Filter	Cor. (mas)[b]	No. of Exp.	Exp. Time (minutes)[c]	Mode[d]	Rotation (°)	Strehl[e] (%)
NLTT 26359	J11072772−1917293	2011 Dec 27	HiCIAO	K_S	300	40	40.0	ADI	14.9	...
		2013 May 2	NIRC2/W	K_S	1500	5	2.5	DI	...	...
G 119-62	J11115215+3332110	2011 Jan 26	HiCIAO	K_S	300	40	40.0	ADI	18.3	...
2MASS J11240434+3808108	J11240434+3808108	2010 Nov 28	NIRC2/N	H	600	51	34.0	ADI	19.0	17
		2011 Mar 25	NIRC2/N	K_S	600	42	42.0	ADI	16.0	54
TWA 30 A	J11321831−3019518	2011 Mar 25	NIRC2/N	K_S	600	20	20.0	ADI	7.9	20
G 10-52	J11483548+0741403	2011 Jan 27	HiCIAO	K_S	300	40	40.0	ADI	15.3	...
LP 734-34	J12102834−1310234	2011 Dec 27	HiCIAO	K_S	300	40	40.0	ADI	17.0	...
G 13-33 AB	J12225061−0404462	2011 Dec 28	HiCIAO	K_S	300	39	39.0	ADI	26.1	...
		2012 May 21	NIRC2/N	K_S	600	30	30.0	ADI	11.9	12
		2013 Feb 4	NIRC2/N	K_S	600	34	34.0	DI	...	25
GJ 3729 AB	J12290290+4143497	2011 Jan 26	HiCIAO	K_S	300	45	45.0	ADI	24.5	...
		2011 Jun 21	NIRC2/N	H	600	35	35.0	ADI	20.9	19
		2012 Jan 3	HiCIAO	H	300	47	47.0	ADI	33.7	...
1RXS J124147.5+564506	J12414736+5645137	2011 Jan 26	HiCIAO	K	300	40	40.0	ADI	20.6	...
		2012 May 10	HiCIAO	K_S	300	40	40.0	ADI	18.5	...
		2013 May 2	NIRC2/W	K_S	1500	5	4.2	DI	...	...
LHS 2613	J12424996+4153469	2011 Dec 27	HiCIAO	K_S	300	20	20.0	ADI	12.6	...
		2012 Jan 3	HiCIAO	H	300	40	40.0	ADI	20.4	...
LHS 2672	J13024751+4131098	2012 May 10	HiCIAO	H	300	40	40.0	ADI	20.8	...
GJ 1167 A	J13093495+2859065	2011 Jan 27	HiCIAO	K_S	300	40	40.0	ADI	21.0	...
		2012 May 10	HiCIAO	K_S	300	40	40.0	ADI	20.4	...
LHS 2686	J13101268+4745190	2011 Jun 21	NIRC2/N	H	600	40	40.0	ADI	18.4	34
2MASS J13233804−2554449	J13233804−2554449	2013 Feb 4	NIRC2/N	K_S	600	40	40.0	ADI	15.0	31
2MASS J13292408−1422122	J13292408−1422122	2011 Mar 25	NIRC2/N	K_S	600	52	52.0	ADI	15.0	53
2MASS J14124864−1629561	J14124864−1629561	2012 May 22	NIRC2/N	K_S	600	40	40.0	ADI	15.6	28
		2013 May 2	NIRC2/N	K_S	600	40	40.0	ADI	18.1	49
GQ Vir	J14130492−1201262	2012 May 21	NIRC2/N	K_S	600	40	40.0	ADI	19.2	18
2MASS J14442809−0424078	J14442809−0424078	2011 Mar 25	NIRC2/N	K_S	600	40	40.0	ADI	10.3	51
G 166-49	J14511044+3106406	2012 May 22	NIRC2/N	H	600	80	40.0	ADI	44.9	24
		2013 Feb 4	NIRC2/N	K_S	600	20	20.0	DI	...	53
1RXS J150907.2+590422 A	J15090696+5904282	2012 May 21	NIRC2/N	K_S	600	40	40.0	ADI	14.9	22
2MASS J15323737+4653048	J15323737+4653048	2012 May 22	NIRC2/N	K_S	600	33	33.0	ADI	13.4	13
		2013 Aug 17	NIRC2/N	K_S	600	40	40.0	ADI	14.9	49
NLTT 40561	J15335062+2510106	2010 Aug 18	NIRC2/N	H	600	40	40.0	ADI	5.8	31
G 202-48	J16252459+5418148	2011 Jun 21	NIRC2/N	H	600	20	20.0	ADI	11.9	37
GJ 3966 AB	J16352740+3500577	2011 Jun 21	NIRC2/N	H	600	10	10.0	ADI	10.2	18
		2012 Apr 12	NIRC2/N	H	600	3	3.0	DI	...	...
LP 447-38 AB	J17182284+1808568	2012 May 10	HiCIAO	H	300	10	10.0	ADI	4.1	...
GJ 669 B	J17195298+2630026	2010 Aug 18	NIRC2/N	H	600	41	43.7	ADI	15.0	31
GJ 669 A	J17195422+2630030	2012 May 10	HiCIAO	H	300	40	40.0	ADI	16.2	...
		2013 May 2	NIRC2/W	K_S	1500	5	4.2	DI	...	...
LHS 3321	J17435595+4322441	2011 Jun 21	NIRC2/N	H	600	80	40.0	ADI	36.5	37
		2012 May 10	HiCIAO	H	300	40	40.0	ADI	19.9	...
G 227-22	J18021660+6415445	2010 Aug 17	NIRC2/N	H	600	30	30.0	ADI	17.9	26
LP 390-16	J18130657+2601519	2011 Mar 25	NIRC2/N	K_S	600	71	71.0	ADI	33.7	53
GJ 9652 A	J19143925+1919025	2011 Aug 20	NIRC2/N	H	600	84	28.0	ADI	1.5	25
		2012 Aug 23	NIRC2/N	H	600	59	19.7	ADI	27.7	17
2MASS J19303829−1335083	J19303829−1335083	2010 Aug 17	NIRC2/N	H	600	46	46.0	ADI	22.0	23
		2011 Jul 1	NIRC2/N	H	600	40	40.0	ADI	15.4	28
1RXS J193528.9+374605	J19352922+3746082	2010 Aug 17	NIRC2/N	H	600	36	36.0	ADI	18.9	32
		2011 Aug 20	NIRC2/N	H	600	20	20.0	ADI	25.5	42
2MASS J19435432−0546363	J19435432−0546363	2012 May 21	NIRC2/N	K_S	600	40	40.0	ADI	16.2	9
		2013 May 2	NIRC2/N	K_S	600	30	30.0	ADI	17.8	43
TYC 7443-1102-1	J19560438−3207376	2012 May 22	NIRC2/N	K_S	600	24	24.0	ADI	12.0	13
NLTT 48651	J20043077−2342018	2011 Jun 21	NIRC2/N	H	600	40	40.0	ADI	14.0	20
		2012 May 21	NIRC2/N	K_S	600	8	4.0	DI	...	...
2MASS J20284361−1128307	J20284361−1128307	2012 May 10	HiCIAO	H	300	18	18.0	ADI	8.6	...
		2013 Aug 17	NIRC2/W	K_S	300	5	2.5	ADI	1.57	...
TYC 523-573-1	J20395460+0620118	2012 Aug 23	NIRC2/N	H	600	120	40.0	ADI	58.8	13
NLTT 50710	J21111366−2248173	2012 May 21	NIRC2/N	K_S	600	28	28.0	ADI	10.6	16
GJ 4186 B	J21160378+2951460	2010 Aug 17	NIRC2/N	H	600	30	30.0	ADI	14.3	26
		2011 Jun 21	NIRC2/N	H	600	40	40.0	ADI	15.1	24

9

Table 3
(Continued)

Name	2MASS ID	UT Date (Y-M-D)	Instrument[a]	Filter	Cor. (mas)[b]	No. of Exp.	Exp. Time (minutes)[c]	Mode[d]	Rotation (°)	Strehl[e] (%)
GJ 4185 Aab	J21160576+2951511	2011 Jun 21	NIRC2/N	H	600	5	5.0	ADI	2.71	...
		2012 May 21	NIRC2/N	K_S	600	10	5.0	DI	...	...
GJ 4274	J22230696−1736250	2011 Jun 21	NIRC2/N	H	600	40	40.0	ADI	15.2	31
NLTT 54873	J22473764+4041253	2010 Aug 18	NIRC2/N	H	600	40	40.0	ADI	11.8	29
		2011 Aug 20	NIRC2/N	H	600	4	4.0	DI	...	...
2MASS J22581643−1104170	J22581643−1104170	2010 Aug 17	NIRC2/N	H	600	30	30.0	ADI	22.8	28
GJ 4337 A	J23292346+4128068	2010 Aug 18	NIRC2/N	H	600	42	42.0	ADI	17.0	37
		2011 Aug 20	NIRC2/N	H	600	40	20.0	DI	...	39
GJ 1290	J23442084+2136050	2011 Nov 15	NIRC2/N	H	600	28	28.0	ADI	43.5	33
		2012 Aug 23	NIRC2/N	H	600	35	17.5	DI	...	6
		2012 Oct 8	NIRC2/N	H	600	37	18.5	DI	...	45
G 68-46	J23512227+2344207	2012 Aug 23	NIRC2/N	K_S	600	40	40.0	ADI	14.9	34
		2013 Aug 17	NIRC2/N	K_S	600	40	40.0	ADI	8.4	55
1RXS J235133.3+312720	J23513366+3127229	2011 Jun 21	NIRC2/N	H	600	41	41.0	ADI	15.8	42
1RXS J235452.2+383129	J23545147+3831363	2011 Aug 20	NIRC2/N	H	600	40	40.0	ADI	21.6	43
		2012 Aug 23	NIRC2/N	H	600	20	20.0	DI	...	14
G 158-8	J23555512−1321238	2011 Aug 20	NIRC2/N	H	600	40	40.0	ADI	16.8	36
G 130-31	J23591986+3241244	2010 Aug 18	NIRC2/N	H	600	39	39.0	ADI	18.1	29

Notes.

[a] NIRC2/N refers to the narrow ($\approx 10'' \times 10''$) camera mode. NIRC2/W refers to the wide ($\approx 40'' \times 40''$) camera.

[b] Angular diameter of coronagraph.

[c] Number of frames × coadds per frame × exposure time per frame. Most of the deep imaging consisted of 60 sec exposures with 1 coadd.

[d] ADI = Angular Differential Imaging; DI = Direct Imaging (rotator on).

[e] Strehl ratios are computed for NIRC2 images with the `nirc2strehl` IDL routine available on the Keck Web site. The quoted value is the median Strehl ratio from unsaturated images taken before and after deep ADI or DI sequences.

[f] NLTT 13844 was observed with on-axis LGS-AO at Keck (Wizinowich et al. 2006; van Dam et al. 2006).

re-observe the stars with the worst data sets at Keck, a few of our observations only reach corresponding masses of $\sim$10–20 $M_{\rm Jup}$.

For HiCIAO, we adopt the following plate scale measurements, which we found slightly vary with wavelength (see Appendix A): 9.81 ± 0.04 mas pixel^{-1} for Y band, 9.75 ± 0.04 mas pixel^{-1} for J band, 9.723 ± 0.011 mas pixel^{-1} for H band, and 9.67 ± 0.03 mas pixel^{-1} for K_S band. A constant plate scale orientation of $0°\!\!.0 \pm 0°\!\!.1$ is adopted for all of the filters. Post-fit residuals from the distortion solution are $\approx$1 pixel.

3.3. IRTF/SpeX Near-infrared Spectroscopy

We obtained a near-infrared spectrum of the young, $5''\!\!.6$ separation substellar companion 2MASS J15594729+4403595 B (Section 5.1.4) with the Infrared Telescope Facility's (IRTF) SpeX spectrograph (Rayner et al. 2003) in short wavelength cross-dispersed (SXD) mode on 2012 August 11 UT in photometric conditions. A slit width of $0''\!\!.5$ yielded a resolving power ($R \equiv \lambda/\Delta\lambda$) of $\approx$1200 from 0.8–2.5 μm. To avoid the host star, we oriented the slit perpendicular to the primary star-companion position angle (P.A.). We obtained a total of 36 minutes of integration time by nodding in an ABBA pattern along the slit. Immediately after, we observed the A0V standard 26 Ser at a similar airmass (1.22) for telluric correction. Flats and arc lamps were acquired at the same sky position. The spectra were extracted, median-combined, and telluric-corrected using Spextool reduction package (Vacca et al. 2003; Cushing et al. 2004). Table 4 summarizes our spectroscopic observations of three substellar companions in our sample.

3.4. Keck/OSIRIS Near-infrared Spectroscopy

On 2013 February 1 UT and 2013 February 2 UT, we observed GJ 3629 B and 1RXS J034231.8+121622 B with the OH-Suppressing Infrared Imaging Spectrograph (OSIRIS; Larkin et al. 2006) at the Keck I telescope using NGS-AO (Table 4). Conditions were clear and both targets were observed at a low airmass of $\approx$1.1. Since the companions are located $<1''$ from their host stars, we chose the 20 mas pixel^{-1} plate scale to finely sample the point-spread function (PSF) structure with a resolving power of $\approx$3800. These observations benefited from a new grating installed in OSIRIS in 2012 December, increasing the average sensitivity by a factor of 1.83 compared to its previous performance on Keck II (Mieda et al. 2014).

We acquired Jbb-, Hbb-, and Kbb-band spectra of GJ 3629 B with the long axis of the $0''\!\!.32 \times 1''\!\!.28$ detector aligned with the primary-companion P.A. The close separation of this system ($0''\!\!.2$) ensured that both components were on the detector. The 1RXS J034231.8+121622 A-B separation is $0''\!\!.83$, so for this system we aligned the long-axis of the detector perpendicular to the primary-companion P.A. so that the primary fell off of the array. We nodded the telescope along the detector by $\approx$1$''$ in an ABBA pattern for pair-wise sky subtraction. A0V standards were observed in each filter at a similar airmass following both science targets.

Basic image reduction, wavelength calibration, assemblage of the two-dimensional (2D) images into three-dimensional spectral cubes, and pair-wise sky subtraction was carried out using version 3.2 of the OSIRIS Data Reduction Pipeline with the latest rectification matrices from 2013 February. The companion and standard star spectra were then extracted from the cubes with aperture photometry. For GJ 3629 B we used aperture radii of 2 spaxels with an annulus of 2.5–4.0 spaxels to remove some contaminating flux from the nearby host star GJ 3629 A. No local sky subtraction was applied for 1RXS J034231.8+121622

Table 4
Spectroscopic Observations

Object	Date (UT)	Telescope/ Instrument	Filter	Slit Width ($''$)	Plate Scale (mas pixel^{-1})	Exp. Time (minutes)	Standard
2MASS J15594729+4403595 B	2012 Aug 11	IRTF/SpeX-SXD	. . .	0.5	150	36	26 Ser
GJ 3629 B	2013 Feb 1	Keck I/OSIRIS	Jbb	. . .	20	20	HD 99960
	2013 Feb 1	Keck I/OSIRIS	Hbb	. . .	20	13.5	HD 99960
	2013 Feb 1	Keck I/OSIRIS	Kbb	. . .	20	10	HD 99960
1RXS J034231.8+121622 B	2013 Feb 2	Keck I/OSIRIS	Hbb	. . .	20	24	HD 31411
	2013 Feb 2	Keck I/OSIRIS	Kbb	. . .	20	24	HD 31411

B and the standards. The spectra were corrected for telluric absorption using the `xtellcor_general` routine in the IRTF Spextool reduction package (Vacca et al. 2003; Cushing et al. 2004). Finally, each band was flux calibrated using photometry from Bowler et al. (2012a) for GJ 3629 B and from Table 7 of this work for 1RXS J034231.8+121622 B.

4. ADI PROCESSING PIPELINE

We developed a processing pipeline for our ADI data to register the images, model and subtract the PSF and speckle pattern for each image, de-rotate and coadd the individual frames, identify point sources in the stacked images, compute contrast curves, and derive the sensitivity in mass and physical separation using information about the primary star coupled with evolutionary models. Below, we describe each step in detail for a typical ADI sequence consisting of forty 60 s coronagraphic images and short unsaturated frames.

4.1. Image Registration

For our NIRC2 images we correct for optical distortions using the narrow camera distortion solution made available by Keck Observatory (B. Cameron 2007, private communication), which yields post-fit residuals of ∼0.6 mas in the *x* and *y* directions. For our HiCIAO data we derive distortion solutions from our own observations of the globular cluster M5 taken before and after the installation of a new camera lens in 2011 April. See Appendix A for details. The post-fit residuals across the entire array are ∼1 pixel (10 mas).

Images are then registered and assembled into cubes. For NIRC2 we fit a 2D elliptical Gaussian to the star itself, which is visible behind the partly transparent coronagraph. For HiCIAO, which has an opaque coronagraph, we infer the position of the star by masking the coronagraph and fitting a 2D elliptical Gaussian to the PSF wings. Sky values are measured, stored, and subtracted from each image after masking the science target. Accurate accounting of the sky values are especially important for NIRC2. Since the coronagraph is not completely opaque, photometric calibration using the apparent brightness of the star behind the mask and the measured transmission of the coronagraph must also account for the background sky value. Once the stellar positions are measured, the images are assembled into a cube and aligned by shifting to a common position using sub-pixel resampling. Parallactic angles and north orientations on the detector are stored for later processing. For NIRC2, the parallactic angle is taken from FITS headers. For HiCIAO, it is computed from the hour angle at the time of the observation, target declination, and latitude of Mauna Kea.

4.2. PSF and Speckle Subtraction

The AO PSF comprises a mixture of static structure from the diffraction pattern and correlated, quasi-static speckle noise from imperfect wavefront correction and changing atmospheric conditions (Racine et al. 1999; Marois et al. 2000; Macintosh et al. 2005; Hinkley et al. 2007; Oppenheimer & Hinkley 2009). Together these conspire to make the detection of faint point sources difficult in the contrast-limited regime, and removing these features requires modeling and subtracting the PSF pattern while minimizing the subtraction of actual companions. Observing strategies based on FOV rotation (Liu 2004; Marois et al. 2006) and/or chromatic dependencies of the PSF pattern (e.g., Sparks & Ford 2002; Marois et al. 2005; Thatte et al. 2007; Biller et al. 2008; Crepp et al. 2011) together with more sophisticated processing techniques (Lafrenière et al. 2007b; Marois et al. 2010a; Soummer et al. 2011; Pueyo et al. 2012) yield contrasts >14 mag at 1$''$ (e.g., Wahhaj et al. 2013b).

We experimented with a variety of PSF subtraction methods spanning a range of sky rotations and variable AO correction (caused both by seeing conditions and target brightness). Each method has advantages and disadvantages depending on the particular data set and instrument. For example, for small sky rotations, aggressive use of the Locally Optimized Combination of Images (LOCI) algorithm (Lafrenière et al. 2007b) results in substantial self-subtraction of real point sources. In these cases, simply subtracting a median-combined PSF model can result in a higher signal-to-noise ratio (S/N) for companions. In other cases where AO quality changes substantially during an ADI sequence, LOCI generally performs better than other simpler methods. We also tested a variation of LOCI described by Marois et al. (2010a) in which a small central portion of the region used to compute the correlation matrix is masked and then used to reconstruct the final image after calculation of the reference image weights. This method keeps noise levels across the processing region relatively constant and better preserves the photometry and astrometry of known point sources, but we found that it was not the best technique to identify real objects in a first (blind) pass.

Altogether we adopt three PSF subtraction methods to homogeneously process our survey data: subtraction of a scaled median-combined PSF model, a "conservative" application of LOCI algorithm, and an "aggressive" form of LOCI. Each technique is applied to the inner (contrast-limited) 3$''$ of our ADI sequences. In the background/read noise-limited regime beyond 3$''$, we subtract a median-combined sky frame created from the data set itself.

For the scaled subtraction method we first create a PSF model by median-combining images in the ADI sequence. For each science image the model is then scaled to the annulus spanning the IWA out to 3$''$ by computing the multiplicative factor *C* that
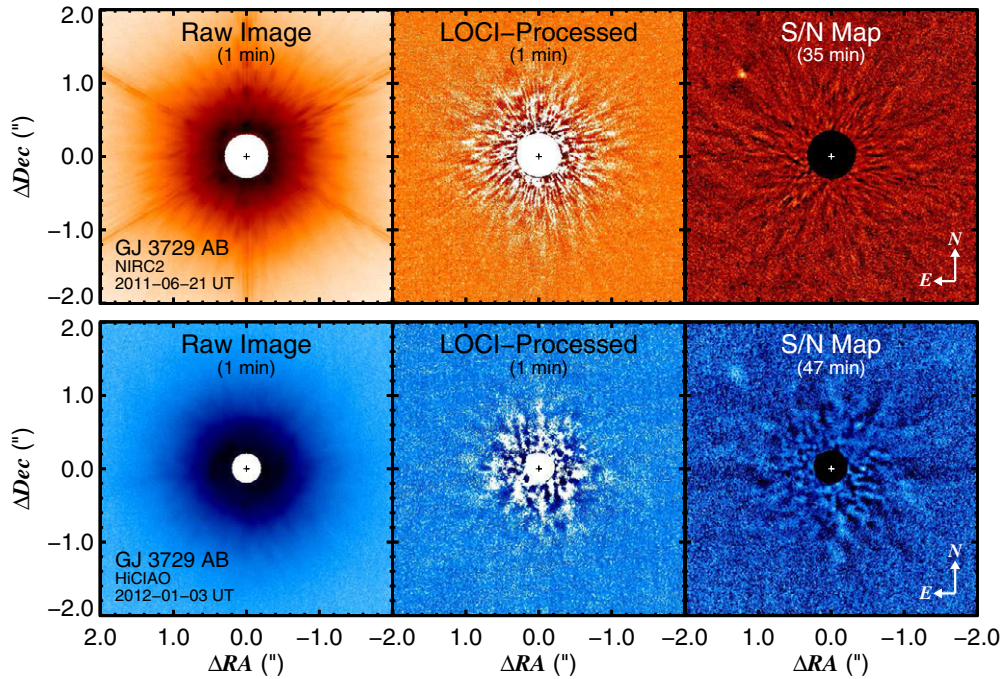
Figure 2. Example of ADI processing to reveal faint companions. The top panels show raw, LOCI-processed, and de-rotated and coadded images from NIRC2. A candidate companion is clearly visible ∼2″ from the star GJ 3729 AB. The bottom panel shows the same sequence for observations with HiCIAO about six months later.

minimizes the χ^2 value over all n pixels:

$$\chi^2 = \sum_{i=1}^{n} \left(\frac{f_i - C\mathcal{F}_i}{\sigma_i} \right)^2, \quad (1)$$

$$C = \frac{\sum f_i \mathcal{F}_i / \sigma_i^2}{\sum \mathcal{F}_i^2 / \sigma_i^2}. \quad (2)$$

Here f_i and $\mathcal{F}_i$ are the flux at pixel i in the science and model images in units of DN, and σ_i is the uncertainty in the science flux. In this flux-limited regime, $\sigma_i \propto \sqrt{f_i}$, in which case C simplifies to $\sum \mathcal{F}_i / \sum (\mathcal{F}_i^2 / f_i)$.

Our implementation of LOCI follows the geometric regions described by Lafrenière et al. (2007b) with the following parameters: $N_A = 300$, $g = 1$, $dr = 2$. We perform two reductions with minimum rotation parameter N_δ equal to 1.5 and 0.5 in units of PSF FWHM for the conservative and aggressive cases, respectively. If no reference frames satisfy the N_δ criterion for a particular annular subsection because of inadequate rotation at small separations then that section for that image is skipped. This affects some of the conservative LOCI processing at small separations near the IWA, but rarely influences the aggressive reduction.

Point sources bright enough to bias the reduction are masked out of the images prior to PSF subtraction. For the scaled median subtraction, masking reduces the influence of bright objects when computing scale factors. For the LOCI reduction, masking excludes these regions from the correlation matrix to avoid influencing the reference image weights.

4.3. Point Source Identification

After PSF subtraction, the individual images are de-rotated to a common P.A., median-combined, and oriented so that celestial north is at a P.A. of $0°$. A map of the noise is created by computing the standard deviation of flux values in concentric annuli with a width of 3 pixels after rejecting outlier pixels with a clipping threshold of 4σ. In addition to outlier rejection, bright point sources are manually masked from the coadded image to minimize their influence on the noise measurements, and, from this, a signal-to-noise map is made to search for point sources in the images.

Automated point source identification is performed on the signal-to-noise maps using the `max_search` routine in the StarFinder AO imaging software package (Diolaiti et al. 2000). `max_search` identifies peak values above a threshold level relative to nearest neighbor pixel intensities. Low threshold values (∼3–5) tend to produce a large number of false positives near the star where the speckle density is high, so we adopted a 7σ limit. However, visual inspection of each image ultimately proved to be the most robust way to identify fainter point sources. In general, we found that artificial point sources injected into the median-combined images with peak values of 7σ are reliably recovered from visual inspection across the entire image.

Figure 2 shows a typical reduction sequence with NIRC2 and HiCIAO. (This particular case is for the 50 mas binary GJ 3729 AB, though it is not included in the final survey statistics because of its binarity.) The right-hand panels show the clear detection of a point source in the NIRC2 S/N maps, which is recovered in the HiCIAO data six months later. Multi-epoch astrometry shows the candidate companion is a background object.

4.4. Contrast Curves

Contrast curves are generated from the reduced images using the noise maps and the flux from the primary star. For NIRC2 we directly measure the star brightness behind the coronagraph. This allows us to monitor AO correction throughout the ADI sequences and calibrate the detection limits

using the coronagraph throughput, which we have measured in the H and K_S filters using a binary star (Appendix B). An important caveat is that the background sky level must be taken into account since the apparent flux of the star behind the mask (f_m) is the filter-dependent attenuation of the sky-plus-stellar flux, rather than simply the attenuated stellar flux alone. Since the sky level was subtracted from the raw images, it must also be taken into account to compute the corrected sky-subtracted stellar flux level (f_c): $f_c = ((f_m + sky)/T_{filt}) - sky$, where T_{filt} is the filter-dependent transmission and sky is the background sky level. This is particularly important for our target sample of M dwarfs since the attenuated fluxes in 60 s exposures can be comparable to the (unattenuated) sky level in the raw frames. Finally, we use the median-corrected, sky-subtracted peak flux of the primary star (f_c) from the sequence together with the noise map to compute contrast curves at the desired σ level.

In a comprehensive analysis of deep ADI and SDI observations from the Gemini NICI Planet-Finding Campaign (Liu 2010a), Wahhaj et al. (2013a) show that the 5σ threshold commonly used for contrast curves in high-contrast imaging surveys corresponds to ≈ 0.2 mag brighter than the 95% recovery rate from Monte Carlo injections and extractions of artificial planets. For this survey we therefore adopt a 7σ threshold as a robust threshold for our sensitivity limits.

The FOV coverage changes for each observation based on the instrument, coronagraph position on the detector, and total sky rotation of the ADI sequence. To make full use of the data (i.e., corners of the array), we also compute the fractional coverage as a function of radial separation from the star for each observation, which we incorporate into our sensitivity limits for the statistical analysis.

For our HiCIAO data we use the short unsaturated images taken in sets during the ADI sequences to photometrically calibrate the coronagraphic frames. For some Subaru data sets, neutral density filters with $\approx 1\%$ and $\approx 10\%$ throughputs were used to prevent saturating the detector. We adopt the following transmission measurements for the neutral density filters kindly provided by T. Kudo (2013, private communication): $9.740\% \pm 0.022\%$ for $ND10$ in the H band, $0.854\% \pm 0.002\%$ for $ND1$ in the H band, $10.460\% \pm 0.020\%$ for $ND10$ in the K_S band, and $1.142\% \pm 0.026\%$ for $ND1$ in the K_S band.

Unsaturated images are processed similarly to the coronagraphic frames: they are first registered, de-rotated to a common P.A. (which is necessary for multiple sets taken during an ADI sequence), median combined, and north aligned. 7σ contrast curves are measured and joined with those from the deep imaging for separations inside the coronagraphic IWA.

Contrasts from the survey are shown in Figures 3–5 and listed in Table 5. Beyond $\approx 2''$ the contrast curves flatten out to the background/read-noise level. The AO performance at both Keck and Subaru is sensitive to seeing conditions and rapidly degrades when seeing exceeds $\sim 1''.5$. Most of our observations with Hi-CIAO suffer from bad seeing, which is reflected in the modest contrast limits. Figure 6 summarizes the survey sensitivity: at $1''$, our NIRC2 contrasts reach 11.5–14 mag, but the HiCIAO observations span a larger range from 8–13 mag. The unsaturated frames reach between ~ 3.5–5.5 mag at $0''.3$. In limiting apparent magnitude, our observations at $1''$ reach 15–23 mag, which translates to 13–23 mag in absolute magnitude. Note that we have excluded contrasts in these histograms for the two substellar companion host stars 1RXS J034231.8+121622 and 2MASS J15594729+4403595, for which we only obtained short images when we discovered the companions (Section 5.1).
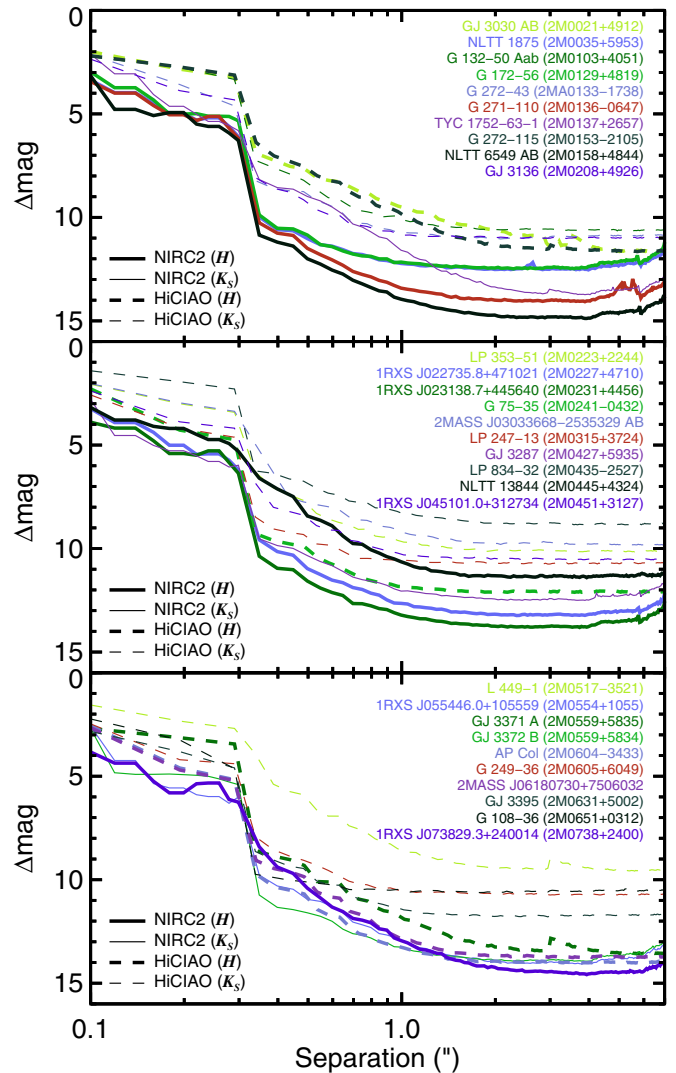
Figure 3. 7σ contrast curves from our survey. Unsaturated frames are joined with the deep imaging at $0''.3$. PSF subtraction with LOCI is performed from $0''.3$–$3''$ and scaled median subtraction is applied beyond $3''$.

These contrast curves are, however, included in our statistical analysis.

The right-most panel in Figure 6 shows the limiting mass at $1''$ as a function of physical separation at $1''$ for our entire sample. The median limiting mass is 5.5 M_{Jup} and we are sensitive to masses below 10 M_{Jup} at $1''$ for 85% of our targets. The median physical separation at $1''$ is 20.3 AU and 85% of our targets correspond to physical separations less than 33 AU at $1''$.

4.5. Astrometry and Photometry

4.5.1. Stellar Binaries

Astrometry for bright companions from our short unsaturated images is computed in the following manner. After correcting each image for distortion, the separation and position angle are measured in one of two ways. For companions with small separations ($\lesssim 1''$) we fit each binary component with a PSF composed of three elliptical Gaussians as described in Liu et al. (2008). This method performs well for both the NIRC2 and HiCIAO data in a variety of seeing conditions. For separations wide enough to avoid contamination from the primary ($\gtrsim 1''$),

Table 5
Contrast Curves

Name	UT Date	Inst.	Filter	Contrast (Δmag) [FOV Coverage]													
				0″.1	0″.2	0″.5	0″.75	1″	1″.5	2″	3″	4″	5″	8″	10″	12″	14″
GJ 3030 AB	2011 Dec 27	HiCIAO	H	1.9	2.8	7.6	8.7	9.5	10.3	10.6	11.4	11.3 [1.0]	11.6 [1.0]	11.7 [1.0]	11.3 [0.9]	10.8 [0.5]	10.4 [0.1]
NLTT 1875	2010 Aug 18	NIRC2/N	H	3.3	5.0	11.0	11.8	12.2	12.4	12.5	12.5	12.5 [1.0]	12.3 [0.7]	11.6 [0.1]	...	...	...
G 132-50 Aab	2011 Dec 28	HiCIAO	K_S	2.2	2.8	8.2	9.7	10.1	10.5	10.6	10.6	10.6 [1.0]	10.6 [1.0]	10.6 [1.0]	10.4 [0.9]	9.8 [0.6]	9.4 [0.1]
G 172-56	2010 Aug 17	NIRC2/N	H	2.9	5.0	10.9	11.9	12.2	12.4	12.4	12.4	12.4 [1.0]	12.1 [0.7]	11.5 [0.1]	...	...	...
G 272-43	2012 Jan 3	HiCIAO	K_S	2.1	3.6	8.8	10.3	10.7	10.9	11.0	10.9	10.9 [1.0]	10.9 [1.0]	10.9 [1.0]	10.6 [0.8]	10.2 [0.5]	9.9 [0.1]
G 271-110	2010 Aug 18	NIRC2/N	H	3.4	5.0	11.5	12.8	13.4	13.8	14.0	14.0	14.0 [1.0]	13.4 [0.7]	13.1 [0.1]	...	...	...
TYC 1752-63-1	2012 Aug 23	NIRC2/N	K_S	2.1	4.6	9.0	10.5	11.6	12.7	13.4	13.5	13.7 [1.0]	13.5 [0.7]	12.9 [0.1]	...	...	...
G 272-115	2011 Dec 27	HiCIAO	H	2.2	2.7	7.5	9.0	9.9	11.0	11.3	11.3	11.6 [1.0]	11.6 [1.0]	11.6 [1.0]	11.4 [0.8]	11.1 [0.4]	10.8 [0.1]
NLTT 6549 AB	2011 Aug 20	NIRC2/N	H	3.1	4.9	12.0	13.2	14.0	14.5	14.7	14.8	14.9 [1.0]	14.6 [0.7]	13.8 [0.1]	...	...	...
GJ 3136	2011 Jan 27	HiCIAO	K_S	2.3	3.9	9.2	10.4	10.9	10.9	10.9	11.0	11.0 [1.0]	11.0 [1.0]	11.0 [1.0]	10.6 [0.8]	10.2 [0.4]	9.6 [0.1]
LP 353-51	2011 Dec 28	HiCIAO	K_S	2.0	3.0	7.7	9.1	9.7	10.0	10.1	10.1	10.1 [1.0]	10.1 [1.0]	10.1 [1.0]	9.9 [0.8]	9.5 [0.4]	9.1 [0.0]
1RXS J022735.8+471021	2010 Aug 17	NIRC2/N	H	3.2	5.0	11.0	12.0	12.6	13.1	13.2	13.2	13.2 [1.0]	13.0 [0.7]	12.4 [0.1]	...	...	...
1RXS J023138.7+445640	2010 Aug 18	NIRC2/N	H	3.9	5.4	11.6	12.7	13.2	13.6	13.8	13.8	13.8 [1.0]	13.5 [0.7]	12.8 [0.1]	...	...	...
G 75-35	2012 Jan 3	HiCIAO	H	2.2	4.3	9.9	11.4	11.8	12.0	12.1	12.1	12.1 [1.0]	12.1 [1.0]	12.1 [1.0]	11.9 [0.8]	11.5 [0.4]	11.1 [0.1]
2MASS J03033668−2535329 AB	2011 Dec 28	HiCIAO	K_S	2.0	3.0	7.7	8.6	9.2	9.6	9.8	9.7	9.8 [1.0]	9.8 [1.0]	9.8 [1.0]	9.7 [0.8]	9.4 [0.3]	9.1 [0.0]
LP 247-13	2011 Aug 20	NIRC2/N	H	3.8	5.1	8.9	10.6	11.6	13.0	13.4	13.5	13.7 [1.0]	13.7 [0.6]	13.8 [0.0]	...	...	...
GJ 3287	2013 Feb 4	NIRC2/N	K_S	2.7	5.3	10.3	11.5	12.1	12.3	12.4	12.4	12.5 [1.0]	12.3 [0.7]	11.6 [0.1]	...	...	...
LP 834-32	2011 Dec 28	HiCIAO	K_S	1.4	1.9	6.7	7.8	8.3	8.6	8.8	8.8	8.8 [1.0]	8.8 [1.0]	8.8 [1.0]	8.5 [0.8]	8.2 [0.4]	7.9 [0.1]
NLTT 13844	2012 Oct 8	NIRC2/N	H	3.2	4.2	8.4	9.8	10.6	11.2	11.3	11.3	11.4 [1.0]	11.3 [0.6]	11.3 [0.0]	...	...	...
1RXS J045101.0+312734	2011 Jan 27	HiCIAO	K_S	2.3	3.9	8.4	9.8	10.3	10.5	10.5	10.5	10.5 [1.0]	10.5 [1.0]	10.5 [1.0]	10.3 [0.8]	9.6 [0.4]	9.3 [0.0]
L 449-1 AB	2011 Dec 28	HiCIAO	K_S	1.5	2.3	5.9	7.7	8.6	9.2	9.4	9.0	9.4 [1.0]	9.5 [1.0]	9.5 [1.0]	9.4 [0.8]	9.1 [0.3]	8.6 [0.0]
1RXS J055446.0+105559	2013 Feb 4	NIRC2/N	K_S	2.5	5.6	10.9	12.2	12.9	13.7	14.0	14.0	14.1 [1.0]	13.7 [0.7]	13.1 [0.1]	...	...	...
GJ 3371 A	2011 Dec 27	HiCIAO	H	2.7	3.1	9.3	10.9	11.9	12.8	13.3	12.8	13.4 [1.0]	13.6 [1.0]	13.6 [1.0]	13.3 [0.9]	12.9 [0.5]	12.5 [0.1]
GJ 3372 B	2011 Mar 25	NIRC2/N	K_S	2.6	4.9	11.6	12.7	13.3	13.7	13.9	13.9	13.9 [1.0]	13.7 [0.7]	13.0 [0.1]	...	...	...
AP Col	2012 Jan 3	HiCIAO	H	2.4	4.6	10.7	12.6	13.3	13.8	13.9	14.0	14.0 [1.0]	14.0 [1.0]	14.0 [1.0]	13.9 [0.8]	13.5 [0.4]	13.1 [0.1]
G 249-36	2011 Jan 27	HiCIAO	K_S	2.4	4.2	9.1	10.2	10.6	10.6	10.7	10.7	10.7 [1.0]	10.7 [1.0]	10.7 [1.0]	10.5 [0.8]	9.9 [0.4]	9.5 [0.0]
2MASS J06180730+7506032	2012 Jan 3	HiCIAO	H	2.5	4.7	9.9	11.7	12.9	13.5	13.7	13.7	13.7 [1.0]	13.7 [1.0]	13.7 [1.0]	13.6 [0.8]	13.2 [0.4]	12.7 [0.1]
GJ 3395	2011 Jan 26	HiCIAO	K_S	2.8	3.8	9.5	11.0	11.5	11.7	11.8	11.7	11.7 [1.0]	11.7 [1.0]	11.7 [1.0]	11.4 [0.8]	10.9 [0.5]	10.3 [0.1]
G 108-36	2012 Jan 3	HiCIAO	K_S	2.2	3.2	10.1	10.5	10.5	10.6	10.6	10.5	10.6 [1.0]	10.5 [1.0]	10.5 [1.0]	10.1 [0.9]	9.6 [0.6]	9.2 [0.1]
1RXS J073829.3+240014	2010 Nov 27	NIRC2/N	H	3.8	5.8	10.4	12.0	12.9	13.9	14.2	14.4	14.6 [1.0]	14.5 [0.7]	13.8 [0.0]	...	...	...
1RXS J091744.5+461229 AB	2011 Dec 28	HiCIAO	K_S	0.7	2.1	7.6	8.8	9.4	9.8	9.9	9.8	10.0 [1.0]	9.9 [1.0]	9.9 [1.0]	9.7 [0.8]	9.2 [0.4]	8.8 [0.1]
GJ 354.1 B	2013 May 2	NIRC2/N	K_S	2.3	5.0	10.4	11.4	11.8	12.1	12.2	12.2	12.2 [1.0]	11.9 [0.7]	11.2 [0.1]	...	...	...
PYC 09362+3731 AB	2012 May 22	NIRC2/N	H	2.9	4.2	11.8	12.8	13.7	14.4	14.7	14.6	14.9 [1.0]	14.6 [0.7]	13.9 [0.1]	...	...	...
G 161-71	2011 Nov 16	NIRC2/N	H	3.2	4.2	11.1	12.3	13.3	14.0	14.3	14.3	13.5 [1.1]	13.1 [0.9]	13.1 [0.1]	...	...	...
NLTT 22741 A	2012 May 21	NIRC2/N	K_S	2.0	3.5	8.9	9.7	10.1	10.5	10.6	10.6	10.6 [1.0]	10.5 [0.7]	9.8 [0.0]	...	...	...
GJ 3577 A	2013 Feb 4	NIRC2/N	K_S	2.3	4.9	10.7	11.8	12.4	12.8	13.0	12.9	13.0 [1.0]	12.6 [0.8]	12.0 [0.1]	...	...	...
GJ 3578 B	2013 Feb 4	NIRC2/N	K_S	2.5	5.1	11.4	12.3	12.7	12.9	13.0	13.0	13.0 [1.0]	12.7 [0.8]	11.9 [0.1]	...	...	...
G 196-3 A	2011 Jan 26	HiCIAO	K_S	2.2	3.5	8.6	10.5	11.2	11.5	11.5	11.5	11.5 [1.0]	11.5 [1.0]	11.5 [1.0]	11.3 [0.7]	10.9 [0.3]	10.5 [0.0]
GJ 2079 AB	2013 Feb 4	NIRC2/N	K_S	1.5	4.7	9.4	11.0	12.1	13.2	13.8	13.1	13.8 [1.0]	13.3 [0.7]	12.7 [0.1]	...	...	...
GJ 3629 AB	2012 May 10	HiCIAO	H	2.4	4.3	9.0	10.3	10.8	11.0	11.1	11.1	11.1 [1.0]	11.1 [1.0]	11.1 [1.0]	10.9 [0.8]	10.3 [0.4]	9.9 [0.1]
GJ 3639	2011 Jan 27	HiCIAO	K_S	3.0	4.3	10.4	10.7	10.7	10.7	10.8	10.8	10.7 [1.0]	10.7 [1.0]	10.8 [1.0]	10.3 [0.9]	9.6 [0.6]	8.8 [0.1]
NLTT 26114	2012 Jan 14	NIRC2/N	K	0.0	9.6	10.0	11.6	12.2	12.6	12.8	12.7	12.8 [1.0]	12.6 [0.7]	11.8 [0.1]	...	...	...
NLTT 26359	2011 Dec 27	HiCIAO	K_S	2.4	4.0	9.6	11.5	12.1	12.5	12.7	12.6	12.7 [1.0]	12.7 [1.0]	12.6 [1.0]	12.4 [0.8]	12.0 [0.4]	11.6 [0.1]
G 119-62	2011 Jan 26	HiCIAO	K_S	2.6	4.4	9.3	11.0	11.4	11.6	11.7	11.7	11.6 [1.0]	11.7 [1.0]	11.6 [1.0]	11.3 [0.8]	10.9 [0.4]	10.4 [0.1]
2MASS J11240434+3808108	2011 Mar 25	NIRC2/N	K_S	2.7	5.3	11.3	12.4	12.9	13.2	13.2	13.2	13.3 [1.0]	13.1 [0.7]	12.3 [0.1]	...	...	...
TWA 30 A	2011 Mar 25	NIRC2/N	K_S	2.1	3.8	9.1	10.1	10.6	10.8	10.9	10.9	11.0 [1.0]	10.8 [0.7]	10.2 [0.0]	...	...	...

Table 5
(Continued)

Name	UT Date	Inst.	Filter	Contrast (Δmag) [FOV Coverage]													
				0″.1	0″.2	0″.5	0″.75	1″	1″.5	2″	3″	4″	5″	8″	10″	12″	14″
G 10-52	2011 Jan 27	HiCIAO	K_S	2.7	4.3	9.8	10.7	10.8	10.8	10.9	10.9	10.9 [1.0]	10.9 [1.0]	10.9 [1.0]	10.6 [0.8]	10.0 [0.3]	9.7 [0.0]
LP 734-34	2011 Dec 27	HiCIAO	K_S	2.3	3.9	9.1	10.1	10.2	10.4	10.4	10.4	10.4 [1.0]	10.4 [1.0]	10.4 [1.0]	10.1 [0.8]	9.7 [0.4]	9.3 [0.1]
G 13-33 AB	2012 May 21	NIRC2/N	K_S	1.9	3.4	9.3	10.2	10.8	11.2	11.4	11.4	11.5 [1.0]	11.3 [0.7]	10.6 [0.0]	...	...	...
GJ 3729 AB	2011 Jun 21	NIRC2/N	H	2.9	4.8	11.1	12.3	13.1	13.8	14.1	14.1	14.2 [1.0]	13.9 [0.7]	13.3 [0.1]	...	...	...
1RXS J124147.5+564506	2011 Jan 26	HiCIAO	K_S	2.5	3.5	8.5	9.5	9.6	9.7	9.8	9.7	9.7 [1.0]	9.7 [1.0]	9.7 [1.0]	9.5 [0.8]	9.0 [0.5]	8.5 [0.1]
LHS 2613	2012 Jan 3	HiCIAO	H	2.5	4.7	9.7	11.5	12.4	13.0	13.2	13.2	13.2 [1.0]	13.3 [1.0]	13.2 [1.0]	13.0 [0.8]	12.5 [0.5]	12.1 [0.1]
LHS 2672	2012 May 10	HiCIAO	H	2.5	4.7	10.5	11.8	12.4	12.5	12.6	12.5	12.6 [1.0]	12.6 [1.0]	12.6 [1.0]	12.3 [0.8]	11.6 [0.5]	11.3 [0.1]
GJ 1167 A	2011 Jan 27	HiCIAO	K_S	2.7	4.0	10.2	10.7	10.7	10.8	10.8	10.8	10.7 [1.0]	10.8 [1.0]	10.8 [1.0]	10.4 [0.8]	9.8 [0.4]	9.3 [0.1]
LHS 2686	2011 Jun 21	NIRC2/N	H	4.1	5.0	11.3	12.4	13.3	13.9	14.1	14.2	14.2 [1.0]	14.0 [1.0]	13.3 [0.1]	...	...	...
2MASS J13233804−2554449	2013 Feb 4	NIRC2/N	K_S	2.5	5.1	9.9	11.0	12.0	12.9	13.3	13.1	13.4 [1.0]	13.0 [0.7]	12.5 [0.1]	...	...	...
2MASS J13292408−1422122	2011 Mar 25	NIRC2/N	K_S	2.7	5.4	10.8	12.4	13.1	13.7	13.9	13.9	14.0 [1.0]	13.8 [0.7]	13.1 [0.1]	...	...	...
2MASS J14124864−1629561	2013 May 2	NIRC2/N	K_S	2.4	4.9	10.6	11.8	12.5	13.1	13.2	13.2	13.3 [1.0]	13.0 [0.7]	12.4 [0.1]	...	...	...
GQ Vir	2012 May 21	NIRC2/N	K_S	2.0	4.3	10.1	11.0	11.7	12.3	12.6	12.6	12.7 [1.0]	12.5 [0.7]	11.8 [0.1]	...	...	...
2MASS J14442809−0424078	2011 Mar 25	NIRC2/N	K_S	2.5	5.2	10.9	11.9	12.6	13.0	13.1	13.1	13.1 [1.0]	13.0 [0.7]	12.5 [0.0]	...	...	...
G 166-49	2012 May 22	NIRC2/N	H	3.5	4.9	11.7	12.6	13.2	13.9	14.2	13.8	13.6 [1.0]	13.5 [0.9]	13.0 [0.1]	...	...	...
1RXS J150907.2+590422 A	2012 May 21	NIRC2/N	K_S	2.2	4.7	9.9	10.9	11.6	12.3	12.5	12.5	12.6 [1.0]	12.4 [0.7]	11.7 [0.1]	...	...	...
2MASS J15323737+4653048	2013 Aug 17	NIRC2/N	K_S	2.5	5.1	10.6	12.0	13.0	13.8	14.1	14.2	14.3 [1.0]	14.2 [0.7]	13.5 [0.1]	...	...	...
NLTT 40561	2010 Aug 18	NIRC2/N	H	3.6	5.2	9.6	11.3	12.0	12.6	12.9	13.0	13.0 [1.0]	12.9 [0.7]	12.4 [0.0]	...	...	...
G 202-48	2011 Jun 21	NIRC2/N	H	3.6	5.0	10.8	12.1	13.4	14.9	15.7	15.7	16.2 [1.0]	16.0 [0.7]	15.5 [0.0]	...	...	...
GJ 669 B	2010 Aug 18	NIRC2/N	H	3.8	5.3	10.9	12.6	13.6	14.3	14.2	14.6	14.6 [1.0]	14.4 [0.7]	13.7 [0.1]	...	...	...
GJ 669 A	2012 May 10	HiCIAO	H	2.4	4.5	10.0	11.8	12.9	13.6	13.8	13.9	13.9 [1.0]	13.9 [1.0]	13.9 [1.0]	13.6 [0.8]	13.0 [0.4]	12.9 [0.1]
LHS 3321	2011 Jun 21	NIRC2/N	H	4.2	5.4	11.9	13.2	14.4	15.5	16.1	15.6	16.2 [1.0]	15.6 [0.8]	15.1 [0.1]	...	...	...
G 227-22	2010 Aug 17	NIRC2/N	H	3.0	4.9	10.6	12.0	13.0	13.9	14.3	14.4	14.4 [1.0]	14.3 [0.7]	13.6 [0.1]	...	...	...
LP 390-16	2011 Mar 25	NIRC2/N	K_S	2.9	5.3	11.1	12.2	13.0	13.7	13.9	13.8	13.8 [1.0]	13.2 [0.8]	12.9 [0.1]	...	...	...
GJ 9652 A	2011 Aug 20	NIRC2/N	H	3.3	4.5	10.5	11.9	12.8	14.0	14.7	15.3	15.5 [1.0]	15.4 [0.6]	15.5 [0.0]	...	...	...
2MASS J19303829−1335083	2011 Jul 1	NIRC2/N	H	3.0	3.7	10.6	11.4	11.7	11.8	11.8	11.9	11.9 [1.0]	11.7 [0.7]	10.8 [0.1]	...	...	...
1RXS J193528.9+374605	2011 Aug 20	NIRC2/N	H	4.2	5.2	11.5	12.8	14.0	15.0	15.4	15.5	15.8 [1.0]	15.6 [0.8]	14.8 [0.1]	...	...	...
2MASS J19435432−0546363	2012 May 21	NIRC2/N	K_S	1.8	3.4	8.9	9.9	10.5	11.1	11.3	11.3	11.4 [1.0]	11.2 [0.7]	10.5 [0.1]	...	...	...
TYC 7443-1102-1	2012 May 22	NIRC2/N	K_S	1.8	3.8	8.6	9.7	10.6	11.4	11.8	11.6	12.0 [1.0]	11.9 [0.7]	11.3 [0.1]	...	...	...
NLTT 48651	2011 Jun 21	NIRC2/N	H	3.1	4.4	10.8	12.1	13.2	14.1	14.4	14.5	14.7 [1.0]	14.5 [0.7]	13.9 [0.1]	...	...	...
2MASS J20284361−1128307	2012 May 10	HiCIAO	H	2.2	4.3	8.5	10.7	11.8	12.3	12.5	12.4	12.4 [1.0]	12.4 [1.0]	12.5 [1.0]	12.3 [0.8]	11.8 [0.3]	11.5 [0.0]
TYC 523-573-1	2012 Aug 23	NIRC2/N	H	2.4	4.2	10.6	11.7	12.9	13.9	14.4	13.3	14.2 [1.0]	14.0 [0.9]	13.4 [0.2]	...	...	...
NLTT 50710	2012 May 21	NIRC2/N	K_S	2.0	3.8	8.6	9.4	10.2	10.7	10.9	10.9	11.0 [1.0]	10.9 [0.7]	10.2 [0.0]	...	...	...
GJ 4186 B	2011 Jun 21	NIRC2/N	H	3.7	4.7	10.8	12.2	13.1	13.8	14.1	14.1	14.2 [1.0]	14.0 [0.7]	13.3 [0.1]	...	...	...
GJ 4274	2011 Jun 21	NIRC2/N	H	3.8	4.9	11.2	12.8	13.8	14.7	15.1	15.0	15.3 [1.0]	15.1 [0.7]	14.4 [0.1]	...	...	...
NLTT 54873	2010 Aug 18	NIRC2/N	H	3.5	5.1	11.0	12.1	12.7	13.1	13.2	13.2	13.2 [1.0]	13.1 [0.7]	12.3 [0.0]	...	...	...
2MASS J22581643−1104170	2010 Aug 17	NIRC2/N	H	3.2	5.0	10.5	12.0	13.0	13.7	14.0	14.1	14.1 [1.0]	13.9 [0.7]	13.3 [0.1]	...	...	...
GJ 4337 A	2010 Aug 18	NIRC2/N	H	3.8	5.8	11.6	13.0	13.8	14.5	14.6	14.6	14.6 [1.0]	14.4 [0.7]	13.6 [0.1]	...	...	...
GJ 1290	2011 Nov 15	NIRC2/N	H	3.8	4.6	11.5	12.9	13.8	14.5	14.8	14.7	14.9 [1.0]	14.3 [0.9]	13.4 [0.1]	...	...	...
G 68-46	2013 Aug 17	NIRC2/N	K_S	2.5	5.2	10.4	11.9	12.6	13.1	13.3	13.3	13.4 [1.0]	13.3 [0.7]	12.8 [0.0]	...	...	...
1RXS J235133.3+312720	2011 Jun 21	NIRC2/N	H	3.7	5.5	10.4	11.7	12.9	13.7	14.0	14.1	14.2 [1.0]	14.0 [0.7]	13.2 [0.1]	...	...	...
1RXS J235452.2+383129	2011 Aug 20	NIRC2/N	H	4.5	5.5	11.7	13.0	13.8	14.5	14.7	14.8	14.9 [1.0]	14.6 [0.7]	14.0 [0.1]	...	...	...
G 158-8	2011 Aug 20	NIRC2/N	H	3.9	4.8	11.4	12.8	13.6	14.2	14.4	14.4	14.5 [1.0]	14.3 [0.7]	13.6 [0.1]	...	...	...
G 130-31	2010 Aug 18	NIRC2/N	H	3.9	5.5	11.3	12.2	12.8	13.1	13.2	13.2	13.2 [1.0]	13.0 [0.7]	12.3 [0.1]	...	...	...
Median NIRC2 Contrast	...	NIRC2/N	...	3.1	5.1	10.8	12.0	12.9	13.6	13.8	13.5	13.7	13.3	12.9	...	...	...
Median HiCIAO Contrast	...	HiCIAO	...	2.4	3.9	9.2	10.5	10.7	10.9	11.0	11.0	11.0	11.0	11.0	10.6	10.2	9.9
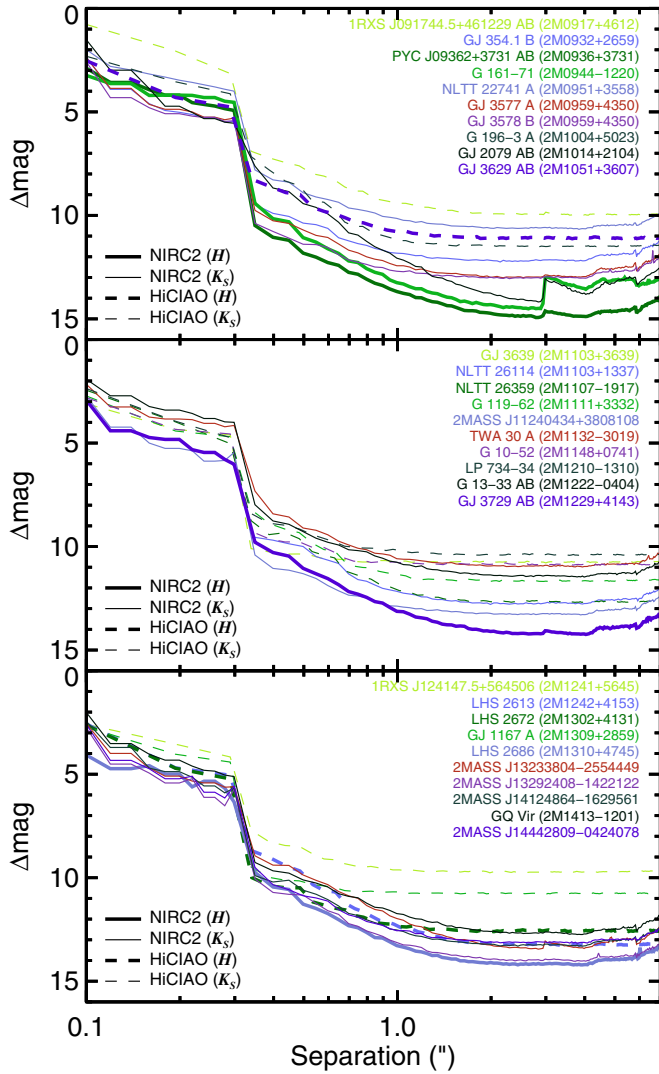
Figure 4. 7σ contrast curves from our survey (continued).
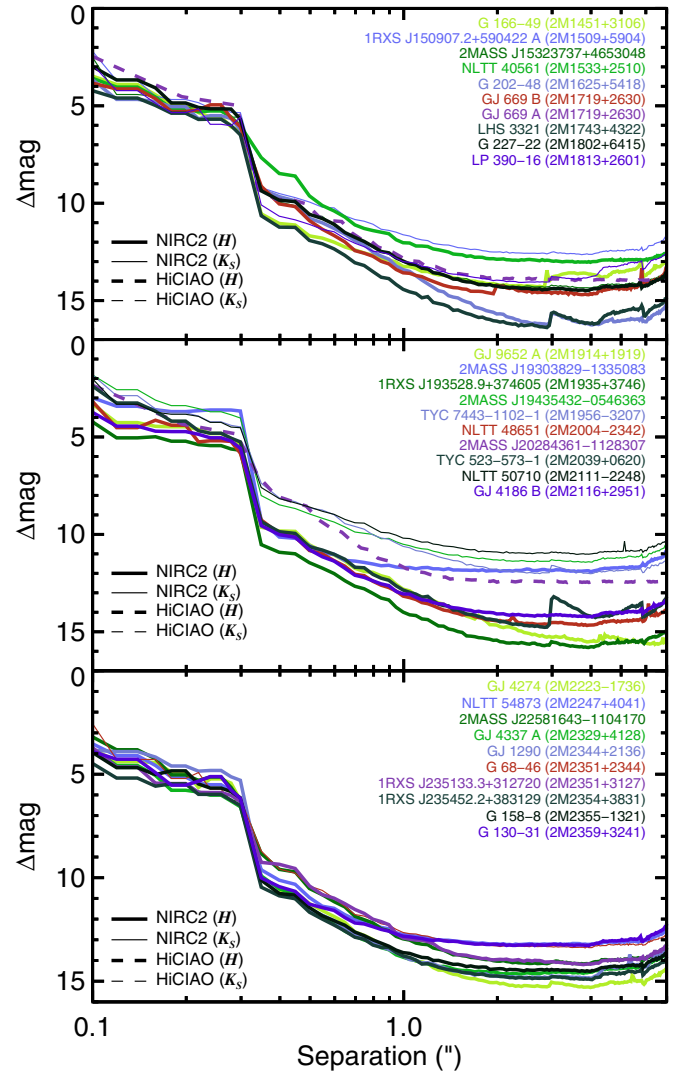
Figure 5. 7σ contrast curves from our survey (continued).

we use aperture photometry after subtracting the sky level from each image. The mean of the separation and P.A. measured from individual images are adopted for our astrometry.

Several sources contribute to the uncertainty in these values: random sub-pixel centroid measurement errors from image to image, systematic effects from residuals in the distortion solution, uncertainties in the absolute sky orientation on the detector, and the finite precision of the measured plate scale. These independent errors are propagated analytically to produce our final astrometric uncertainties. The separation ρ is therefore

$$\rho = s\,\bar{\rho}_{\mathrm{meas}} \pm s\,\bar{\rho}_{\mathrm{meas}} \left(\left(\frac{\sigma_s}{s}\right)^2 + \left(\frac{\sigma_{\bar{\rho},\mathrm{tot}}}{\sigma_{\bar{\rho},\mathrm{meas}}}\right)^2 \right)^{1/2}, \qquad (3)$$

$$\sigma_{\bar{\rho},\mathrm{tot}}^2 = \sigma_{\bar{\rho},\mathrm{meas}}^2 + 2\sigma_d^2, \qquad (4)$$

where s and σ_s are the plate scale and associated uncertainty in mas pixel^{-1}, $\bar{\rho}_{\mathrm{meas}}$ and $\sigma_{\bar{\rho},\mathrm{meas}}$ are the mean and standard deviation of the measured separations for the individual images (in pixels), and σ_d is the typical residual positional displacement after applying the distortion correction (in pixels, one for each

binary component). Likewise, the P.A. (θ) is

$$\theta = \bar{\theta}_{\mathrm{meas}} + \theta_{\mathrm{North}} \pm \left(\sigma_{\theta,\mathrm{meas}}^2 + \sigma_{\theta,\mathrm{North}}^2 \right)^{1/2}, \qquad (5)$$

where $\bar{\theta}_{\mathrm{meas}}$ is the mean P.A. of the individual images, θ_{North} is the orientation of the detector relative to north, $\sigma_{\theta,\mathrm{meas}}$ is the standard deviation of the P.A. measurements, and $\sigma_{\theta,\mathrm{North}}$ is the uncertainty in the sky orientation on the detector.

4.5.2. Faint Point Sources

Astrometry and photometry for faint point sources are measured from our final processed images. The error budget for the separation measurement consists of positional uncertainties of the star behind the mask, centroid errors for the candidate, and systematic errors in the distortion solution (Equation (3)). For NIRC2, we adopt random measurement uncertainties ($\sigma_{\rho,\mathrm{meas}}$) of 0.3 pixel, which is typical of our binary star measurements.

The dominant source of astrometric uncertainty for our HiCIAO data are from the image registration process since the peak of the PSF is hidden under the opaque 300 mas focal plane mask. To estimate the typical magnitude of this uncertainty, we use our ADI sequence of the $\sim 2''$ binary system
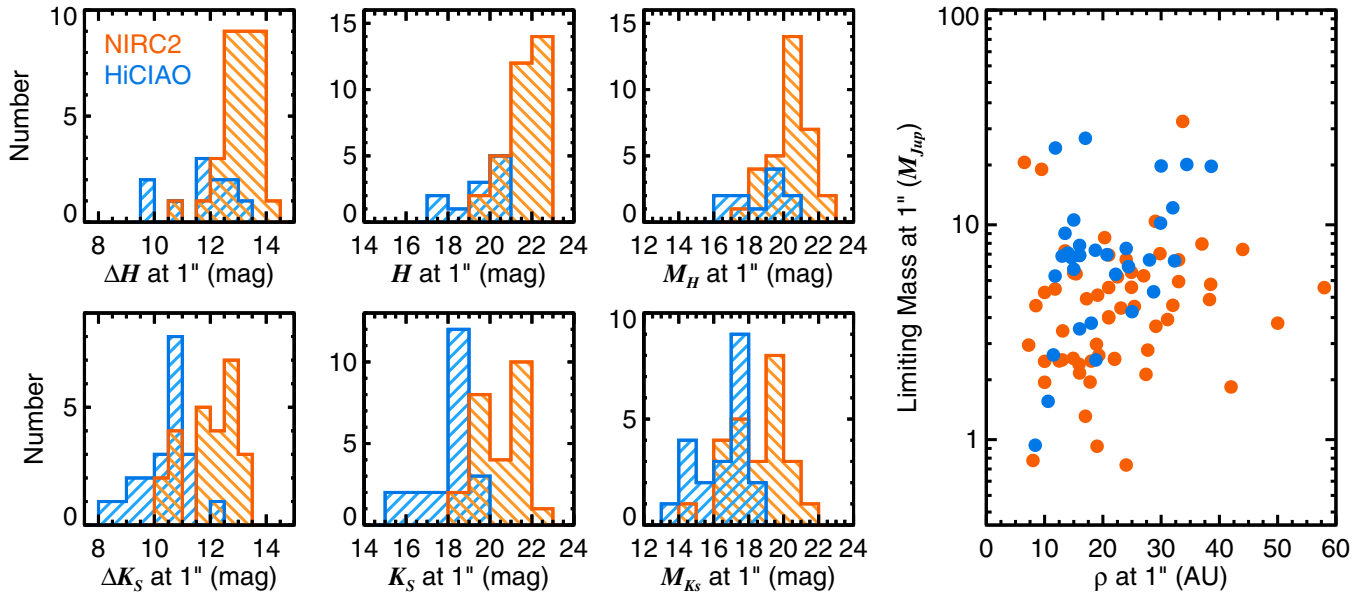
Figure 6. Summary of our measured contrasts, limiting apparent magnitudes, and limiting absolute magnitudes at $1''$. The right panel shows the limiting planet masses and projected physical separations at $1''$ for NIRC2 (red) and HiCIAO (blue). We are sensitive to planets below 10 $M_{\rm Jup}$ at separations less than 33 AU at $1''$ for 85% of our sample.

GJ 3030 AB. The R-band magnitude of this system from UCAC4 ($\sim$12.2 mag) is typical for our targets and, as with most of our HiCIAO observations in this program, these data were taken in unusually poor seeing conditions (1.5–2″0). Here GJ 3030 A was behind the mask and the following test was performed on the B component. We first determine the centroid of the companion GJ 3030 B in each image, then mask the central 150 mas, fit a 2D elliptical Gaussian to the wing of the PSF following our general method for HiCIAO image registration (see Section 4.1), and compute the relative difference of the inferred to the actual measured stellar position. The inferred position is generally $\sim$1–2.5 pixel from the actual center (the mean value is 1.6 pixel for this representative sequence), so we conservatively adopt an uncertainty of 2 pixel, or $\sim$20 mas, for the HiCIAO registration term ($\sigma_{\bar{\rho},{\rm meas}}$). For the random error term $\sigma_{\theta,{\rm meas}}$ we adopt characteristic uncertainties from our moderate-contrast binary star astrometry of 0°.2 and 0°.1 for NIRC2 and HiCIAO, respectively.

Position angle uncertainties originate from centroid errors for the candidate companion, systematic errors in the north alignment, and, for HiCIAO, uncertainties associated with image registration. In this latter case we add an additional term, $\sigma_{\rm reg}$, in quadrature with the random and systematic errors in Equation (5). $\sigma_{\rm reg}$ refers to the angular uncertainty associated with a positional error (from image registration) orthogonal to the primary-candidate companion direction; for HiCIAO we adopt a 2 pixel positional uncertainty, so $\sigma_{\rm reg}$ (in deg) scales as arcsin(2 pixel/$\rho_{\rm meas}$).

Many of the wide-separation ($\gtrsim 5''$) candidates identified in first epoch imaging were followed up with the NIRC2 wide camera mode, which has a plate scale of 39.884 $\pm$ 0.039 mas pixel^{-1} (Pravdo et al. 2006) and FOV ($\approx$40″ $\times$ 40″). For these observations, we use the distortion solution from Fu et al. (2014) and estimate a residual positional uncertainty σ_d of 1 pixel from the residual map.[10] Even behind the partly opaque

coronagraph, the primary stars were usually saturated in this wide camera mode. Although this had a minimal impact on relative astrometry, it prevented accurate relative photometry for these observations.

Aperture photometry is measured for all point sources to derive contrasts relative to the star. We use aperture radii of 6 pixel for candidates identified in our NIRC2 data. For our HiCIAO observations, which typically suffered from poor seeing and modest AO correction, we use larger aperture radii of 15 pixel. Photometric errors incorporate measurement errors computed at the source location in the noise map, uncertainties in the coronagraph transmission (for NIRC2), uncertainties in the neutral density filters (for HiCIAO, when applicable), and uncertainties in the measured flux of the primary star itself. This last term is the standard deviation of flux measurements from the star (behind the mask for NIRC2, and from unsaturated images for HiCIAO).

5. SURVEY RESULTS

Out of 122 targets imaged in our survey, 44 are close stellar binaries, 27 of which are new or spatially resolved for the first time. We discovered four new young brown dwarf companions confirmed to be comoving with their host stars. Over 150 planet candidates were identified out to projected separations of $\approx$400 AU; we recovered the majority (56%) of these in second-epoch imaging, and all of these are background stars. Below, we describe these results in detail.

5.1. Substellar Companions from the PALMS Survey

Our four brown dwarf discoveries span masses of 30–70 $M_{\rm Jup}$ at projected separations of 6–190 AU. Two have already been published as part of this series (1RXS J235133.3+312720 B in Bowler et al. 2012b; GJ 3629 B in Bowler et al. 2012a) and here we present two new companions, 1RXS J034231.8+121622 B and 2MASS J15594729+4403595 B. Note that the young stars G 196-3 A (2MASS J10042148+5023135) and NLTT 22741 A (2MASS J09510459+3558098; LP 261-75) in our sample have

---

[10] http://www2.keck.hawaii.edu/inst/nirc2/dewarp.html
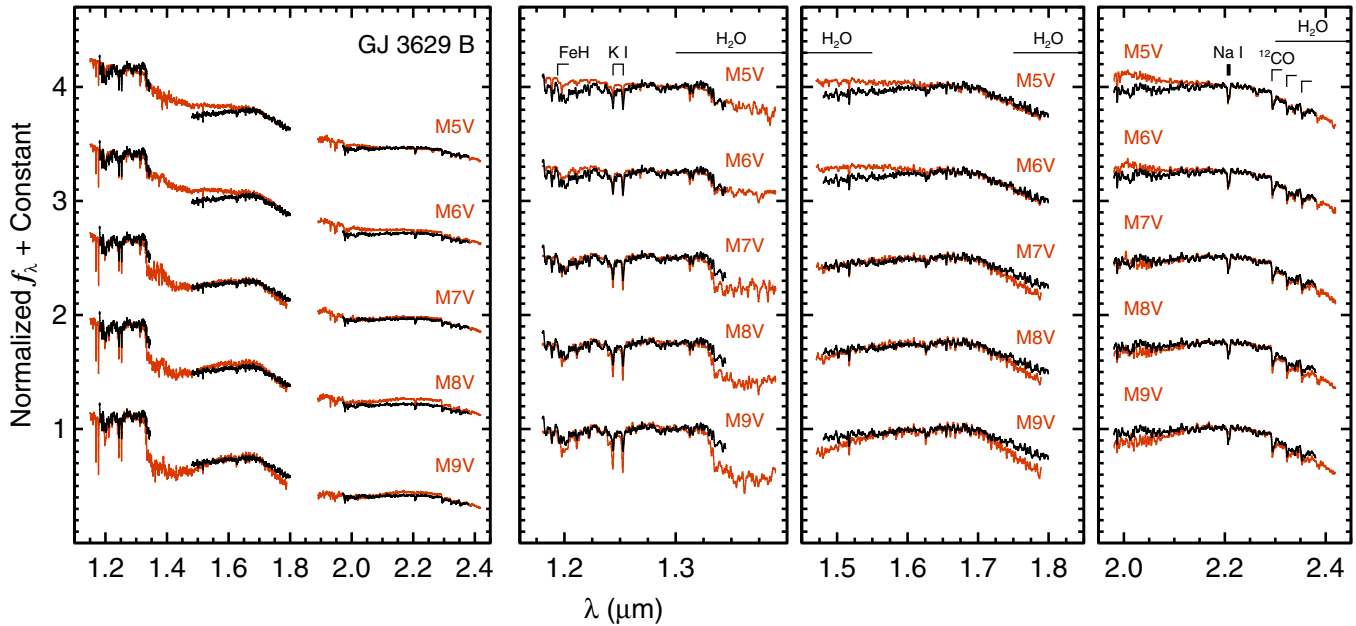
Figure 7. Our OSIRIS spectrum of GJ 3629 B compared with field objects from the IRTF SpeX Spectral Library (Cushing et al. 2005; Rayner et al. 2009). Overall the 1.15–2.40 μm spectrum of GJ 3629 B, which is largely driven by relative band-to-band flux calibration, best resembles M7 field template (left panel). Compared to individual bandpasses, GJ 3629 B is similar to both M7 and M8 objects in J, H, and K spectral regions. Altogether we adopt a spectral type of M7.5 $\pm$ 0.5 for GJ 3629 B. The IRTF library templates are Gl 51 (M5V), Gl 406 (M6V), Gl 644 C (M7V), Gl 752 B (M8V), and DENIS-P J104814.7–395606.1 (M9V). All spectra have been smoothed to a common resolving power of $R \approx 2000$.

previously known wide-separation brown dwarf companions with L spectral types (Rebolo et al. 1998; Reid & Walkowicz 2006). However, neither companion falls in the FOV of our observations so they are not included in our statistical analysis (Section 6). Below we summarize our discoveries and present new photometry and astrometry for each system.

5.1.1. 1RXS J235133.3+312720 B (2MASS J23513366+3127229)

1RXS J235133.3+312720 B is a 32 $\pm$ 6 $M_{\rm Jup}$ companion to the active M2.0 star 1RXS J235133.3+312720 A and was the first discovery from our PALMS survey (Bowler et al. 2012b). Shkolnik et al. (2012), Schlieder et al. (2012b), and Malo et al. (2013) independently identify the primary as a likely member of the AB Dor YMG ($\sim$120 Myr) based on its kinematics and activity. We found a near-IR spectral type of L0$^{+2}_{-1}$ for the companion along with subtle spectroscopic hints of low surface gravity (Bowler et al. 2012b). Based on the photometric distance to the primary (50 $\pm$ 10 pc), the 2$\farcs$4 projected separation corresponds to 120 $\pm$ 20 AU.

In Bowler et al. (2012b), we presented two epochs of relative astrometry for 1RXS J235133.3+312720 AB based on AO imaging with NIRC2 in 2011 in the H and K' bands. In addition, we also obtained seeing-limited relative photometry from IRTF in $YJHKs$ filters. Here we present new, more precise 1–3.8 μm relative photometry obtained with NIRC2 in 2013 (Table 7). We infer a Y–J color of 1.17 $\pm$ 0.17 mag for 1RXS J235133.3+312720 B assuming a Y–J color of 0.459 $\pm$ 0.001 mag for the primary, which is the mean color for M2.0 dwarfs from Rayner et al. (2009). Based on the MKO photometry of the primary from Bowler et al. (2012b), we derive the following colors for 1RXS J235133.3+312720 B: $(J$–$H)_{\rm MKO}$ = 0.73 $\pm$ 0.12 mag, $(H$–$K)_{\rm MKO}$ = 0.64 $\pm$ 0.08 mag, $(J$–$K)_{\rm MKO}$ = 1.37 $\pm$ 0.12 mag. Finally, based on the typical $K_{\rm MKO}$–L' color of 0.2 $\pm$ 0.1 mag for M2 dwarfs

from Golimowski et al. (2004), we derive a $K_{\rm MKO}$–L' color of 0.8 $\pm$ 0.2 mag for the companion. Compared to typical colors of M/L dwarfs (e.g., Bowler et al. 2012a; Golimowski et al. 2004), our new photometry for 1RXS J235133.3+312720 B corresponds to spectral types of $\approx$L0–L3, which is consistent with our published classification based on near-IR spectroscopy.

Altogether, our astrometry over 3 yr shows tentative signs of orbital motion. The reduced χ^2 values for constant and linear fits to the separation measurements are 1.58 and 1.38, respectively. Reduced χ^2 values for the P.A. are 3.91 and 0.47 for the constant and linear models, suggesting a slight change of $-0.076 \pm 0\fdg017$ yr^{-1}. Additional astrometry in the future will be needed for confirmation.

5.1.2. GJ 3629 B (2MASS J10512059+3607255 B)

GJ 3629 B is a modest-contrast companion located a mere 0$\farcs$2 from its active M3.0Ve host star GJ 3629 A (Bowler et al. 2012a). Based on its photometric distance of 22 $\pm$ 3 pc and age of 25–300 Myr (Shkolnik et al. 2009), Bowler et al. inferred a mass of 46 $\pm$ 16 $M_{\rm Jup}$ for the companion. Recently, Dittmann et al. (2013) measured a parallactic distance of 32.3 $\pm$ 2.4 pc to the system. This corresponds to a somewhat higher luminosity of $\log(L/L_{\odot})$ = -2.89 ± 0.10 dex. At the system age of 25–300 Myr, the Burrows et al. (1997) evolutionary models imply a mass much closer to the hydrogen burning limit. Assuming a log-normal luminosity distribution and a linearly uniform age distribution, the resulting mass distribution from Monte Carlo simulations has a median value of 64 $M_{\rm Jup}$. The 68.3% confidence range about the median is 41–94 $M_{\rm Jup}$, and the 95.4% range spans 31–114 $M_{\rm Jup}$. Altogether, the probability that GJ 3629 B is substellar ($<$75 $M_{\rm Jup}$) is 62%.

Figure 7 shows our resolved 1.15–2.4 μm Keck/OSIRIS spectrum of GJ 3629 B compared to M5–M8 field stars from the IRTF SpeX Spectral Library (Cushing et al. 2005; Rayner

Table 6
Spectral Types and Gravity Indices for Substellar Companions

Object	NIR SpT	FeH$_z$ Index	FeH$_J$ Index	VO$_z$ Index	K I$_J$ Index	H-cont Index	Gravity Score[a]	Gravity Class
GJ 3629 B	M7.5 ± 0.5	. . .	1.098 ± 0.015	. . .	1.055 ± 0.006	1.003 ± 0.004	nn12	INT-G?
1RXS J034231.8+121622 B	L0 ± 1	. . .	. . .	. . .	. . .	0.948 ± 0.004	nnn1	INT-G?
2MASS J15594729+4403595 B	M8.0 ± 0.5	1.097 ± 0.008	1.087 ± 0.010	1.049 ± 0.006	1.058 ± 0.004	1.018 ± 0.006	1n12	INT-G

Note. [a] Gravity scores are listed in order of FeH, VO, alkali lines, and H-band shape following Allers & Liu (2013).

et al. 2009). Overall the spectrum of GJ 3629 B is typical of an ultracool M dwarf, exhibiting deep ≈1.4 μm and 1.9 μm steam bands, strong 2.2935 μm CO band heads, FeH absorption at ≈1.2 μm, and K I and Na I doublets at 1.25 μm and 2.21 μm. GJ 3629 B is an excellent match to the M7 template across the entire spectrum (left-most panel) and M7–M8 objects among individual bandpasses (right three panels). Altogether we adopt a spectral type of M7.5 ± 0.5. Compared to a low- and high-gravity templates from Allers & Liu (2013) in Figure 8, there are no obvious signs of low surface gravity in GJ 3629 B, which is prominently manifested as a angular H-band shape and shallow J-band alkali line strengths in young brown dwarfs (e.g., McLean et al. 2000; Allers et al. 2007). Our OSIRIS spectrum does not span the entire wavelength range to compute all gravity indices using the Allers & Liu (2013) scheme, but the K I$_J$ and H-cont indices tentatively show signs of youth (Table 6 and Figure 9).

We also take the opportunity to update the physical properties of the primary with this new trigonometric distance. Following the same methods as in Bowler et al. (2012a), the luminosity of the primary is $\log(L_{\rm Bol}/L_\odot) = -1.54 \pm 0.08$ dex and its mass is 0.3–0.5 $M_\odot$ using the Baraffe et al. (1998) evolutionary models. Taking into account the updated component masses and projected separation (6.5 ± 0.5 AU), the expected orbital period for this system is 30^{+30}_{-13} yr assuming a projected-to-physical conversion scale of $1.16^{+0.81}_{-0.31}$ from Dupuy & Liu (2011). Our new astrometry taken with HiCIAO only a few months after our last published epoch is consistent with our previously reported measurements. Finally, we note that the system kinematics, $UVW = \{-28.9 \pm 0.8, -15.8 \pm 1.0, -0.9 \pm 0.5\}$ km s^{-1}, do not correspond to any known moving group.

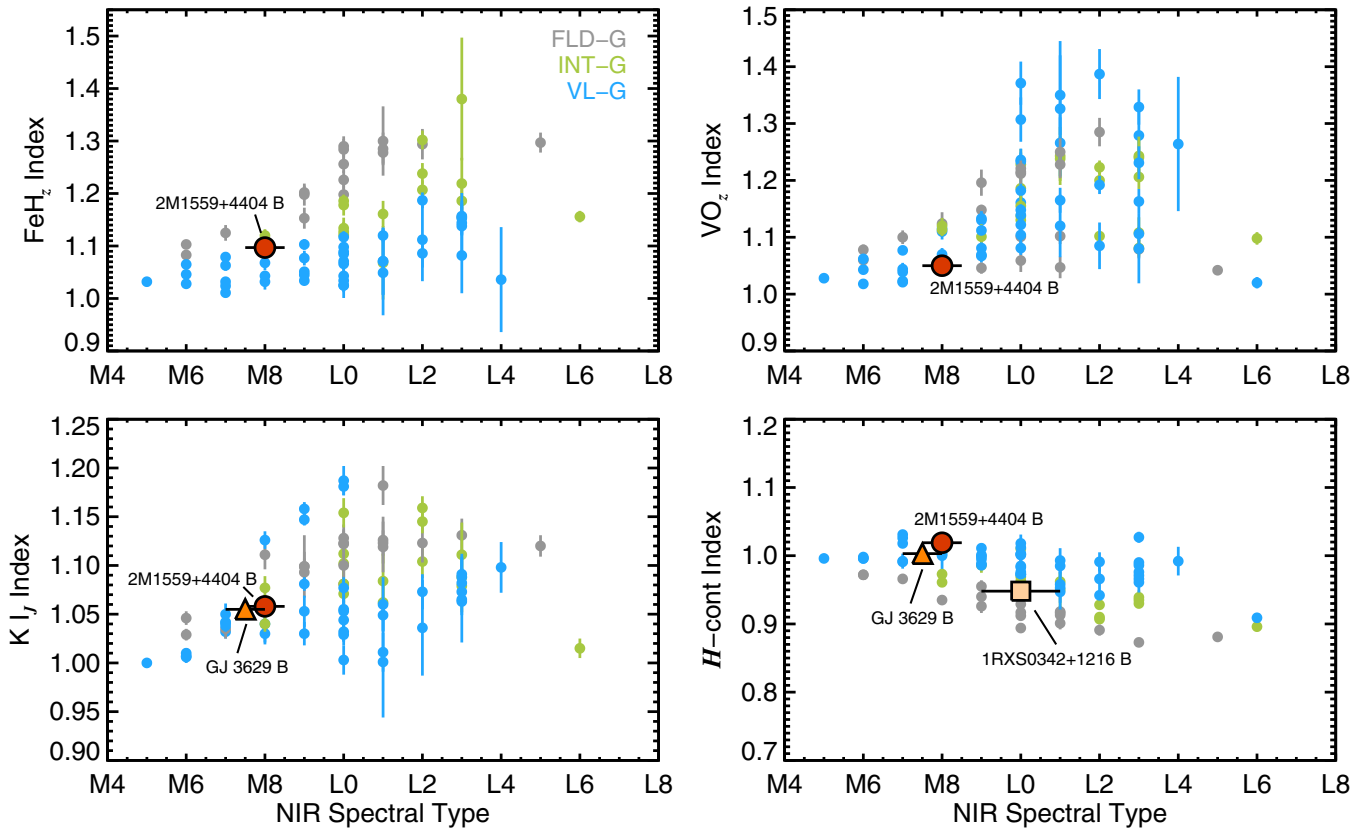### 5.1.3. 1RXS J034231.8+121622 B (2MASS J03423180+1216225 B)

1RXS J034231.8+121622 A is an active M4.0Ve star detected in the *ROSAT* and *GALEX* surveys (Riaz et al. 2006). Shkolnik et al. (2009) first noted hints of youth (60–300 Myr) from its X-ray emission and ruled out spectroscopic binarity from two epochs of high-resolution ($R \sim 58,000$) optical spectroscopy.

Recently, Dittmann et al. (2013) measured a parallactic distance of 23.9 ± 1.1 pc to this star. Its distance and radial velocity (35.4 ± 0.4 km s^{-1}) from Shkolnik et al. (2012) imply UVW space velocities of $\{-39.0 \pm 0.6, -13.4 \pm 0.8, -6.8 \pm 0.7$ km s$^{-1}\}$, which are similar to, though not formally consistent with, the Hyades moving group ($UVW_{\rm Hyades} = \{-41.7, -19.3, -1.1\} \pm 0.4$ km s^{-1}; Perryman et al. 1998). 1RXS J034231.8+121622 A also shares a similar sky position with the Hyades and is only 24 pc from the cluster center (Röser et al. 2011), suggesting a possible association with the larger but less coherent Hyades Supercluster or Stream (Eggen 1958). However, the origin and relationship of this kinematic
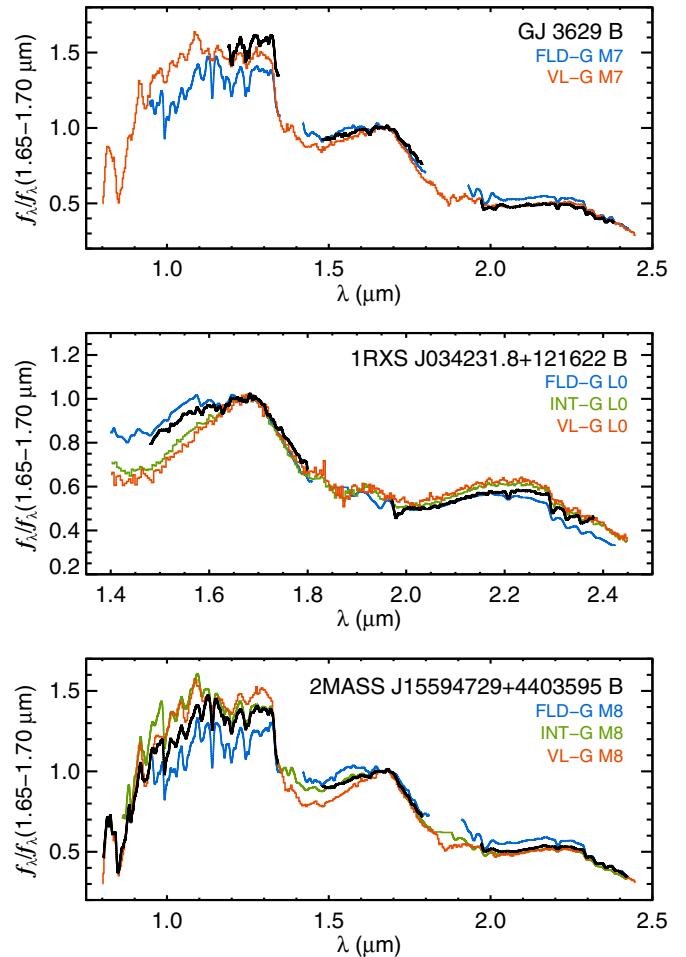
Figure 8. Comparison of GJ 3629 B, 1RXS J034231.8+121622 B, and 2MASS J15594729+4403595 B with very low gravity (VL-G), intermediate-gravity (INT-G), and field high-gravity (FLD-G) ultracool objects from Allers & Liu (2013). GJ 3629 B does not appear to differ substantially from the FLD-G M7 object. The H-band shape of 1RXS J034231.8+121622 B is somewhat less angular than the INT-G L0 template but is noticeably more pronounced than the field object. 2MASS J15594729+4403595 B agrees well with the INT-G M8 template. The comparison objects from Allers & Liu (2013) are 2MASSJ00034227-2822410 (FLD-G M7), 2MASS J03350208+2342356 (VL-G M7), 2MASS J17312974+2721233 (FLD-G L0), 2MASS J15525906+2948485 (INT-G L0), 2MASS J22134491−2136079 (VL-G L0), 2MASS J08040580+615333 (FLD-G M8), and 2MASS J00192626+4614078 (INT-G M8). TWA 27 A (VL-G M8) is from Looper et al. (2007). All spectra are smoothed to $R \sim 120$ and normalized to the 1.65–1.70 μm region.

overdensity with the Hyades cluster is not clear and is unlikely to be useful for age-dating purposes (e.g., Famaey et al. 2005). So for this work we adopt the 60–300 Myr statistical age constraint from Shkolnik et al. (2009) based on the X-ray luminosity and spectroscopic youth indicators of 1RXS J034231.8+121622 A.

Figure 9. Gravity indices as a function of NIR spectral type for 2MASS J15594729+4403595 B, GJ 3629 B, and 1RXS J034231.8+121622 B following the Allers & Liu (2013) classification scheme. 2MASS J15594729+4403595 B is an INT-G brown dwarf; the other two companions show signs of low surface gravity but the limited spectral coverage prevents definitive assignments. Objects with final gravity classes of field-gravity (FLD-G), intermediate-gravity (INT-G), and very low gravity (VL-G) from Allers & Liu (2013) are plotted in gray, green, and blue for comparison.

Janson et al. (2012) used Lucky imaging to resolve a close (0″8) candidate companion, 1RXS J034231.8+121622 B, at two epochs in 2008. However, they were not able to distinguish a background object from a comoving companion from these data. Their contrast measurement in z band (5.20 ± 0.27 mag) imply a spectral type of $\gtrsim$L0 for the companion.

We imaged 1RXS J034231.8+121622 on 2012 August 23 UT and 2013 January 17 UT with NIRC2 in the Y, J, H, K_S, and L' bands (Table 7). The companion was easily identified in all the data with contrasts between 4.3–3.6 mag (Figure 10). Figure 11 shows our astrometry and that from Janson et al. between 2008 and 2013 compared to the expected track from a background object. We confirm that 1RXS J034231.8+121622 B is physically bound and detect slight orbital motion in both P.A. and separation. The reduced χ^2 value for a constant fit in separation is 6.97 and for a linear fit is 0.98. Similarly, for the P.A., the constant fit gives 6.75 and 5.23. Removing the 2012.645 epoch Y-band P.A. point, in which the companion was only identified in three exposures, gives a reduced χ^2 value of 3.67 and 0.46 for the constant and linear P.A. fits, respectively. These imply orbital motion of -8.1 ± 1.5 mas yr^{-1} in separation and $+0.33 \pm 0°09$ yr^{-1} in P.A. At a distance of 23.9 ± 1.1 pc, the projected separation of the pair is 19.8 ± 0.9 AU.

We use our measured contrasts to compute J_{MKO}-, H_{MKO}-, and K_S-band magnitudes for 1RXS J034231.8+121622 B based on photometry of the primary, which was first converted from the Two Micron Sky Survey (2MASS) to MKO filter system for the J and H filters with the relations from Leggett et al. (2006).

Based on the typical Y–J color of 0.524 ± 0.01 mag for M4 stars from Rayner et al. (2009), we derive a Y–J color of 0.86 ± 0.13 mag for 1RXS J034231.8+121622 B, which suggests a photometric spectral type of M8 $\pm$ 1.

Figure 12 shows our resolved Keck/OSIRIS H- and K-band spectra of 1RXS J034231.8+121622 B compared to field templates. 1RXS J034231.8+121622 B is most similar to L0–L1 objects in the 1.4–2.4 μm region and in H-band alone. The K-band spectrum resembles field M9–L0 templates. Altogether we adopt a spectral type of L0 $\pm$ 1. Compared to younger L0 objects from Allers & Liu (2013) in Figure 8, the blue side of the H band of 1RXS J034231.8+121622 B appears somewhat shallower than the H-band spectral shape of the field object, but not as much as the intermediate- or very low gravity brown dwarfs (Figure 9).

Using this spectral type and the system distance, we compute an H-band bolometric correction from Liu et al. (2010b) and a bolometric luminosity of log $L/L_\odot = -3.81 \pm 0.05$ dex. Uncertainties in distance, spectral type, and photometry are incorporated into our final error in an Monte Carlo fashion. Based on the age of the system, the evolutionary models of Burrows et al. (1997) imply a mass of 35 ± 8 M_{Jup}.

5.1.4. 2MASS J15594729+4403595 B

2MASS J15594729+4403595 A is an M2.0 star exhibiting Hα emission and saturated X-ray emission (Riaz et al. 2006). As part of an ongoing search for young low-mass members, E. L. Shkolnik et al. (in preparation) identify this active star from its

Table 7
Astrometry of Stellar and Substellar Companions

Name	2MASS ID	Epoch (UT)	Instrument	Filt.	N_{images}	Separation (mas)	P.A. (°)	Δmag	m_A[a] (mag)	m_B[b] (mag)	FWHM (mas)
						Substellar Companions					
1RXS J034231.8+121622 AB	J03423180+1216225	2012.645	NIRC2/N	Y	3	850 ± 30	17.8 ± 0.2	4.25 ± 0.12	10.70 ± 0.02[c]	14.95 ± 0.12[c]	68 ± 16
		2012.645	NIRC2/N	J	10	829 ± 2	18.5 ± 0.2	3.91 ± 0.05	10.19 ± 0.02	14.10 ± 0.05	52 ± 4
		2012.645	NIRC2/N	H	10	831 ± 2	18.71 ± 0.07	3.93 ± 0.05	9.58 ± 0.019	13.51 ± 0.05	53 ± 4
		2012.645	NIRC2/N	K_S	10	832.4 ± 1.0	18.70 ± 0.04	3.76 ± 0.07	9.31 ± 0.018	13.07 ± 0.07	54.8 ± 1.8
		2013.044	NIRC2/N	L'	10	822 ± 8	19.1 ± 0.7	3.56 ± 0.17	9.22 ± 0.10[d]	12.78 ± 0.19[d]	110 ± 9
GJ 3629 AB	J10512059+3607255	2012.357	HiCIAO	H	28	206 ± 19	119.6 ± 2.3	3.3 ± 0.3	8.87 ± 0.02	12.2 ± 0.3	79 ± 11
2MASS J15594729+4403595 AB	J15594729+4403595	2012.357	HiCIAO	Y	10	5646 ± 27	284.47 ± 0.10	5.06 ± 0.04	8.98 ± 0.02[c]	14.04 ± 0.05[c]	94 ± 6
		2012.357	HiCIAO	J	10	5647 ± 27	284.48 ± 0.10	4.72 ± 0.03	8.52 ± 0.02	13.24 ± 0.04	82 ± 8
		2012.357	HiCIAO	H	20	5647 ± 15	284.46 ± 0.10	4.76 ± 0.03	7.86 ± 0.02	12.62 ± 0.04	73 ± 4
		2012.357	HiCIAO	K_S	20	5644 ± 22	284.47 ± 0.10	4.11 ± 0.02	7.65 ± 0.02	11.76 ± 0.03	78 ± 3
1RXS J235133.3+312720 AB	J23513366+3127229	2013.626	NIRC2/N	Y	10	2391 ± 4	91.63 ± 0.02	6.24 ± 0.14	10.28 ± 0.02[c]	16.52 ± 0.14[c]	31.4 ± 1.8
		2013.626	NIRC2/N	J	14	2391 ± 3	91.647 ± 0.015	5.53 ± 0.10	9.83 ± 0.02	15.36 ± 0.10	33.6 ± 1.6
		2013.626	NIRC2/N	H	8	2390.7 ± 1.1	91.65 ± 0.010	5.39 ± 0.05	9.18 ± 0.019	14.57 ± 0.05	40.7 ± 0.8
		2013.626	NIRC2/N	Ks	5	2391.2 ± 1.1	91.63 ± 0.03	4.96 ± 0.05	8.98 ± 0.018	13.94 ± 0.05	49.4 ± 0.3
		2013.626	NIRC2/N	K	6	2391.6 ± 1.7	91.643 ± 0.014	4.98 ± 0.05	8.95 ± 0.02[e]	13.93 ± 0.05[e]	50.4 ± 0.3
		2013.626	NIRC2/N	L'	20	2390 ± 5	91.64 ± 0.08	4.40 ± 0.19	8.99 ± 0.10[d]	13.39 ± 0.21[d]	83.6 ± 0.4
						Stellar Companions					
G 217-32 AB	J00074264+6022543	2010.628	NIRC2/N	H	3	528.9 ± 0.9	74.22 ± 0.11	0.475 ± 0.011	8.87 ± 0.02	9.35 ± 0.03	44.3 ± 0.3
1RXS J001557.5−163659 AB	J00155808−1636578	2011.634	NIRC2/N	H	10	104.5 ± 0.9	90.37 ± 0.05	0.06 ± 0.05	8.91 ± 0.03	8.97 ± 0.03	45 ± 2
		2012.644	NIRC2/N	K_S	20	<59	…	…	…	…	58.9 ± 1.0
		2012.770	NIRC2/N	H	10	<54	…	…	…	…	54.1 ± 1.3
GJ 3030 AB	J00215781+4912379	2011.986	HiCIAO	H	13	2267 ± 14	300.30 ± 0.11	2.16 ± 0.04	8.59 ± 0.02	10.75 ± 0.04	120 ± 20
G 132-50 Aab	J01034013+4051288	2011.989	HiCIAO	H	5	270 ± 15	308 ± 3	2.8 ± 0.3	7.55 ± 0.07	10.3 ± 0.3	100 ± 30
		2011.989	HiCIAO	K_S	14	264 ± 17	308.9 ± 1.2	2.34 ± 0.18	7.45 ± 0.03	9.78 ± 0.16	87 ± 6
NLTT 6549 AB	J01581361+4844197	2011.069	HiCIAO	H	15	<120	…	…	…	…	120 ± 30
		2011.634	NIRC2/N	H	5	49.6 ± 1.2	51 ± 2	1.44 ± 0.09	8.69 ± 0.03	10.13 ± 0.07	40.7 ± 0.4
2MASS J03033668−2535329 AB	J03033668−2535329	2011.989	HiCIAO	K_S	25	830 ± 14	359.84 ± 0.13	2.99 ± 0.06	7.17 ± 0.03	10.16 ± 0.06	93 ± 14
G 160-54 AB	J04134585−0509049	2012.006	HiCIAO	Y	5	195 ± 14	127.10 ± 0.12	0.177 ± 0.011	10.91 ± 0.03[c]	11.09 ± 0.03[c]	123 ± 2
		2012.006	HiCIAO	J	20	195 ± 14	127.49 ± 0.08	0.181 ± 0.012	10.38 ± 0.03	10.56 ± 0.03	123 ± 5
		2012.006	HiCIAO	H	20	193 ± 14	128.02 ± 0.17	0.134 ± 0.015	9.80 ± 0.03	9.94 ± 0.03	111 ± 7
		2012.006	HiCIAO	K_S	20	195 ± 14	127.78 ± 0.14	0.12 ± 0.03	9.52 ± 0.03	9.64 ± 0.03	96 ± 3
		2012.645	NIRC2/N	K_S	10	166.7 ± 1.9	123.2 ± 0.3	0.42 ± 0.11	9.39 ± 0.05	9.81 ± 0.07	62 ± 6
G 160-54 AC	J04134585−0509049	2012.006	HiCIAO	Y	5	3355 ± 20	108.50 ± 0.10	3.039 ± 0.012	10.91 ± 0.03[c]	14.01 ± 0.03[c]	123 ± 2
		2012.006	HiCIAO	J	20	3350 ± 19	108.59 ± 0.10	2.780 ± 0.013	10.38 ± 0.03	13.24 ± 0.03	123 ± 5
		2012.006	HiCIAO	H	20	3349 ± 14	108.65 ± 0.10	2.735 ± 0.014	9.80 ± 0.02	12.62 ± 0.03	111 ± 7
		2012.006	HiCIAO	K_S	20	3348 ± 17	108.61 ± 0.10	2.279 ± 0.013	9.52 ± 0.02	11.93 ± 0.03	96 ± 3
		2012.645	NIRC2/N	K_S	10	3332 ± 1.8	108.47 ± 0.03	2.77 ± 0.06	9.39 ± 0.02	12.24 ± 0.06	62 ± 6
2MASS J04220833−2849053 AB	J04220833−2849053	2012.006	HiCIAO	H	10	745 ± 14	241.83 ± 0.11	0.048 ± 0.011	8.29 ± 0.02	8.34 ± 0.02	57 ± 4
2MASS J04472312−2750358	J04472312−2750358	2011.069	HiCIAO	K_S	5	8848 ± 31	133.80 ± 0.10	0.57 ± 0.014	7.33 ± 0.02	7.90 ± 0.02	80 ± 6
G 81-34 AB	J04492947+4828459	2011.072	HiCIAO	K_S	5	637 ± 14	234.18 ± 0.13	0.564 ± 0.016	8.68 ± 0.03	9.24 ± 0.03	76 ± 3
		2011.634	NIRC2/N	H	6	636.5 ± 1.9	237.68 ± 0.08	0.57 ± 0.03	8.94 ± 0.06	9.51 ± 0.06	40 ± 2
2MASS J06131330−2742054 AB	J06131330−2742054	2011.987	HiCIAO	K_S	17	130 ± 14	215.3 ± 0.8	0.31 ± 0.10	7.75 ± 0.05	8.06 ± 0.06	70 ± 20
LHS 1864 AB	J06434969+5108209	2011.987	HiCIAO	K_S	10	1765 ± 15	271.0 ± 0.10	0.674 ± 0.012	8.012 ± 0.018	8.69 ± 0.02	62 ± 3
1RXS J091744.5+461229 AB	J09174473+4612246	2011.073	HiCIAO	K_S	10	204 ± 14	37.5 ± 0.3	0.102 ± 0.019	7.948 ± 0.019	8.05 ± 0.02	55 ± 7

Table 7
(Continued)

Name	2MASS ID	Epoch (UT)	Instrument	Filt.	N_{images}	Separation (mas)	P.A. (°)	Δmag	m_A[a] (mag)	m_B[b] (mag)	FWHM (mas)
GJ 2079 AB	J10141918+2104297	2011.228	NIRC2/N	K_S	10	99 ± 2	129.99 ± 0.17	1.87 ± 0.06	6.44 ± 0.03	8.31 ± 0.06	48.2 ± 0.2
		2011.990	HiCIAO	K_S	23	<83	. . .	. . .	. . .	. . .	83 ± 9
		2013.094	NIRC2/N	K_S	20	95 ± 3	320.2 ± 1.2	1.8 ± 0.2	6.45 ± 0.04	8.25 ± 0.17	51.4 ± 1.2
PYC J10571+0544 AB	J10571139+0544547	2012.390	NIRC2/N	H	14	1005.6 ± 1.3	155.96 ± 0.04	0.82 ± 0.02	9.63 ± 0.02	10.45 ± 0.03	46 ± 2
2MASS J12062214−1314559 AB	J12062214−1314559	2012.007	HiCIAO	H	25	422 ± 15	54.6 ± 0.3	1.94 ± 0.02	8.24 ± 0.04	10.18 ± 0.04	100 ± 20
		2012.007	HiCIAO	K_S	10	423 ± 14	54.62 ± 0.19	1.90 ± 0.02	7.99 ± 0.03	9.89 ± 0.03	68 ± 3
G 13-33 AB	J12225061−0404462	2011.990	HiCIAO	K_S	19	<170	. . .	. . .	. . .	. . .	170 ± 16
		2012.387	NIRC2/N	K_S	21	57.1 ± 1.3	64.7 ± 1.1	0.27 ± 0.09	9.45 ± 0.05	9.72 ± 0.06	71 ± 6
		2013.095	NIRC2/N	K_S	17	129.7 ± 0.9	36.6 ± 0.09	0.18 ± 0.05	9.49 ± 0.03	9.67 ± 0.03	79 ± 16
LP 735-48 AB	J12264413−1229175	2011.987	HiCIAO	K_S	10	1889 ± 15	71.23 ± 0.11	0.285 ± 0.018	8.49 ± 0.02	8.78 ± 0.02	119 ± 18
GJ 3729 AB	J12290290+4143497	2011.070	HiCIAO	K_S	10	<88	. . .	. . .	. . .	. . .	88 ± 13
		2011.469	NIRC2/N	H	15	50.3 ± 0.9	255.5 ± 0.8	0.647 ± 0.06	8.66 ± 0.03	9.31 ± 0.04	44.3 ± 1.5
		2012.007	HiCIAO	H	10	<86	. . .	. . .	. . .	. . .	86 ± 10
		2013.095	NIRC2/N	K_S	20	<58	. . .	. . .	. . .	. . .	58.5 ± 1.1
2MASS J12383713−2703348 AB	J12383713−2703348	2012.007	HiCIAO	H	10	215 ± 14	286.4 ± 0.3	2.25 ± 0.08	8.21 ± 0.04	10.46 ± 0.08	67 ± 4
		2012.007	HiCIAO	K_S	10	220 ± 14	286.5 ± 0.5	2.28 ± 0.15	7.97 ± 0.03	10.25 ± 0.14	74 ± 5
GJ 490 Bab	J12574030+3513306	2011.229	NIRC2/N	K_S	10	171.0 ± 0.9	310.06 ± 0.02	0.061 ± 0.011	8.74 ± 0.02	8.80 ± 0.02	49.7 ± 1.0
GJ 490 Aab	J12573935+3513194	2011.229	NIRC2/N	K_{cont}	10	106.4 ± 0.9	309.54 ± 0.13	1.91 ± 0.05	8.17 ± 0.03	10.08 ± 0.05	49.92 ± 0.11
		2012.037	NIRC2/N	K	9	112.8 ± 1.6	239.8 ± 0.2	2.06 ± 0.04	8.14 ± 0.03[e]	10.20 ± 0.04[e]	54 ± 4
NLTT 34410 AB	J13323908+3059065	2011.387	NIRC2/N	K_S	14	136.5 ± 1.1	213.8 ± 0.5	0.11 ± 0.06	9.46 ± 0.04	9.57 ± 0.04	71 ± 2
2MASS J14215503-3125537 AB	J14215503−3125537	2011.229	NIRC2/N	K_S	20	70.4 ± 0.9	59.5 ± 0.2	0.10 ± 0.05	9.44 ± 0.03	9.54 ± 0.03	66 ± 3
LHS 3122 AB	J15493833+3448555	2011.469	NIRC2/N	H	5	209.1 ± 0.9	85.28 ± 0.04	1.462 ± 0.012	8.40 ± 0.03	9.86 ± 0.03	38.8 ± 0.3
2MASS J16074132−1103073 AB	J16074132−1103073	2012.387	NIRC2/N	K_S	6	739.4 ± 1.2	149.64 ± 0.07	0.014 ± 0.014	9.74 ± 0.02	9.75 ± 0.02	75 ± 15
GJ 3966 AB	J16352740+3500577	2011.469	NIRC2/N	H	8	92.2 ± 0.9	25.62 ± 0.12	0.406 ± 0.06	8.62 ± 0.03	9.02 ± 0.04	48 ± 2
GJ 3997 AB	J17155010+1900000	2012.390	NIRC2/N	K_S	10	1672.4 ± 1.0	271.39 ± 0.02	1.886 ± 0.013	6.626 ± 0.017	8.51 ± 0.02	56 ± 3
LP 447-38 AB	J17182284+1808568	2012.358	HiCIAO	H	10	411 ± 14	298.41 ± 0.12	1.182 ± 0.012	8.810 ± 0.017	9.99 ± 0.02	106 ± 6
2MASS J19560294−3207186 AB	J19560294−3207186	2012.358	HiCIAO	H	10	199 ± 14	228.4 ± 0.2	1.22 ± 0.04	8.65 ± 0.04	9.87 ± 0.05	75 ± 8
2MASS J20003177+5921289 AB	J20003177+5921289	2010.628	NIRC2/N	H	1	320.4	274.9	0.029	9.81	9.84	49
2MASS J20100002−2801410 AB	J20100002−2801410	2012.358	HiCIAO	H	10	676 ± 14	282.6 ± 0.12	0.25 ± 0.02	8.65 ± 0.05	8.90 ± 0.05	86 ± 13
NLTT 50066 AB	J20531465−0221218	2010.628	NIRC2/N	H	2	138.0 ± 0.9	327.323 ± 0.014	0.11 ± 0.05	9.41 ± 0.03	9.52 ± 0.04	40.92 ± 0.10
GJ 4185 Aab	J21160576+2951511	2011.470	NIRC2/N	H	5	54.3 ± 0.9	354.6 ± 0.4	0.37 ± 0.07	8.44 ± 0.03	8.81 ± 0.04	42.6 ± 0.5
		2011.633	NIRC2/N	H	9	49.5 ± 0.9	47.8 ± 0.8	0.34 ± 0.09	8.46 ± 0.04	8.80 ± 0.05	41.0 ± 1.3
PYC J21376+0137 AB	J21374019+0137137	2012.388	NIRC2/N	K_S	18	439.5 ± 1.4	342.6 ± 0.14	0.83 ± 0.03	8.30 ± 0.02	9.13 ± 0.03	51.0 ± 1.6
1RXS J221419.3+253411 AB	J22141765+2534066	2011.470	NIRC2/N	H	5	141.3 ± 0.8	304.09 ± 0.05	1.077 ± 0.05	9.68 ± 0.02	10.76 ± 0.04	41.7 ± 0.8
GJ 4338 Bab	J23292258+4127522	2010.628	NIRC2/N	H	3	46.7 ± 0.9	192.3 ± 0.4	0.27 ± 0.06	8.03 ± 0.04	8.30 ± 0.04	47 ± 2
		2011.470	NIRC2/N	H	4	78.2 ± 0.9	269.3 ± 0.2	0.43 ± 0.06	7.97 ± 0.04	8.40 ± 0.05	48 ± 6
GJ 4381 AB	J23574989+3837468	2011.634	NIRC2/N	H	9	537.4 ± 0.9	247.365 ± 0.016	1.469 ± 0.011	8.30 ± 0.02	9.77 ± 0.02	38.2 ± 0.4

Notes.

[a] Magnitude of the primary (m_A) decomposed from the integrated-light magnitude of the A and B components (m_{AB}) as follows: $m_A = m_{AB} + 2.5 \log(1 + 10^{-\Delta mag/2.5})$. Uncertainties are derived in a Monte Carlo fashion. Unless otherwise noted, J, H, and K_S magnitudes are from 2MASS (Skrutskie et al. 2006).

[b] Magnitude of the companion (m_B) is computed from Δmag and m_A.

[c] Y-band integrated-light magnitude is derived from the typical $Y-J$ color of dwarfs for the system spectral type from Rayner et al. (2009) and the integrated-light J-band magnitude.

[d] L'-band integrated-light magnitude is derived from the typical $K_S - L'$ color of dwarfs for the system spectral type from Golimowski et al. (2004) and the integrated-light K_S-band magnitude.

[e] Integrated-light K_S-band magnitude is converted to K_{MKO} using relations from Leggett et al. (2006).
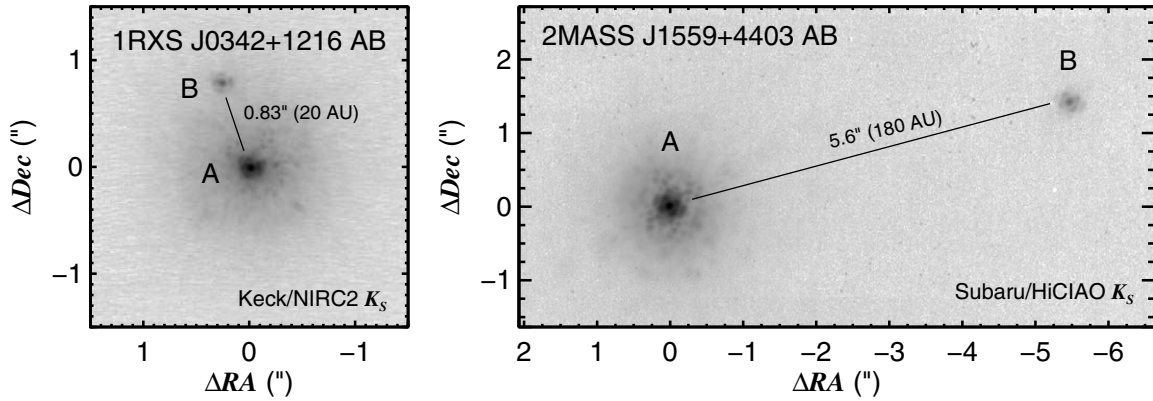
Figure 10. NIRC2 and HiCIAO images of two new brown dwarf companions identified in this survey. The inferred masses of 1RXS J034231.8+121622 B (L0 ± 1) and 2MASS J15594729+4403595 B (M8.0 ± 0.5) are 35 ± 8 M_{Jup} and 43 ± 9 M_{Jup}, respectively. North is up and east is left.
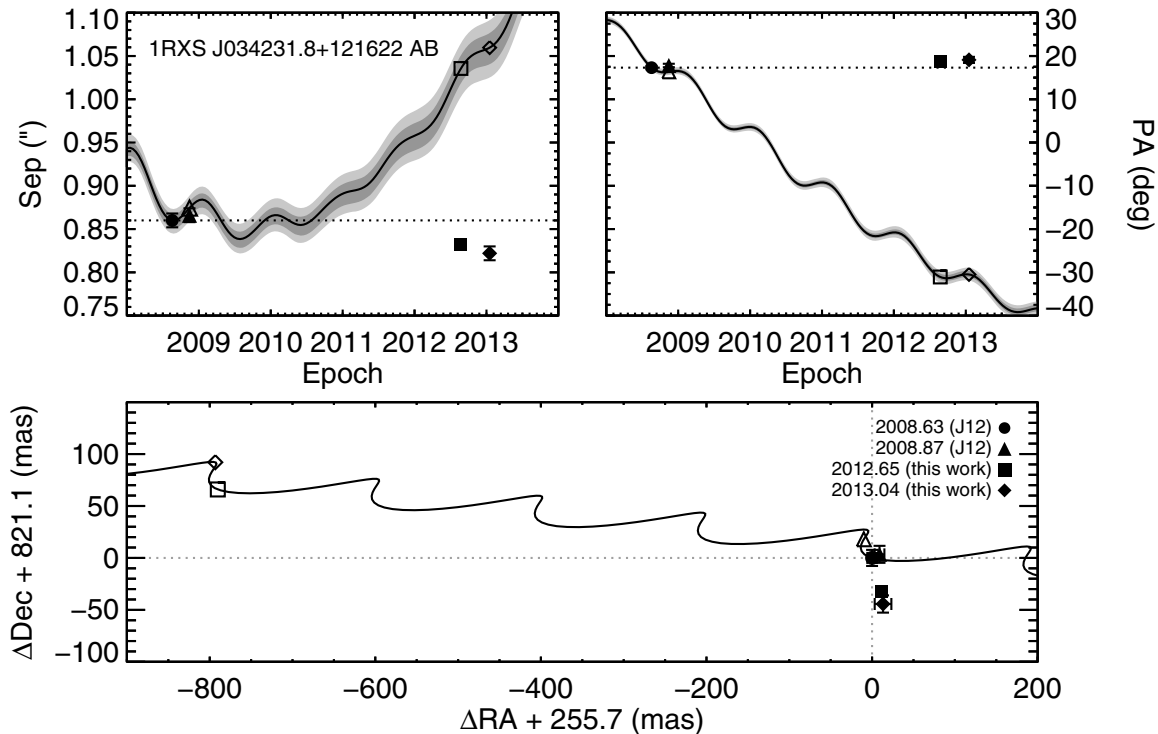
Figure 11. Test for physical association for the companion to 1RXS J034231.8+121622. The first two epochs in 2008 are from Janson et al. (2012). We confirm the companion is comoving and detect orbital motion with our AO imaging in 2012.

GALEX photometry (using Shkolnik et al. 2011 criteria), which is similar to known YMG members in $NUV-W1$ color (11.11 ± 0.04 mag; see Rodriguez et al. 2013). Malo et al. (2013) found that 2MASS J15594729+4403595 A is a likely member of the 120 Myr AB Dor YMG based on its sky position, proper motion, and high-energy emission. Assuming group membership, they find a kinematic distance of 33 ± 4 pc to the primary and predict a radial velocity of −28.9 ± 1.8 km s^{-1}.

E. L. Shkolnik et al. (in preparation) measure a radial velocity of −19.6 ± 0.6 km s^{-1} for 2MASS J15594729+4403595 as part of their follow-up efforts to kinematically associate nearby young stars with moving groups. Assuming the primary is not a single-lined spectroscopic binary, this velocity disagrees with the prediction by Malo et al. for AB Dor. In Figure 13 we show the partial kinematic constraints for distances between 20–60 pc. 2MASS J15594729+4403595 is consistent with β Pic and Carina at ∼20 pc and ∼50 pc. However, the *XYZ*

positions disagree with all moving groups so we conclude that it is probably not a member of these known groups, which prevents precise age-dating through coevality with a young cluster. Additional radial velocities will help determine whether the primary is radial velocity stable and this measurement represents the systemic radial velocity.

Janson et al. (2012) imaged the system three times between 2008 and 2009, identifying 2MASS J15594729+4403595 B at 5″.6 (187 ± 23 AU) and confirming its physical association with the primary. Their i'- and z-band contrasts imply a spectral type of ≈M8 for the companion. We imaged the system in five filters at a single epoch in 2012 with HiCIAO (Figure 10). Our astrometry listed in Table 7 are consistent with that of Janson et al. and do not show signs of orbital motion (Figure 14).

We derive a $Y-J$ color of 0.80 ± 0.05 mag for 2MASS J15594729+4403595 B in a similar fashion as for 1RXS J034231.8+121622 B. Compared to ultracool dwarfs in Rayner
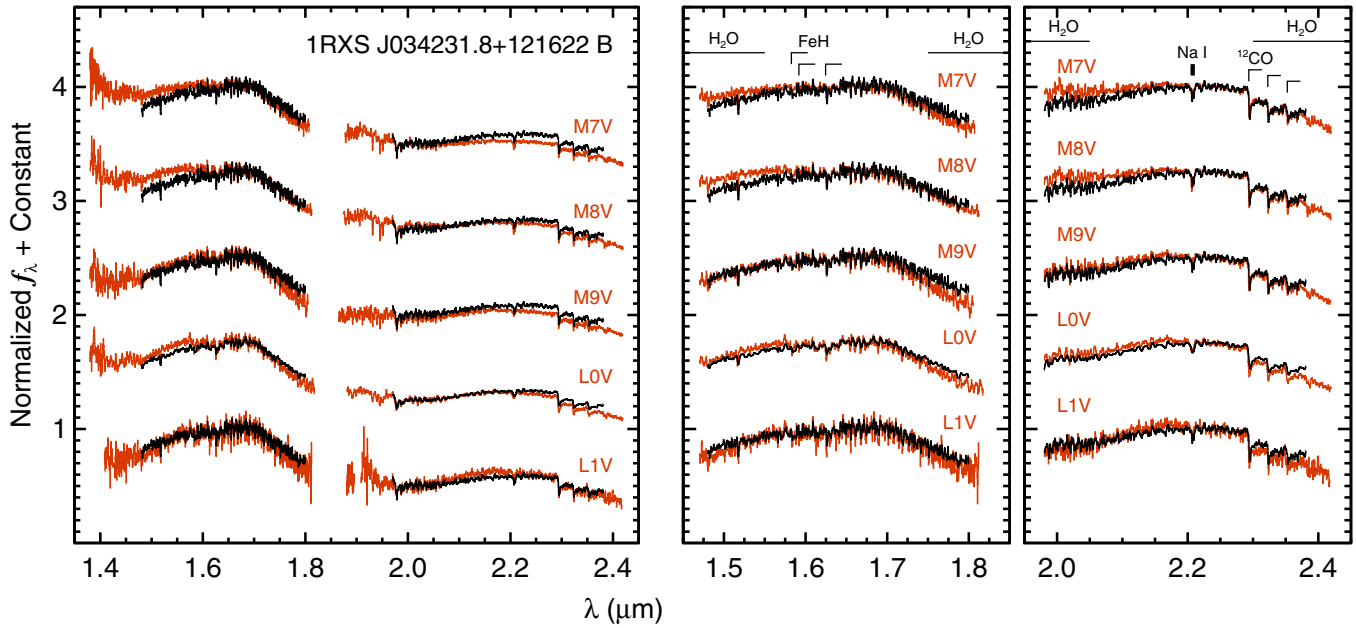
Figure 12. Our Keck/OSIRIS 1.4–2.4 μm spectrum of 1RXS J034231.8+121622 B compared to field objects from the IRTF SpeX Spectral Library. We adopt a spectral type of L0 ± 1 for 1RXS J034231.8+121622 B. M7–M9 templates are listed in Figure 7. The L0 template is 2MASS J17312974+2721233 from Allers & Liu (2013) and the L1 template is 2MASS J02081833+2542533 from Cushing et al. (2005). All spectra have been smoothed to a common resolving power of $R \approx 2000$ except for the L0 template, which has $R \approx 750$.
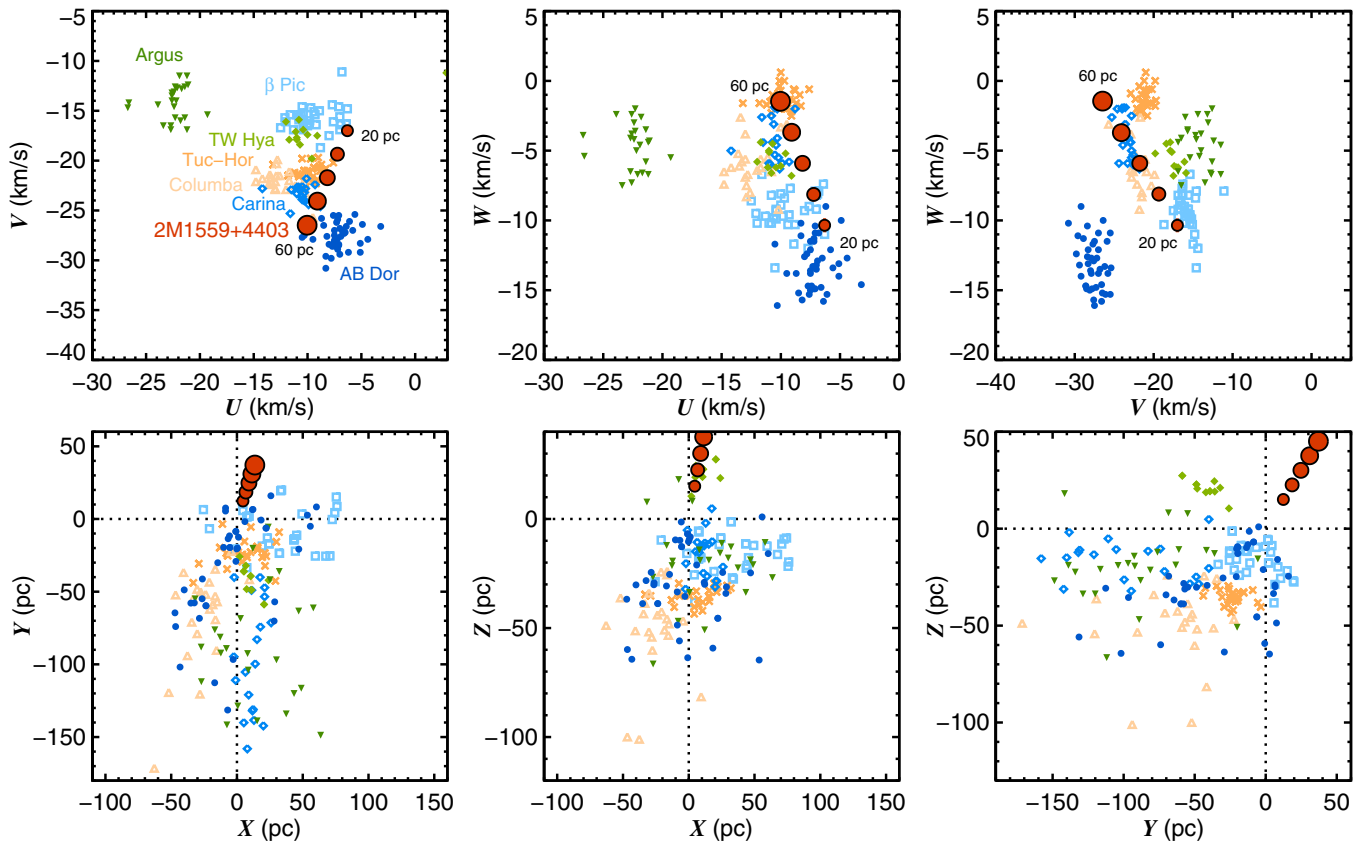
Figure 13. UVW galactic velocities and XYZ space positions of 2MASS J15594729+4403595 AB compared to nearby young moving groups from Torres et al. (2008). Although we lack a parallactic distance, the measured radial velocity to the primary enables partial kinematic constraints. 2MASS J15594729+4403595 AB is consistent with several moving groups in UVW space for distances between ∼20–50 pc, but physically appears to be tens of parsecs from these same groups. Given this physical discrepancy, we find no convincing association with a known moving group.
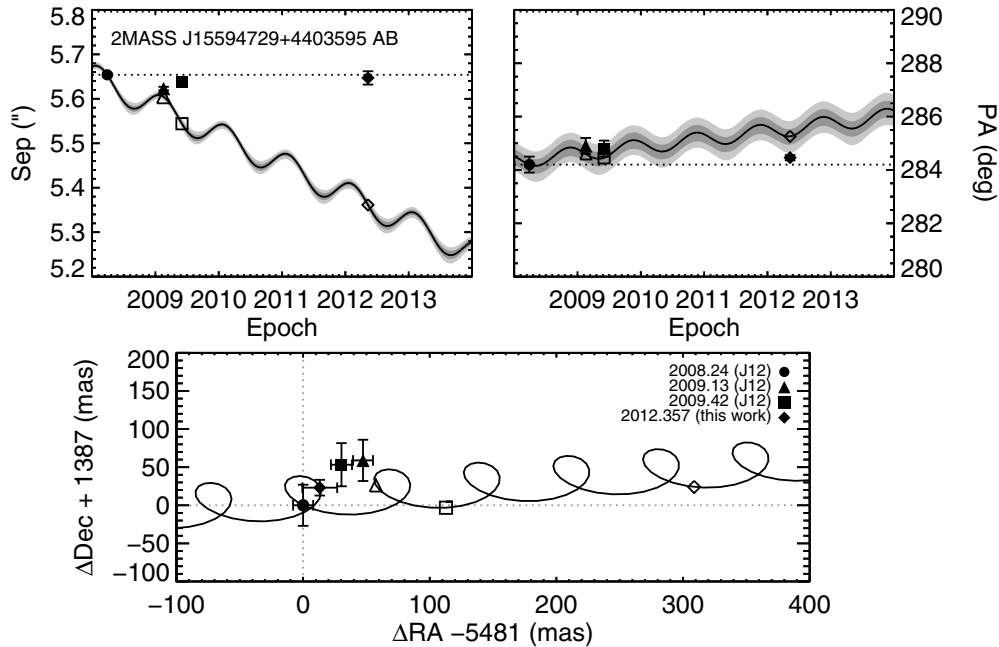
Figure 14. Relative astrometry of 2MASS J15594729+4403595 B compared to the expected background track of a stationary object (solid line). The first three epochs in 2008 and 2009 are from Janson et al. (2012). We verify the companion is unambiguously comoving from our AO imaging in 2012.
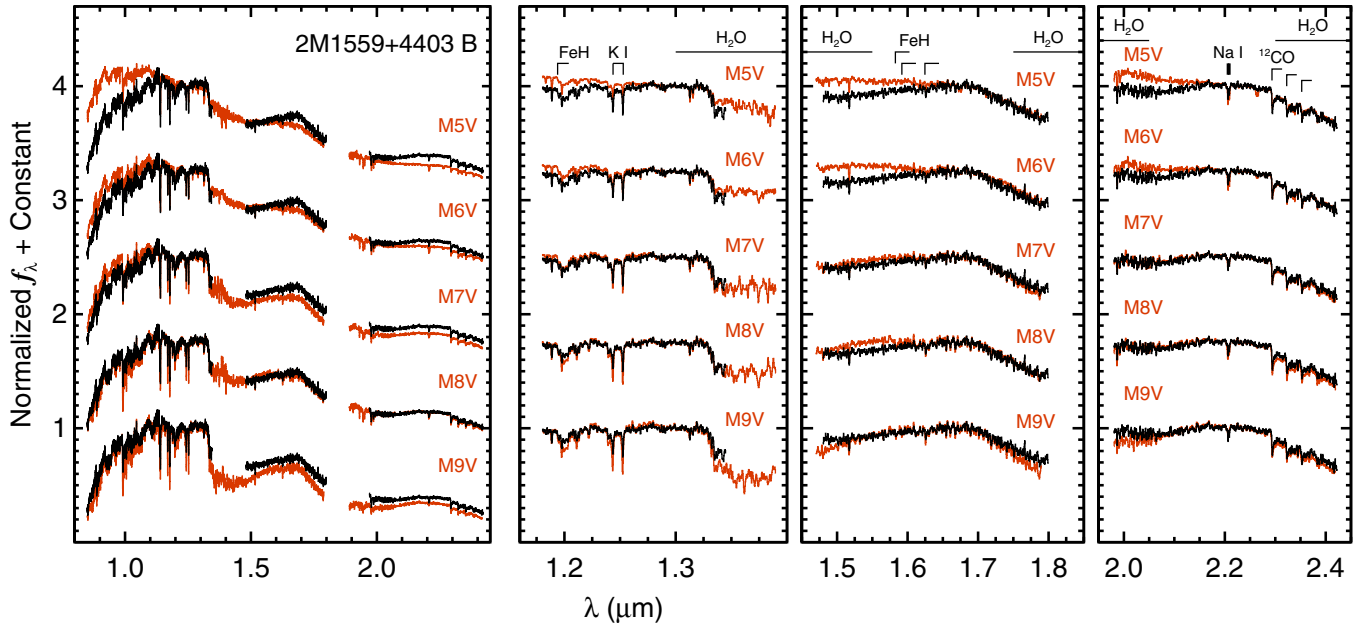
Figure 15. Our IRTF/SpeX SXD spectrum of 2MASS J15594729+4403595 B compared to field templates from the IRTF SpeX Spectral Library. 2MASS J15594729+4403595 B is a good match to the field M8 template across all bandpasses, though the H-band shape is noticeably more angular in 2MASS J15594729+4403595 B. We adopt a spectral type of M8.0 ± 0.5. The comparison objects are the same as in Figure 7. All spectra have been smoothed to a common resolving power of $R \approx 1200$.

et al. (2009), we infer a photometric spectral type of M7.5 ± 1. Our 0.8–2.45 μm IRTF/SpeX spectrum of 2MASS J15594729+4403595 B is shown in Figure 15. The best-fit spectral type across the entire spectrum is M8. M8, M7, and M7–M8 templates provide the best matches to field templates (Table 6). The gravity-insensitive index-based near-infrared classification schemes of Allers et al. (2007) and Slesnick et al. (2004) imply spectral types of M6.8 ± 0.4, M7.6 ± 1.1, and M7.6 ± 0.4. Altogether we adopt a spectral type of M8.0 ± 0.5. The shallow J-band alkali lines and angular H band are immediately clear and

point to low surface gravity, which is supported by an "INT-G" gravity classification using the indices of Allers & Liu (2013, see Table 6 and Figure 9). Indeed, 2MASS J15594729+4403595 B closely resembles the intermediate-gravity M8 object 2MASS J00192626+4614078 from Allers & Liu (2013) in Figure 8.

Although low-gravity features in young brown dwarfs are not yet fully calibrated with empirical benchmarks, Allers & Liu (2013) find that objects with intermediate-gravity spectra like 2MASS J15594729+4403595 B are most closely linked to brown dwarfs with ages between ~50–200 Myr. Lacking
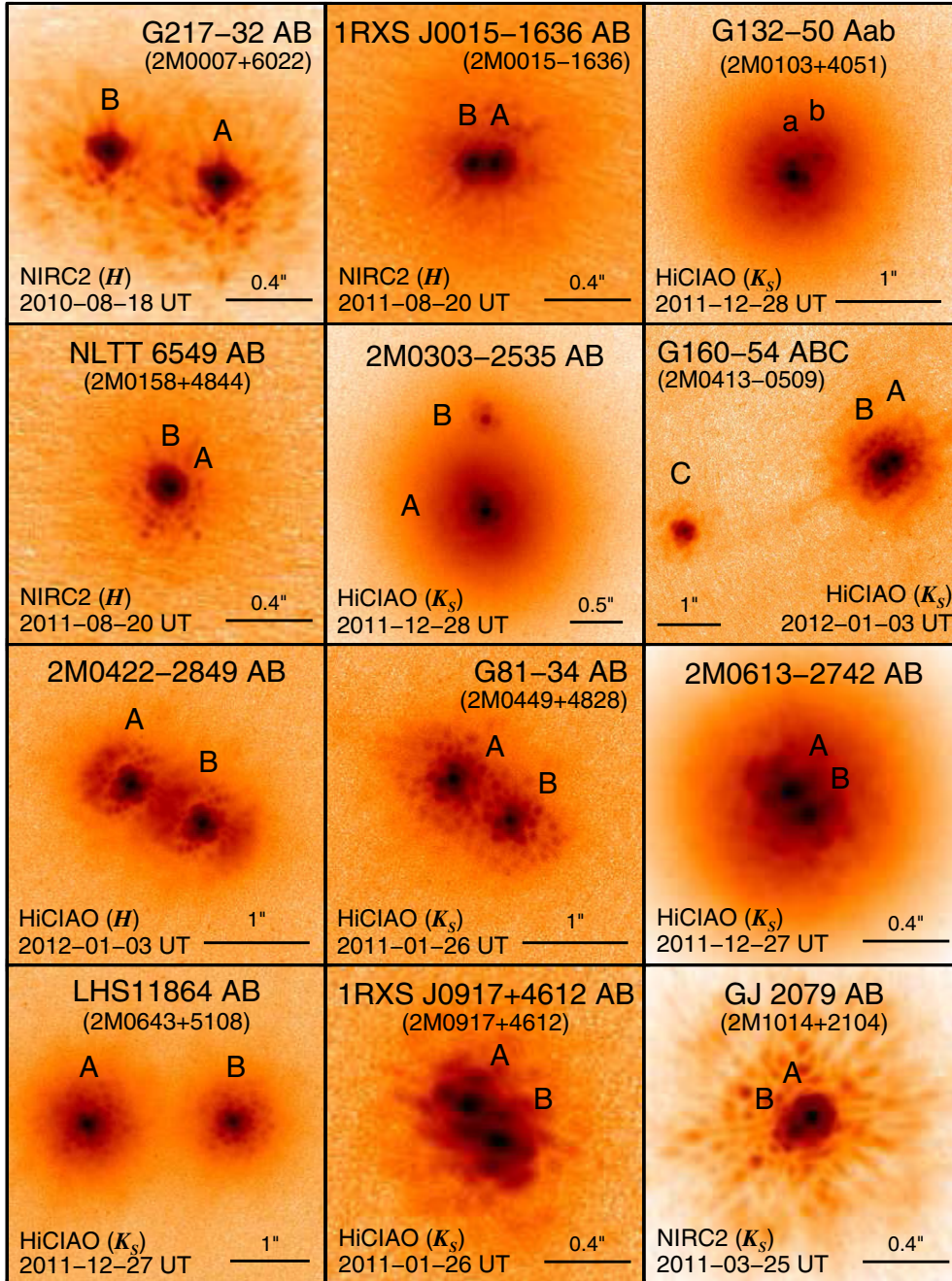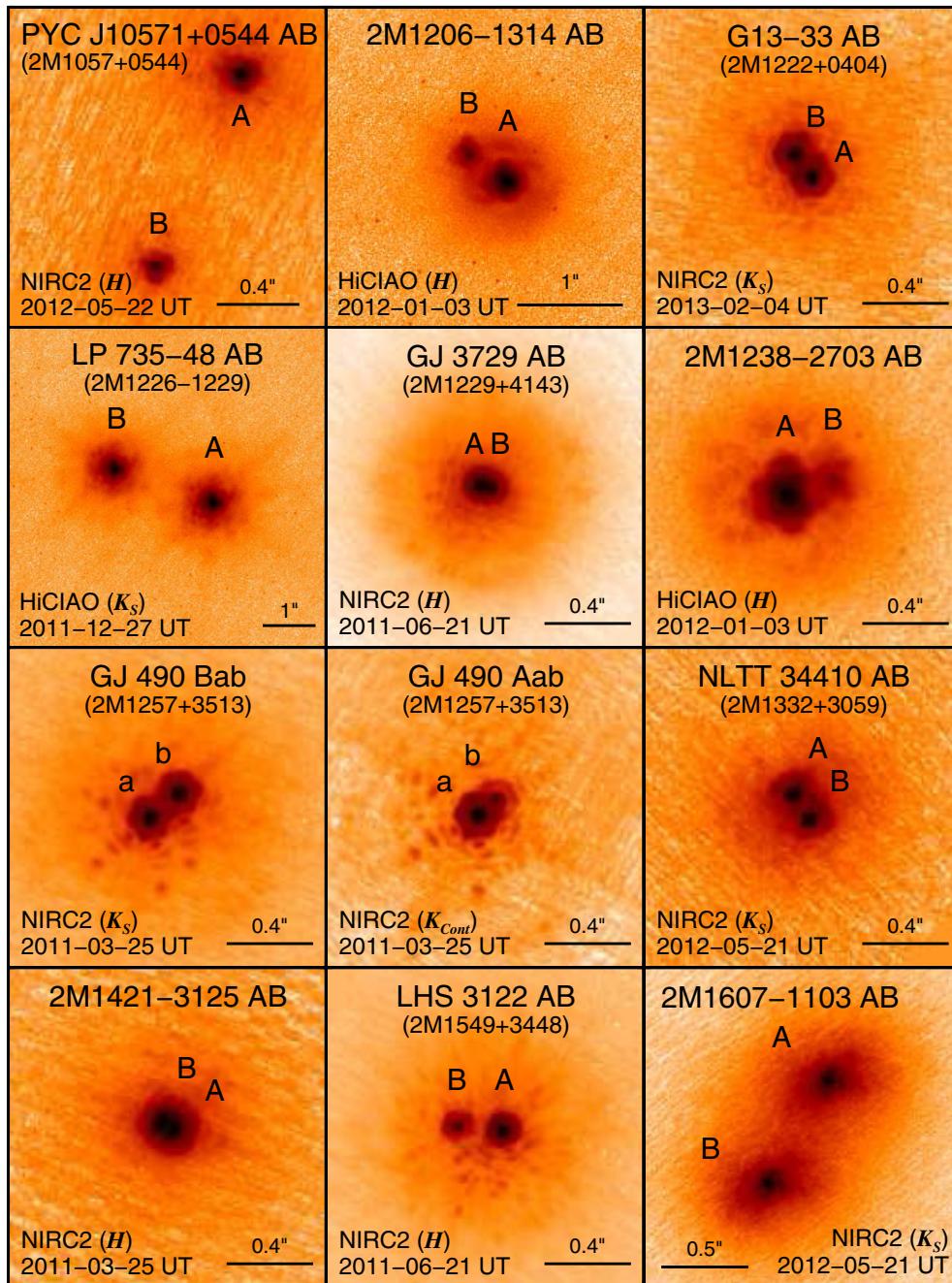
Figure 16. Binary stars detected in our survey. North is up and east is left.

a convincing association with a YMG, we adopt this spectroscopically inferred age for the system. The H-band photometric distance to the companion is 27 ± 2 pc using the absolute magnitude-spectral type relation from Dupuy & Liu (2012). An H-band bolometric correction from Liu et al. (2010b) gives a bolometric luminosity of -3.32 ± 0.07 dex which together with the system age implies a mass of $43 \pm 9 \, M_{\rm Jup}$ for 2MASS J15594729+4403595 B based on the evolutionary models of Burrows et al. (1997).

5.2. Stellar Binaries and Multiples from the PALMS Survey

Most of our targets have not been previously imaged with AO and, as expected, many were found to be close binaries (Table 7 and Figures 16–18). Altogether 43 stars in our sample have stellar companions with projected separations less than 100 AU. We resolve 38 systems into binaries with angular separations from 50 mas to several arcseconds; 17 of these are separated by <5 AU in projection, 29 are separated by <20 AU, and 37 of these are separated by <100 AU. Among these, 27 are either new or spatially resolved for the first time in this work. An additional five targets not resolved in our data were found to be close spectroscopic binaries either from the literature or from E. L. Shkolnik et al. (in preparation). One additional target not resolved in our survey, LP 449-1 AB, was identified as a 50 mas binary by Riedel et al. (2014) with *Hubble Space Telescope* (*HST*) Fine Guidance Sensor interferometry.

Figure 17. Binary stars detected in our survey (continued). North is up and east is left.

We intentionally vetted our initial target sample for previously known close binary systems which were found in heterogeneous studies. Since measuring the stellar companion mass function was not an original goal of this survey, we make no attempt to analyze the statistical properties of the multiples we uncovered. Nevertheless, we find that at least 43 out of 122 of our targets have stellar companions within 100 AU, implying a minimum companion frequency of $>35.4\% \pm 4.3\%$. This agrees well with the established close companion fraction of $33\% \pm 5\%$ (Duchêne & Kraus 2013).

Several binaries were not seen in our first epoch of deep imaging and were only resolved in follow-up observations of

wide planet candidates. These data are not incorporated into our statistical analysis so as to maintain a homogeneous sample of single stars. Note that the closest binaries with projected separations less than a few AU will yield dynamical masses on short timescales.

Seven targets in our sample form higher order hierarchical multiple systems. Five of these are triple systems (G 160-54 ABC, GJ 9652 Aab + GJ 9652 B, 2MASS J19560294–3207186 AB + TYC 7443-1102-1, GJ 4185 Aab + GJ 4186 B, GJ 4338 Bab + GJ 4337 A) and two make up quadruple systems (G 132-50 Aab + G 132-51 Bab, GJ 490 Aab+ GJ 490 Bab).
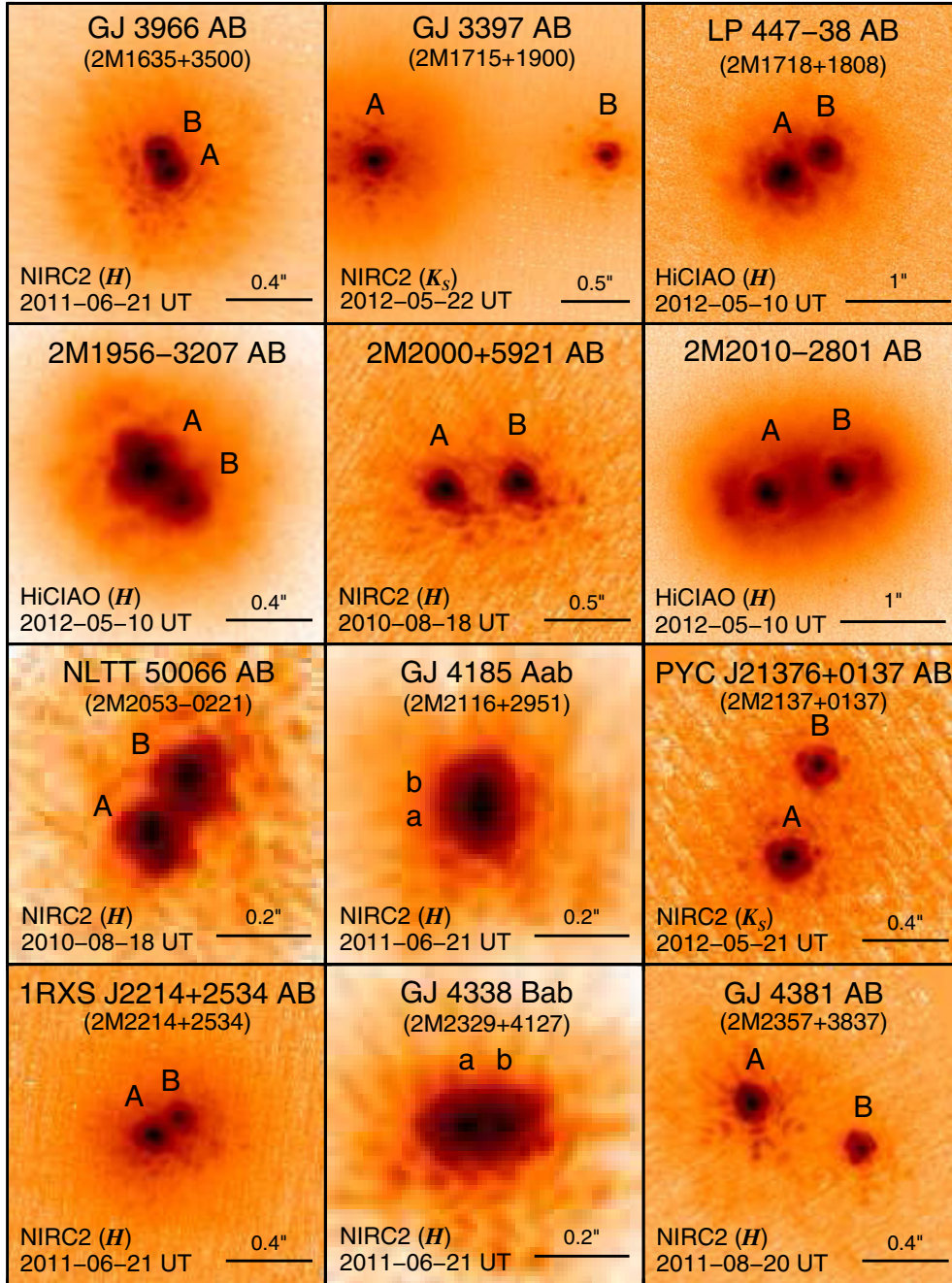
Figure 18. Binary stars detected in our survey (continued). North is up and east is left.

5.3. Candidate Planets from the PALMS Survey

Altogether 167 faint point sources were identified around 45 stars (singles and binaries) in our deep imaging (Figure 19). 42 of these candidates are in the crowded low-galactic latitude field surrounding the single-line spectroscopic binary GJ 9652 A. Astrometry and relative photometry are listed in Table 8. Background stars are distinguished from comoving gravitationally bound companions using two or more epochs of follow-up imaging, with a prioritization for those at small projected separations under 100 AU. In some cases, candidates are visible in archival wide-field imaging surveys like the Digitized Sky Survey (first and second generations), the Sloan Digital Sky Survey (Abazajian et al. 2009), and 2MASS (Skrutskie et al. 2006) and

were rejected if their astrometry and/or colors were inconsistent with cool, comoving companions. Inevitably our second-epoch observations uncovered candidates not seen in our first epoch data, but most of these reside at wide separations beyond the main region of interest (∼10–100 AU).

For candidates with multiple epochs of astrometry we calculate a reduced chi-squared value for a background scenario, $\chi^2_{\nu,BG}$, and a common proper motion scenario, $\chi^2_{\nu,CPM}$. Here

$$\chi^2_{\nu} = \frac{1}{\nu} \sum_{i=1}^{N-1} \left(\frac{(\theta_{\mathrm{meas},i} - \theta_{\mathrm{pred},i})^2}{\sigma^2_{\theta,\mathrm{meas},i} + \sigma^2_{\theta,\mathrm{pred},i}} + \frac{(\rho_{\mathrm{meas},i} - \rho_{\mathrm{pred},i})^2}{\sigma^2_{\rho,\mathrm{meas},i} + \sigma^2_{\rho,\mathrm{pred},i}} \right),$$

Table 8
Candidate Companions

Name	Cand.	UT Date (Y-M-D)	Epoch	Instrument[a]	Filt.	Contrast (mag)	Measured Position ρ ('')	Measured Position P.A. (°)	Background Position ρ ('')	Background Position P.A. (°)	Proj. Sep. (AU)	Comp.?[b]
GJ 3030 AB	CC1	2011 Dec 27	2011.9862	HiCIAO	H	9.65 ± 0.60	5.411 ± 0.020	67.58 ± 0.25	. . .	. . .	135.3	BG[d]
GJ 3030 AB	CC1	2013 Aug 17	2013.6259	NIRC2/W	K_S	. . . [c]	5.139 ± 0.074	65.59 ± 0.20	5.029 ± 0.041	65.56 ± 0.36	128.5	BG
GJ 3030 AB	CC2	2011 Dec 27	2011.9862	HiCIAO	H	7.88 ± 0.59	5.785 ± 0.021	1.01 ± 0.24	. . .	. . .	144.6	BG[d]
GJ 3030 AB	CC2	2013 Aug 17	2013.6259	NIRC2/W	K_S	. . . [c]	5.894 ± 0.074	357.88 ± 0.20	5.810 ± 0.033	356.82 ± 0.39	147.4	BG
NLTT 1875	CC1	2010 Aug 18	2010.6283	NIRC2/N	H	8.57 ± 0.16	5.588 ± 0.003	339.65 ± 0.20	. . .	. . .	214.0	. . .
NLTT 1875	CC1	2011 Aug 20	2011.6339	NIRC2/N	H	8.78 ± 0.16	5.687 ± 0.003	337.35 ± 0.20	5.673 ± 0.004	337.52 ± 0.19	217.8	BG
NLTT 1875	CC2	2010 Aug 18	2010.6283	NIRC2/N	H	9.69 ± 0.16	3.562 ± 0.003	331.45 ± 0.20	. . .	. . .	136.4	. . .
NLTT 1875	CC2	2011 Aug 20	2011.6339	NIRC2/N	H	10.05 ± 0.21	3.690 ± 0.003	328.32 ± 0.20	3.677 ± 0.004	328.40 ± 0.20	141.3	BG
NLTT 1875	CC3	2010 Aug 18	2010.6283	NIRC2/N	H	11.51 ± 0.30	5.096 ± 0.003	249.85 ± 0.20	. . .	. . .	195.2	. . .
NLTT 1875	CC3	2011 Aug 20	2011.6339	NIRC2/N	H	11.75 ± 0.92	5.312 ± 0.003	250.68 ± 0.20	5.306 ± 0.004	250.72 ± 0.20	203.4	BG
NLTT 1875	CC4	2010 Aug 18	2010.6283	NIRC2/N	H	8.59 ± 0.16	2.612 ± 0.003	210.23 ± 0.20	. . .	. . .	100.0	. . .
NLTT 1875	CC4	2011 Aug 20	2011.6339	NIRC2/N	H	8.53 ± 0.16	2.718 ± 0.003	214.37 ± 0.20	2.729 ± 0.004	214.33 ± 0.19	104.1	BG
NLTT 1875	CC5	2010 Aug 18	2010.6283	NIRC2/N	H	9.24 ± 0.16	3.839 ± 0.003	191.60 ± 0.20	. . .	. . .	147.0	. . .
NLTT 1875	CC5	2011 Aug 20	2011.6339	NIRC2/N	H	9.45 ± 0.17	3.874 ± 0.003	194.74 ± 0.20	3.887 ± 0.004	194.84 ± 0.19	148.4	BG
NLTT 1875	CC6	2010 Aug 18	2010.6283	NIRC2/N	H	10.25 ± 0.17	5.939 ± 0.003	169.58 ± 0.20	. . .	. . .	227.5	. . .
NLTT 1875	CC6	2011 Aug 20	2011.6339	NIRC2/N	H	10.32 ± 0.26	5.884 ± 0.003	171.54 ± 0.20	5.899 ± 0.004	171.72 ± 0.20	225.3	BG
G 132-50 Aab	CC1	2011 Dec 28	2011.9889	HiCIAO	K_S	8.96 ± 0.54	11.897 ± 0.042	335.01 ± 0.17	. . .	. . .	355.7	BG[d]
G 172-56	CC1	2010 Aug 17	2010.6257	NIRC2/N	H	12.67 ± 0.84	4.534 ± 0.003	33.54 ± 0.20	. . .	. . .	81.6	SE
G 172-56	CC2	2010 Aug 17	2010.6257	NIRC2/N	H	12.15 ± 0.60	5.061 ± 0.003	143.38 ± 0.20	. . .	. . .	91.1	BG[e]
G 172-56	CC3	2010 Aug 17	2010.6257	NIRC2/N	H	11.28 ± 0.35	6.590 ± 0.003	160.71 ± 0.20	. . .	. . .	118.6	SE
G 271-110	CC1	2010 Aug 18	2010.6284	NIRC2/N	H	13.82 ± 0.98	6.662 ± 0.003	23.18 ± 0.20	. . .	. . .	159.9	SE
NLTT 6549 AB	CC1	2011 Aug 20	2011.6342	NIRC2/N	H	15.09 ± 0.91	3.803 ± 0.003	222.87 ± 0.20	. . .	. . .	167.3	SE
GJ 3136	CC1	2011 Jan 27	2011.0718	HiCIAO	K_S	6.90 ± 0.20	9.846 ± 0.036	302.19 ± 0.18	. . .	. . .	147.7	BG[d]
1RXS J022735.8+471021	CC1	2010 Aug 17	2010.6256	NIRC2/N	H	13.38 ± 0.76	3.244 ± 0.003	233.25 ± 0.20	. . .	. . .	88.9	SE
1RXS J022735.8+471021	CC2	2013 Feb 4	2013.0938	NIRC2/N	H	10.50 ± 0.23	4.779 ± 0.003	163.80 ± 0.20	. . .	. . .	130.9	SE
1RXS J022735.8+471021	CC3	2013 Feb 4	2013.0938	NIRC2/N	H	9.12 ± 0.19	5.660 ± 0.003	155.87 ± 0.20	. . .	. . .	155.1	SE
1RXS J023138.7+445640	CC1	2010 Aug 18	2010.6285	NIRC2/N	H	8.57 ± 0.16	7.438 ± 0.003	269.99 ± 0.20	. . .	. . .	119.0	SE
G 75-35	CC1	2012 Jan 3	2012.0062	HiCIAO	H	10.77 ± 0.45	11.762 ± 0.024	255.20 ± 0.17	. . .	. . .	188.2	BG[d]
LP 247-13	CC1	2011 Jan 26	2011.0692	HiCIAO	K_S	11.09 ± 1.17	1.799 ± 0.020	341.64 ± 0.63	. . .	. . .	61.9	. . .
LP 247-13	CC1	2011 Aug 20	2011.6340	NIRC2/N	H	10.92 ± 0.21	1.894 ± 0.003	338.21 ± 0.20	1.900 ± 0.021	337.11 ± 0.62	65.1	BG
LP 247-13	CC1	2011 Aug 20	2011.6340	NIRC2/N	K_S	13.13 ± 0.85	1.903 ± 0.003	338.20 ± 0.20	1.900 ± 0.021	337.11 ± 0.62	65.4	BG
LP 247-13	CC1	2012 Jan 14	2012.0365	NIRC2/N	H	11.27 ± 0.17	1.941 ± 0.003	337.87 ± 0.20	1.957 ± 0.022	336.80 ± 0.63	66.8	BG
LP 247-13	CC1	2012 Jan 14	2012.0365	NIRC2/N	K	11.15 ± 0.15	1.956 ± 0.003	338.17 ± 0.20	1.957 ± 0.022	336.80 ± 0.63	67.3	BG
LP 247-13	CC2	2011 Jan 26	2011.0692	HiCIAO	K_S	11.12 ± 1.16	6.692 ± 0.028	317.87 ± 0.22	. . .	. . .	230.2	SE
GJ 3287	CC1	2013 Feb 4	2013.0939	NIRC2/N	K_S	9.29 ± 0.22	4.239 ± 0.003	184.13 ± 0.20	. . .	. . .	95.4	SE
NLTT13844	CC1	2012 Oct 8	2012.7710	NIRC2/N	H	10.24 ± 0.22	3.870 ± 0.003	353.14 ± 0.20	. . .	. . .	81.3	. . .
NLTT13844	CC1	2013 Jan 17	2013.0448	NIRC2/N	K	9.70 ± 0.32	4.060 ± 0.003	353.01 ± 0.20	4.053 ± 0.004	352.97 ± 0.19	85.3	BG
NLTT13844	CC2	2012 Oct 8	2012.7710	NIRC2/N	H	10.74 ± 0.31	2.832 ± 0.003	165.37 ± 0.20	. . .	. . .	59.5	. . .
NLTT13844	CC2	2013 Jan 17	2013.0448	NIRC2/N	K	10.20 ± 0.64	2.647 ± 0.003	165.03 ± 0.20	2.649 ± 0.004	165.10 ± 0.23	55.6	BG
1RXS J045101.0+312734	CC1	2011 Jan 27	2011.0721	HiCIAO	K_S	4.93 ± 0.26	10.410 ± 0.038	282.58 ± 0.18	. . .	. . .	135.3	. . .
1RXS J045101.0+312734	CC1	2011 Dec 28	2011.9894	HiCIAO	K_S	5.81 ± 0.41	10.615 ± 0.038	282.66 ± 0.18	10.623 ± 0.041	282.48 ± 0.18	138.0	BG
1RXS J045101.0+312734	CC1	2012 Jan 3	2012.0068	HiCIAO	K_S	5.24 ± 0.06	10.623 ± 0.038	282.55 ± 0.18	10.618 ± 0.040	282.50 ± 0.18	138.1	BG
1RXS J045101.0+312734	CC2	2011 Jan 27	2011.0721	HiCIAO	K_S	10.20 ± 0.78	9.393 ± 0.035	281.59 ± 0.18	. . .	. . .	122.1	. . .
1RXS J045101.0+312734	CC2	2012 Jan 3	2012.0068	HiCIAO	K_S	10.28 ± 1.08	9.622 ± 0.036	281.59 ± 0.18	9.603 ± 0.037	281.52 ± 0.19	125.1	BG

Table 8
(Continued)

Name	Cand.	UT Date (Y-M-D)	Epoch	Instrument[a]	Filt.	Contrast (mag)	Measured Position ρ ('')	Measured Position P.A. (°)	Background Position ρ ('')	Background Position P.A. (°)	Proj. Sep. (AU)	Comp.?[b]
1RXS J055446.0+105559	CC1	2013 Feb 4	2013.0940	NIRC2/N	K_S	14.38 ± 0.92	3.770 ± 0.003	34.37 ± 0.20	. . .	. . .	95.8	SE
1RXS J055446.0+105559	CC2	2013 Feb 4	2013.0940	NIRC2/N	K_S	14.04 ± 1.07	6.443 ± 0.003	107.95 ± 0.20	. . .	. . .	163.7	SE
1RXS J055446.0+105559	CC3	2013 Feb 4	2013.0940	NIRC2/N	K_S	11.86 ± 0.15	4.920 ± 0.003	148.42 ± 0.20	. . .	. . .	125.0	SE
1RXS J055446.0+105559	CC4	2013 Feb 4	2013.0940	NIRC2/N	K_S	11.65 ± 0.14	4.991 ± 0.003	171.31 ± 0.20	. . .	. . .	126.8	SE
1RXS J055446.0+105559	CC5	2013 Feb 4	2013.0940	NIRC2/N	K_S	11.48 ± 0.15	6.469 ± 0.003	191.22 ± 0.20	. . .	. . .	164.3	SE
AP Col	CC1	2011 Dec 27	2011.9867	HiCIAO	K_S	11.16 ± 1.16	6.899 ± 0.029	141.80 ± 0.21	. . .	. . .	57.9	. . .
AP Col	CC1	2012 Jan 3	2012.0065	HiCIAO	H	11.30 ± 0.10	6.853 ± 0.021	142.10 ± 0.22	6.914 ± 0.028	141.75 ± 0.21	57.5	. . .
AP Col	CC1	2012 Oct 8	2012.7711	NIRC2/W	H	. . . [c]	7.040 ± 0.074	145.09 ± 0.20	7.089 ± 0.030	144.38 ± 0.22	59.1	BG
AP Col	CC2	2012 Oct 8	2012.7711	NIRC2/W	H	. . . [c]	16.649 ± 0.076	171.49 ± 0.20	. . .	. . .	139.7	SE
AP Col	CC3	2012 Oct 8	2012.7711	NIRC2/W	H	. . . [c]	18.780 ± 0.076	115.67 ± 0.20	. . .	. . .	157.6	SE
GJ 3395	CC1	2011 Jan 26	2011.0695	HiCIAO	K_S	10.12 ± 0.61	11.833 ± 0.042	203.89 ± 0.17	. . .	. . .	331.3	BG[d]
G 108-36	CC1	2011 Jan 27	2011.0719	HiCIAO	K_S	9.73 ± 0.52	7.962 ± 0.031	0.56 ± 0.20	. . .	. . .	176.8	. . .
G 108-36	CC1	2012 Jan 3	2012.0066	HiCIAO	K_S	9.51 ± 0.35	8.017 ± 0.032	1.84 ± 0.20	8.009 ± 0.033	1.86 ± 0.21	178.0	BG
G 108-36	CC2	2011 Jan 27	2011.0719	HiCIAO	K_S	9.47 ± 0.40	8.246 ± 0.032	359.33 ± 0.20	. . .	. . .	183.1	. . .
G 108-36	CC2	2012 Jan 3	2012.0066	HiCIAO	K_S	9.20 ± 0.25	8.301 ± 0.032	0.62 ± 0.19	8.292 ± 0.034	0.58 ± 0.20	184.3	BG
G 108-36	CC3	2011 Jan 27	2011.0719	HiCIAO	K_S	8.39 ± 0.18	5.307 ± 0.025	331.19 ± 0.25	. . .	. . .	117.8	. . .
G 108-36	CC3	2012 Jan 3	2012.0066	HiCIAO	K_S	8.16 ± 0.09	5.274 ± 0.025	333.21 ± 0.25	5.263 ± 0.028	333.15 ± 0.27	117.1	BG
G 108-36	CC4	2011 Jan 27	2011.0719	HiCIAO	K_S	10.69 ± 1.05	8.603 ± 0.033	281.31 ± 0.19	. . .	. . .	191.0	. . .
G 108-36	CC4	2012 Jan 3	2012.0066	HiCIAO	K_S	10.50 ± 0.94	8.458 ± 0.033	282.07 ± 0.19	8.438 ± 0.033	281.86 ± 0.20	187.8	BG
G 108-36	CC5	2011 Jan 27	2011.0719	HiCIAO	K_S	8.97 ± 0.28	9.317 ± 0.035	262.90 ± 0.18	. . .	. . .	206.8	BG[d]
G 108-36	CC5	2012 Jan 3	2012.0066	HiCIAO	K_S	8.83 ± 0.21	9.152 ± 0.034	263.25 ± 0.19	9.135 ± 0.035	263.06 ± 0.19	203.2	BG
G 108-36	CC6	2011 Jan 27	2011.0719	HiCIAO	K_S	9.14 ± 0.71	12.358 ± 0.043	178.39 ± 0.17	. . .	. . .	274.3	BG[d]
G 108-36	CC7	2012 Jan 3	2012.0066	HiCIAO	K_S	10.98 ± 1.13	8.376 ± 0.032	20.57 ± 0.19	. . .	. . .	185.9	SE
G 108-36	CC8	2012 Jan 3	2012.0066	HiCIAO	K_S	7.07 ± 0.07	11.346 ± 0.040	233.06 ± 0.17	. . .	. . .	251.9	SE
1RXS J073829.3+240014	CC1	2010 Nov 27	2010.9052	NIRC2/N	H	13.47 ± 0.28	5.481 ± 0.003	227.50 ± 0.20	. . .	. . .	103.6	. . .
1RXS J073829.3+240014	CC1	2013 Jan 17	2013.0448	NIRC2/N	K	13.44 ± 1.24	5.061 ± 0.003	226.11 ± 0.20	5.020 ± 0.017	226.07 ± 0.30	95.7	BG
GJ 3577 A	CC1	2013 Feb 4	2013.0944	NIRC2/N	K_S	13.59 ± 1.04	2.634 ± 0.003	311.27 ± 0.20	. . .	. . .	65.6	SE
GJ 3577 A	CC2	2013 Feb 4	2013.0944	NIRC2/N	K_S	12.22 ± 0.49	4.541 ± 0.003	34.21 ± 0.20	. . .	. . .	113.1	SE
GJ 3578 B	CC1	2013 Feb 4	2013.0942	NIRC2/N	K_S	13.57 ± 1.00	3.573 ± 0.003	129.33 ± 0.20	. . .	. . .	89.0	SE
NLTT 26359	CC1	2011 Dec 27	2011.9872	HiCIAO	K_S	11.98 ± 0.77	9.617 ± 0.036	40.93 ± 0.18	. . .	. . .	179.8	. . .
NLTT 26359	CC1	2013 May 2	2013.3323	NIRC2/W	K_S	. . . [c]	9.907 ± 0.075	42.79 ± 0.20	9.916 ± 0.037	42.57 ± 0.18	185.3	BG
NLTT 26359	CC2	2011 Dec 27	2011.9872	HiCIAO	K_S	12.39 ± 0.97	9.084 ± 0.034	107.07 ± 0.19	. . .	. . .	169.9	. . .
NLTT 26359	CC2	2013 May 2	2013.3323	NIRC2/W	K_S	. . . [c]	9.448 ± 0.075	106.32 ± 0.20	9.463 ± 0.036	106.12 ± 0.17	176.7	BG
NLTT 26359	CC3	2013 May 2	2013.3323	NIRC2/W	K_S	. . . [c]	14.789 ± 0.075	37.22 ± 0.20	. . .	. . .	276.5	SE
NLTT 26359	CC4	2013 May 2	2013.3323	NIRC2/W	K_S	. . . [c]	19.331 ± 0.076	133.89 ± 0.20	. . .	. . .	361.5	SE
NLTT 26359	CC5	2013 May 2	2013.3323	NIRC2/W	K_S	. . . [c]	12.568 ± 0.075	275.07 ± 0.20	. . .	. . .	235.0	SE
NLTT 26359	CC6	2013 May 2	2013.3323	NIRC2/W	K_S	. . . [c]	15.287 ± 0.076	344.78 ± 0.20	. . .	. . .	285.9	SE
G 13-33 AB	CC1	2011 Dec 28	2011.9901	HiCIAO	K_S	4.70 ± 0.47	6.094 ± 0.027	224.03 ± 0.23	. . .	. . .	91.4	BG[d]
G 13-33 AB	CC1	2013 Feb 4	2013.0947	NIRC2/N	K_S	. . . [c]	5.776 ± 0.003	223.06 ± 0.20	5.842 ± 0.028	222.41 ± 0.26	86.6	BG
G 13-33 AB	CC2	2012 May 21	2012.3870	NIRC2/N	K_S	12.22 ± 0.68	4.498 ± 0.003	166.19 ± 0.20	. . .	. . .	67.5	. . .
G 13-33 AB	CC2	2013 Feb 4	2013.0947	NIRC2/N	K_S	11.53 ± 0.41	4.424 ± 0.003	163.66 ± 0.20	4.433 ± 0.015	164.86 ± 0.32	66.4	BG
GJ 3729 AB	CC1	2011 Jan 26	2011.0698	HiCIAO	K_S	10.95 ± 1.06	9.384 ± 0.035	110.53 ± 0.18	. . .	. . .	159.5	BG[d]
GJ 3729 AB	CC1	2012 Jan 3	2012.0072	HiCIAO	H	10.98 ± 0.20	9.471 ± 0.022	109.32 ± 0.18	9.474 ± 0.037	108.88 ± 0.19	161.0	BG
GJ 3729 AB	CC2	2011 Jun 21	2011.4689	NIRC2/N	H	13.04 ± 0.28	1.627 ± 0.003	47.93 ± 0.20	. . .	. . .	27.7	. . .
GJ 3729 AB	CC2	2012 Jan 3	2012.0072	HiCIAO	H	12.61 ± 0.97	1.765 ± 0.020	45.68 ± 0.65	1.734 ± 0.015	44.06 ± 1.06	30.0	BG

Table 8
(Continued)

Name	Cand.	UT Date (Y-M-D)	Epoch	Instrument[a]	Filt.	Contrast (mag)	Measured Position ρ ('')	Measured Position P.A. (°)	Background Position ρ ('')	Background Position P.A. (°)	Proj. Sep. (AU)	Comp.?[b]
GJ 3729 AB	CC3	2012 Jan 3	2012.0072	HiCIAO	H	12.60 ± 0.98	9.489 ± 0.022	7.76 ± 0.18	. . .	. . .	161.3	SE
GJ 3729 AB	CC4	2012 Jan 3	2012.0072	HiCIAO	H	11.79 ± 0.80	11.195 ± 0.023	252.88 ± 0.17	. . .	. . .	190.3	SE
1RXS J124147.5+564506	CC1	2012 May 10	2012.3568	HiCIAO	K_S	10.31 ± 0.92	8.995 ± 0.034	7.56 ± 0.19	. . .	. . .	269.9	. . .
1RXS J124147.5+564506	CC1	2013 May 2	2013.3323	NIRC2/W	K_S	. . . [c]	9.042 ± 0.075	7.55 ± 0.20	8.978 ± 0.035	6.85 ± 0.19	271.3	AMB
1RXS J124147.5+564506	CC2	2013 May 2	2013.3323	NIRC2/W	K_S	. . . [c]	12.437 ± 0.075	238.98 ± 0.20	. . .	. . .	373.1	SE
1RXS J124147.5+564506	CC3	2013 May 2	2013.3323	NIRC2/W	K_S	. . . [c]	22.692 ± 0.077	240.72 ± 0.20	. . .	. . .	680.8	BG[d]
LHS 2613	CC1	2012 Jan 3	2012.0071	HiCIAO	H	9.97 ± 0.09	11.596 ± 0.024	23.13 ± 0.17	. . .	. . .	122.9	BG[d, e]
2MASS J14124864−1629561	CC1	2012 May 22	2012.3899	NIRC2/N	K_S	11.92 ± 0.39	2.774 ± 0.003	233.63 ± 0.20	. . .	. . .	74.9	. . .
2MASS J14124864−1629561	CC1	2013 May 2	2013.3324	NIRC2/N	K_S	11.87 ± 0.25	2.645 ± 0.003	233.86 ± 0.20	2.644 ± 0.004	234.08 ± 0.22	71.4	BG
2MASS J14124864−1629561	CC2	2012 May 22	2012.3899	NIRC2/N	K_S	12.41 ± 0.92	6.656 ± 0.003	147.53 ± 0.20	. . .	. . .	179.7	SE
2MASS J14124864−1629561	CC3	2013 May 2	2013.3324	NIRC2/N	K_S	13.39 ± 0.93	5.018 ± 0.003	131.30 ± 0.20	. . .	. . .	135.5	SE
G 166-49	CC1	2012 May 22	2012.3896	NIRC2/N	H	14.01 ± 0.46	2.481 ± 0.003	265.28 ± 0.20	. . .	. . .	31.0	. . .
G 166-49	CC1	2013 Feb 4	2013.0948	NIRC2/N	K_S	13.15 ± 0.43	2.326 ± 0.003	269.62 ± 0.20	2.325 ± 0.008	270.03 ± 0.26	29.1	BG
G 166-49	CC2	2012 May 22	2012.3896	NIRC2/N	H	13.50 ± 0.45	4.455 ± 0.003	226.01 ± 0.20	. . .	. . .	55.7	. . .
G 166-49	CC2	2013 Feb 4	2013.0948	NIRC2/N	K_S	12.84 ± 0.68	4.207 ± 0.003	226.38 ± 0.20	4.206 ± 0.006	226.63 ± 0.23	52.6	BG
G 166-49	CC3	2012 May 22	2012.3896	NIRC2/N	H	6.09 ± 0.31	3.809 ± 0.003	54.11 ± 0.20	. . .	. . .	47.6	BG[d]
G 166-49	CC3	2013 Feb 4	2013.0948	NIRC2/N	K_S	. . . [c]	4.035 ± 0.003	52.93 ± 0.20	4.049 ± 0.007	52.96 ± 0.22	50.4	BG
2MASS J15323737+4653048	CC1	2012 May 22	2012.3901	NIRC2/N	K_S	13.16 ± 0.99	2.658 ± 0.003	208.35 ± 0.20	. . .	. . .	87.7	. . .
2MASS J15323737+4653048	CC1	2013 Aug 17	2013.6249	NIRC2/N	K_S	13.06 ± 0.23	2.515 ± 0.003	205.17 ± 0.20	2.547 ± 0.015	205.23 ± 0.25	83.0	BG
G 202-48	CC1	2011 Jun 21	2011.4691	NIRC2/N	H	15.91 ± 0.89	5.426 ± 0.003	201.15 ± 0.20	. . .	. . .	35.4	SE
GJ 3966 AB	CC1	2011 Jun 21	2011.4692	NIRC2/N	H	12.19 ± 0.23	2.246 ± 0.003	202.44 ± 0.20	. . .	. . .	36.4	. . .
GJ 3966 AB	CC1	2012 Apr 12	2012.2810	NIRC2/N	H	12.04 ± 1.22	2.235 ± 0.003	207.39 ± 0.20	2.201 ± 0.007	208.15 ± 0.28	36.2	BG
GJ 669 A	CC1	2012 May 10	2012.3574	HiCIAO	H	13.62 ± 0.76	3.694 ± 0.020	297.88 ± 0.33	. . .	. . .	43.2	. . .
GJ 669 A	CC1	2013 May 2	2013.3329	NIRC2/W	K_S	. . . [c]	3.233 ± 0.074	293.43 ± 0.20	3.370 ± 0.020	294.29 ± 0.36	37.8	BG
GJ 669 A	CC2	2012 May 10	2012.3574	HiCIAO	H	13.64 ± 0.79	8.801 ± 0.022	22.80 ± 0.19	. . .	. . .	103.0	. . .
GJ 669 A	CC2	2013 May 2	2013.3329	NIRC2/W	K_S	. . . [c]	8.584 ± 0.075	25.28 ± 0.20	8.568 ± 0.023	24.88 ± 0.20	100.4	BG
GJ 669 A	CC3	2012 May 10	2012.3574	HiCIAO	H	9.10 ± 0.08	10.380 ± 0.023	156.61 ± 0.18	. . .	. . .	121.4	. . .
GJ 669 A	CC3	2013 May 2	2013.3329	NIRC2/W	K_S	. . . [c]	10.753 ± 0.075	157.09 ± 0.20	10.769 ± 0.023	156.39 ± 0.17	125.8	BG
GJ 669 A	CC4	2012 May 10	2012.3574	HiCIAO	H	9.68 ± 0.08	10.538 ± 0.023	160.77 ± 0.18	. . .	. . .	123.3	. . .
GJ 669 A	CC4	2013 May 2	2013.3329	NIRC2/W	K_S	. . . [c]	10.916 ± 0.075	161.16 ± 0.20	10.924 ± 0.022	160.39 ± 0.17	127.7	BG
GJ 669 A	CC5	2012 May 10	2012.3574	HiCIAO	H	12.99 ± 0.41	8.960 ± 0.022	200.63 ± 0.19	. . .	. . .	104.8	. . .
GJ 669 A	CC5	2013 May 2	2013.3329	NIRC2/W	K_S	. . . [c]	9.270 ± 0.075	199.43 ± 0.20	9.215 ± 0.023	198.76 ± 0.19	108.5	BG
GJ 669 A	CC6	2013 May 2	2013.3329	NIRC2/W	K_S	. . . [c]	11.173 ± 0.075	91.22 ± 0.20	. . .	. . .	130.7	SE
LHS 3321	CC1	2011 Jun 21	2011.4692	NIRC2/N	H	13.58 ± 0.18	2.615 ± 0.003	279.74 ± 0.20	. . .	. . .	24.8	. . .
LHS 3321	CC1	2012 May 10	2012.3572	HiCIAO	H	13.06 ± 0.27	2.812 ± 0.020	289.50 ± 0.42	2.835 ± 0.008	290.63 ± 0.23	26.7	BG
LHS 3321	CC2	2012 May 10	2012.3572	HiCIAO	H	12.12 ± 0.11	9.222 ± 0.022	314.35 ± 0.19	. . .	. . .	87.4	SE
LP 390-16	CC1	2011 Mar 25	2011.2289	NIRC2/N	K_S	7.35 ± 0.36	4.086 ± 0.003	262.30 ± 0.20	. . .	. . .	70.3	BG[d]
GJ 9652 A	CC1	2011 Aug 20	2011.6334	NIRC2/N	H	. . . [c]	2.770 ± 0.003	341.09 ± 0.20	. . .	. . .	52.9	BG[d]
GJ 9652 A	CC1	2012 Aug 23	2012.6442	NIRC2/N	H	. . . [c]	2.201 ± 0.003	353.00 ± 0.20	2.199 ± 0.009	352.92 ± 0.33	42.0	BG
GJ 9652 A	CC2	2011 Aug 20	2011.6334	NIRC2/N	H	. . . [c]	2.844 ± 0.003	10.26 ± 0.20	. . .	. . .	54.3	. . .
GJ 9652 A	CC2	2012 Aug 23	2012.6442	NIRC2/N	H	. . . [c]	2.619 ± 0.003	25.62 ± 0.20	2.619 ± 0.009	25.64 ± 0.28	50.0	BG
GJ 9652 A	CC3	2011 Aug 20	2011.6334	NIRC2/N	H	12.45 ± 0.99	3.302 ± 0.003	44.01 ± 0.20	. . .	. . .	63.1	. . .
GJ 9652 A	CC3	2012 Aug 23	2012.6442	NIRC2/N	H	12.77 ± 0.20	3.503 ± 0.003	56.39 ± 0.20	3.504 ± 0.009	56.44 ± 0.23	66.9	BG
GJ 9652 A	CC4	2011 Aug 20	2011.6334	NIRC2/N	H	13.60 ± 1.26	4.048 ± 0.003	52.10 ± 0.20	. . .	. . .	77.3	. . .
GJ 9652 A	CC4	2012 Aug 23	2012.6442	NIRC2/N	H	13.80 ± 1.17	4.327 ± 0.003	61.63 ± 0.20	4.335 ± 0.009	61.80 ± 0.22	82.6	BG

Table 8
(Continued)

Name	Cand.	UT Date (Y-M-D)	Epoch	Instrument[a]	Filt.	Contrast (mag)	Measured Position		Background Position		Proj. Sep. (AU)	Comp.?[b]
							ρ ($''$)	P.A. ($°$)	ρ ($''$)	P.A. ($°$)		
GJ 9652 A	CC5	2011 Aug 20	2011.6334	NIRC2/N	H	12.87 ± 1.14	3.290 ± 0.003	61.39 ± 0.20	. . .	. . .	62.8	. . .
GJ 9652 A	CC5	2012 Aug 23	2012.6442	NIRC2/N	H	14.12 ± 0.97	3.690 ± 0.003	71.99 ± 0.20	3.694 ± 0.009	72.06 ± 0.22	70.5	BG
GJ 9652 A	CC6	2011 Aug 20	2011.6334	NIRC2/N	H	13.68 ± 1.26	4.122 ± 0.003	64.75 ± 0.20	. . .	. . .	78.7	. . .
GJ 9652 A	CC6	2012 Aug 23	2012.6442	NIRC2/N	H	14.49 ± 1.19	4.553 ± 0.003	73.13 ± 0.20	4.550 ± 0.009	73.12 ± 0.21	87.0	BG
GJ 9652 A	CC7	2011 Aug 20	2011.6334	NIRC2/N	H	14.07 ± 1.22	5.043 ± 0.003	60.39 ± 0.20	. . .	. . .	96.3	. . .
GJ 9652 A	CC7	2012 Aug 23	2012.6442	NIRC2/N	H	13.61 ± 0.73	5.420 ± 0.003	67.35 ± 0.20	5.416 ± 0.009	67.71 ± 0.20	103.5	BG
GJ 9652 A	CC8	2011 Aug 20	2011.6334	NIRC2/N	H	14.92 ± 1.33	4.975 ± 0.003	63.07 ± 0.20	. . .	. . .	95.0	SE
GJ 9652 A	CC9	2011 Aug 20	2011.6334	NIRC2/N	H	12.27 ± 0.32	6.776 ± 0.003	48.88 ± 0.20	. . .	. . .	129.4	SE
GJ 9652 A	CC10	2011 Aug 20	2011.6334	NIRC2/N	H	7.64 ± 0.28	6.923 ± 0.003	51.68 ± 0.20	. . .	. . .	132.2	BG[d]
GJ 9652 A	CC10	2012 Aug 23	2012.6442	NIRC2/N	H	7.67 ± 0.17	7.177 ± 0.003	57.19 ± 0.20	7.180 ± 0.009	57.53 ± 0.21	137.1	BG
GJ 9652 A	CC11	2011 Aug 20	2011.6334	NIRC2/N	H	11.64 ± 0.39	4.283 ± 0.003	90.74 ± 0.20	. . .	. . .	81.8	SE
GJ 9652 A	CC12	2011 Aug 20	2011.6334	NIRC2/N	H	13.37 ± 1.14	4.650 ± 0.003	87.70 ± 0.20	. . .	. . .	88.8	SE
GJ 9652 A	CC13	2011 Aug 20	2011.6334	NIRC2/N	H	12.32 ± 1.13	2.566 ± 0.003	95.62 ± 0.20	. . .	. . .	49.0	. . .
GJ 9652 A	CC13	2012 Aug 23	2012.6442	NIRC2/N	H	13.91 ± 0.32	3.255 ± 0.003	102.11 ± 0.20	3.254 ± 0.009	102.24 ± 0.21	62.2	BG
GJ 9652 A	CC14	2011 Aug 20	2011.6334	NIRC2/N	H	13.91 ± 1.06	5.873 ± 0.003	128.27 ± 0.20	. . .	. . .	112.2	SE
GJ 9652 A	CC15	2011 Aug 20	2011.6334	NIRC2/N	H	14.30 ± 1.12	6.833 ± 0.003	134.76 ± 0.20	. . .	. . .	130.5	SE
GJ 9652 A	CC16	2011 Aug 20	2011.6334	NIRC2/N	H	10.86 ± 0.28	7.759 ± 0.003	134.48 ± 0.20	. . .	. . .	148.2	SE
GJ 9652 A	CC17	2011 Aug 20	2011.6334	NIRC2/N	H	14.32 ± 1.34	4.752 ± 0.003	175.02 ± 0.20	. . .	. . .	90.8	SE
GJ 9652 A	CC18	2011 Aug 20	2011.6334	NIRC2/N	H	11.64 ± 1.19	1.766 ± 0.003	167.88 ± 0.20	. . .	. . .	33.7	. . .
GJ 9652 A	CC18	2012 Aug 23	2012.6442	NIRC2/N	H	12.59 ± 0.20	2.384 ± 0.003	155.25 ± 0.20	2.383 ± 0.009	155.26 ± 0.24	45.5	BG
GJ 9652 A	CC19	2011 Aug 20	2011.6334	NIRC2/N	H	10.63 ± 0.76	1.770 ± 0.003	174.79 ± 0.20	. . .	. . .	33.8	. . .
GJ 9652 A	CC19	2012 Aug 23	2012.6442	NIRC2/N	H	10.74 ± 0.17	2.332 ± 0.003	160.20 ± 0.20	2.337 ± 0.009	160.30 ± 0.24	44.5	BG
GJ 9652 A	CC20	2011 Aug 20	2011.6334	NIRC2/N	H	11.62 ± 0.59	3.108 ± 0.003	255.69 ± 0.20	. . .	. . .	59.4	. . .
GJ 9652 A	CC20	2012 Aug 23	2012.6442	NIRC2/N	H	11.43 ± 0.17	2.674 ± 0.003	243.29 ± 0.20	2.673 ± 0.009	243.17 ± 0.29	51.1	BG
GJ 9652 A	CC21	2011 Aug 20	2011.6334	NIRC2/N	H	15.65 ± 2.22	4.879 ± 0.003	299.76 ± 0.20	. . .	. . .	93.2	. . .
GJ 9652 A	CC21	2012 Aug 23	2012.6442	NIRC2/N	H	10.81 ± 1.26	4.118 ± 0.003	298.81 ± 0.20	4.118 ± 0.009	298.79 ± 0.26	78.7	BG
GJ 9652 A	CC22	2011 Aug 20	2011.6334	NIRC2/N	H	5.29 ± 0.28	4.868 ± 0.003	318.20 ± 0.20	. . .	. . .	93.0	BG[d]
GJ 9652 A	CC22	2012 Aug 23	2012.6442	NIRC2/N	H	5.23 ± 0.17	4.129 ± 0.003	320.70 ± 0.20	4.127 ± 0.009	320.64 ± 0.26	78.9	BG
GJ 9652 A	CC23	2012 Aug 23	2012.6442	NIRC2/N	H	13.97 ± 1.19	3.931 ± 0.003	13.79 ± 0.20	. . .	. . .	75.1	SE
GJ 9652 A	CC24	2012 Aug 23	2012.6442	NIRC2/N	H	13.84 ± 1.16	4.390 ± 0.003	10.93 ± 0.20	. . .	. . .	83.8	SE
GJ 9652 A	CC25	2012 Aug 23	2012.6442	NIRC2/N	H	14.36 ± 0.79	5.068 ± 0.003	6.62 ± 0.20	. . .	. . .	96.8	SE
GJ 9652 A	CC26	2012 Aug 23	2012.6442	NIRC2/N	H	14.77 ± 1.03	5.471 ± 0.003	6.19 ± 0.20	. . .	. . .	104.5	SE
GJ 9652 A	CC27	2012 Aug 23	2012.6442	NIRC2/N	H	15.06 ± 1.11	5.117 ± 0.003	24.63 ± 0.20	. . .	. . .	97.7	SE
GJ 9652 A	CC28	2012 Aug 23	2012.6442	NIRC2/N	H	13.32 ± 0.29	5.102 ± 0.003	236.82 ± 0.20	. . .	. . .	97.5	SE
GJ 9652 A	CC29	2012 Aug 23	2012.6442	NIRC2/N	H	13.16 ± 0.83	5.354 ± 0.003	254.07 ± 0.20	. . .	. . .	102.3	SE
GJ 9652 A	CC30	2012 Aug 23	2012.6442	NIRC2/N	H	9.02 ± 0.17	5.360 ± 0.003	258.03 ± 0.20	. . .	. . .	102.4	SE
GJ 9652 A	CC31	2012 Aug 23	2012.6442	NIRC2/N	H	13.79 ± 0.97	6.927 ± 0.003	241.92 ± 0.20	. . .	. . .	132.3	SE
GJ 9652 A	CC32	2012 Aug 23	2012.6442	NIRC2/N	H	10.86 ± 0.17	5.766 ± 0.003	271.95 ± 0.20	. . .	. . .	110.1	SE
GJ 9652 A	CC33	2012 Aug 23	2012.6442	NIRC2/N	H	15.13 ± 1.19	5.460 ± 0.003	269.50 ± 0.20	. . .	. . .	104.3	SE
GJ 9652 A	CC34	2012 Aug 23	2012.6442	NIRC2/N	H	14.85 ± 1.01	5.153 ± 0.003	295.41 ± 0.20	. . .	. . .	98.4	SE
GJ 9652 A	CC35	2012 Aug 23	2012.6442	NIRC2/N	H	13.11 ± 0.27	4.875 ± 0.003	299.09 ± 0.20	. . .	. . .	93.1	SE
GJ 9652 A	CC36	2012 Aug 23	2012.6442	NIRC2/N	H	14.04 ± 0.89	6.482 ± 0.003	312.68 ± 0.20	. . .	. . .	123.8	SE
GJ 9652 A	CC37	2012 Aug 23	2012.6442	NIRC2/N	H	10.19 ± 0.17	6.564 ± 0.003	319.50 ± 0.20	. . .	. . .	125.4	SE
GJ 9652 A	CC38	2012 Aug 23	2012.6442	NIRC2/N	H	14.35 ± 1.19	6.994 ± 0.003	323.57 ± 0.20	. . .	. . .	133.6	SE

Table 8
(Continued)

Name	Cand.	UT Date (Y-M-D)	Epoch	Instrument[a]	Filt.	Contrast (mag)	Measured Position ρ ($''$)	Measured Position P.A. ($^\circ$)	Background Position ρ ($''$)	Background Position P.A. ($^\circ$)	Proj. Sep. (AU)	Comp.?[b]
GJ 9652 A	CC39	2012 Aug 23	2012.6442	NIRC2/N	H	14.49 ± 1.06	6.465 ± 0.003	329.59 ± 0.20	...	...	123.5	SE
GJ 9652 A	CC40	2012 Aug 23	2012.6442	NIRC2/N	H	13.07 ± 0.34	7.556 ± 0.003	335.78 ± 0.20	...	...	144.3	SE
GJ 9652 A	CC41	2012 Aug 23	2012.6442	NIRC2/N	H	15.04 ± 1.10	5.578 ± 0.003	352.79 ± 0.20	...	...	106.5	SE
GJ 9652 A	CC42	2012 Aug 23	2012.6442	NIRC2/N	H	12.45 ± 1.26	4.023 ± 0.003	1.14 ± 0.20	...	...	76.8	SE
2MASS J19303829−1335083	CC1	2010 Aug 17	2010.6251	NIRC2/N	H	9.68 ± 0.22	7.214 ± 0.003	70.62 ± 0.20	...	...	199.8	...
2MASS J19303829−1335083	CC1	2011 Jul 1	2011.4969	NIRC2/N	H	10.18 ± 0.30	6.942 ± 0.003	72.64 ± 0.20	6.949 ± 0.010	72.40 ± 0.22	192.3	BG
2MASS J19303829−1335083	CC2	2010 Aug 17	2010.6251	NIRC2/N	H	10.79 ± 0.31	4.481 ± 0.003	83.86 ± 0.20	...	...	124.1	...
2MASS J19303829−1335083	CC2	2011 Jul 1	2011.4969	NIRC2/N	H	11.19 ± 0.37	4.276 ± 0.003	87.91 ± 0.20	4.278 ± 0.010	87.51 ± 0.24	118.4	BG
2MASS J19303829−1335083	CC3	2010 Aug 17	2010.6251	NIRC2/N	H	5.85 ± 0.16	2.174 ± 0.003	177.62 ± 0.20	...	...	60.2	...
2MASS J19303829−1335083	CC3	2011 Jul 1	2011.4969	NIRC2/N	H	6.34 ± 0.18	2.503 ± 0.003	182.17 ± 0.20	2.467 ± 0.010	182.11 ± 0.28	69.3	BG
2MASS J19303829−1335083	CC4	2010 Aug 17	2010.6251	NIRC2/N	H	9.98 ± 0.19	3.528 ± 0.003	229.57 ± 0.20	...	...	97.7	...
2MASS J19303829−1335083	CC4	2011 Jul 1	2011.4969	NIRC2/N	H	10.46 ± 0.23	3.875 ± 0.003	227.84 ± 0.20	3.857 ± 0.010	228.00 ± 0.23	107.3	BG
1RXS J193528.9+374605	CC1	2010 Aug 17	2010.6249	NIRC2/N	H	14.28 ± 0.36	5.844 ± 0.003	343.10 ± 0.20	...	...	58.4	...
1RXS J193528.9+374605	CC1	2011 Aug 20	2011.6333	NIRC2/N	H	14.36 ± 0.26	5.891 ± 0.003	344.86 ± 0.20	5.903 ± 0.006	344.68 ± 0.21	58.9	BG
1RXS J193528.9+374605	CC2	2010 Aug 17	2010.6249	NIRC2/N	H	8.73 ± 0.30	2.759 ± 0.003	87.94 ± 0.20	...	...	27.6	...
1RXS J193528.9+374605	CC2	2011 Aug 20	2011.6333	NIRC2/N	H	8.86 ± 0.15	2.903 ± 0.003	86.40 ± 0.20	2.904 ± 0.007	86.02 ± 0.21	29.0	BG
1RXS J193528.9+374605	CC3	2010 Aug 17	2010.6249	NIRC2/N	H	13.91 ± 0.32	3.902 ± 0.003	88.24 ± 0.20	...	...	39.0	...
1RXS J193528.9+374605	CC3	2011 Aug 20	2011.6333	NIRC2/N	H	14.03 ± 0.20	4.041 ± 0.003	87.20 ± 0.20	4.046 ± 0.007	86.87 ± 0.20	40.4	BG
1RXS J193528.9+374605	CC4	2010 Aug 17	2010.6249	NIRC2/N	H	15.90 ± 0.98	4.070 ± 0.003	89.21 ± 0.20	...	...	40.7	...
1RXS J193528.9+374605	CC4	2011 Aug 20	2011.6333	NIRC2/N	H	15.69 ± 0.78	4.213 ± 0.003	88.23 ± 0.20	4.212 ± 0.007	87.86 ± 0.20	42.1	BG
1RXS J193528.9+374605	CC5	2010 Aug 17	2010.6249	NIRC2/N	H	14.97 ± 0.49	4.006 ± 0.003	210.25 ± 0.20	...	...	40.1	...
1RXS J193528.9+374605	CC5	2011 Aug 20	2011.6333	NIRC2/N	H	15.05 ± 0.40	3.863 ± 0.003	209.36 ± 0.20	3.848 ± 0.006	209.22 ± 0.23	38.6	BG
1RXS J193528.9+374605	CC6	2010 Aug 17	2010.6249	NIRC2/N	H	15.85 ± 1.00	5.134 ± 0.003	238.69 ± 0.20	...	...	51.3	...
1RXS J193528.9+374605	CC6	2011 Aug 20	2011.6333	NIRC2/N	H	16.16 ± 1.07	4.971 ± 0.003	239.02 ± 0.20	4.962 ± 0.007	238.86 ± 0.22	49.7	BG
1RXS J193528.9+374605	CC7	2010 Aug 17	2010.6249	NIRC2/N	H	15.07 ± 0.59	4.329 ± 0.003	262.36 ± 0.20	...	...	43.3	...
1RXS J193528.9+374605	CC7	2011 Aug 20	2011.6333	NIRC2/N	H	15.31 ± 0.57	4.191 ± 0.003	263.51 ± 0.20	4.178 ± 0.007	263.49 ± 0.21	41.9	BG
1RXS J193528.9+374605	CC8	2010 Aug 17	2010.6249	NIRC2/N	H	10.77 ± 0.30	4.437 ± 0.003	281.59 ± 0.20	...	...	44.4	...
1RXS J193528.9+374605	CC8	2011 Aug 20	2011.6333	NIRC2/N	H	10.83 ± 0.15	4.322 ± 0.003	283.31 ± 0.20	4.323 ± 0.007	283.28 ± 0.21	43.2	BG
1RXS J193528.9+374605	CC9	2011 Aug 20	2011.6333	NIRC2/N	H	16.10 ± 1.06	3.088 ± 0.003	129.53 ± 0.20	...	...	30.9	SE
2MASS J19435432−0546363	CC1	2012 May 21	2012.3875	NIRC2/N	K_S	11.11 ± 0.33	4.321 ± 0.003	108.66 ± 0.20	...	...	138.3	...
2MASS J19435432−0546363	CC1	2013 May 2	2013.3330	NIRC2/N	K_S	10.64 ± 0.12	4.236 ± 0.003	109.52 ± 0.20	4.267 ± 0.008	108.97 ± 0.23	135.6	BG
2MASS J19435432−0546363	CC2	2012 May 21	2012.3875	NIRC2/N	K_S	11.78 ± 0.63	5.284 ± 0.003	192.63 ± 0.20	...	...	169.1	SE
2MASS J19435432−0546363	CC3	2012 May 21	2012.3875	NIRC2/N	K_S	11.70 ± 0.57	2.405 ± 0.003	244.72 ± 0.20	...	...	77.0	...
2MASS J19435432−0546363	CC3	2013 May 2	2013.3330	NIRC2/N	K_S	11.06 ± 0.13	2.471 ± 0.003	244.92 ± 0.20	2.461 ± 0.008	245.20 ± 0.27	79.1	BG
2MASS J19435432−0546363	CC4	2012 May 21	2012.3875	NIRC2/N	K_S	11.61 ± 0.49	4.849 ± 0.003	281.46 ± 0.20	...	...	155.2	...
2MASS J19435432−0546363	CC4	2013 May 2	2013.3330	NIRC2/N	K_S	... [f]	4.912 ± 0.003	281.20 ± 0.20	4.898 ± 0.008	281.26 ± 0.22	157.2	BG
2MASS J19435432−0546363	CC5	2013 May 2	2013.3330	NIRC2/N	K_S	13.50 ± 1.01	5.971 ± 0.003	82.84 ± 0.20	...	...	191.1	SE
2MASS J19435432−0546363	CC6	2013 May 2	2013.3330	NIRC2/N	K_S	13.61 ± 1.04	4.851 ± 0.003	94.24 ± 0.20	...	...	155.2	SE
2MASS J19435432−0546363	CC7	2013 May 2	2013.3330	NIRC2/N	K_S	13.44 ± 0.99	5.790 ± 0.003	332.96 ± 0.20	...	...	185.3	SE
NLTT 48651	CC1	2011 Jun 21	2011.4694	NIRC2/N	H	10.22 ± 0.16	2.273 ± 0.003	252.47 ± 0.20	...	...	22.7	...
NLTT 48651	CC1	2012 May 21	2012.3876	NIRC2/N	K_S	9.99 ± 0.73	2.340 ± 0.003	260.78 ± 0.20	2.346 ± 0.010	260.62 ± 0.25	23.4	BG
NLTT 48651	CC2	2011 Jun 21	2011.4694	NIRC2/N	H	10.67 ± 0.16	6.131 ± 0.003	0.86 ± 0.20	...	...	61.3	...
NLTT 48651	CC2	2012 May 21	2012.3876	NIRC2/N	K_S	10.37 ± 0.52	6.431 ± 0.003	359.76 ± 0.20	6.433 ± 0.008	359.50 ± 35.78	64.3	BG
2MASS J20284361−1128307	CC1	2012 May 10	2012.3577	HiCIAO	H	7.48 ± 0.05	5.644 ± 0.021	38.68 ± 0.24	...	...	79.0	...
2MASS J20284361−1128307	CC1	2013 Aug 17	2013.6254	NIRC2/W	K_S	... [c]	5.704 ± 0.074	36.80 ± 0.20	5.675 ± 0.026	36.88 ± 0.29	79.9	BG

Table 8
(Continued)

Name	Cand.	UT Date (Y-M-D)	Epoch	Instrument[a]	Filt.	Contrast (mag)	Measured Position ρ (″)	Measured Position P.A. (°)	Background Position ρ (″)	Background Position P.A. (°)	Proj. Sep. (AU)	Comp.?[b]
2MASS J20284361−1128307	CC2	2012 May 10	2012.3577	HiCIAO	H	10.22 ± 0.12	3.073 ± 0.020	128.96 ± 0.39	. . .	. . .	43.0	. . .
2MASS J20284361−1128307	CC2	2013 Aug 17	2013.6254	NIRC2/W	K_S	. . . [c]	2.834 ± 0.074	128.39 ± 0.20	2.895 ± 0.025	128.42 ± 0.54	39.7	BG
2MASS J20284361−1128307	CC3	2012 May 10	2012.3577	HiCIAO	H	11.02 ± 0.25	5.579 ± 0.020	231.00 ± 0.24	. . .	. . .	78.1	. . .
2MASS J20284361−1128307	CC3	2013 Aug 17	2013.6254	NIRC2/W	K_S	. . . [c]	5.632 ± 0.074	233.89 ± 0.20	5.594 ± 0.028	232.84 ± 0.27	78.8	BG
2MASS J20284361−1128307	CC4	2013 Aug 17	2013.6254	NIRC2/W	K_S	. . . [c]	21.666 ± 0.077	81.81 ± 0.20	. . .	. . .	303.3	SE
2MASS J20284361−1128307	CC5	2013 Aug 17	2013.6254	NIRC2/W	K_S	. . . [c]	20.218 ± 0.077	95.04 ± 0.20	. . .	. . .	283.1	SE
2MASS J20284361−1128307	CC6	2013 Aug 17	2013.6254	NIRC2/W	K_S	. . . [c]	20.209 ± 0.077	100.03 ± 0.20	. . .	. . .	282.9	SE
2MASS J20284361−1128307	CC7	2013 Aug 17	2013.6254	NIRC2/W	K_S	. . . [c]	12.948 ± 0.075	110.23 ± 0.20	. . .	. . .	181.3	SE
2MASS J20284361−1128307	CC8	2013 Aug 17	2013.6254	NIRC2/W	K_S	. . . [c]	21.073 ± 0.077	122.73 ± 0.20	. . .	. . .	295.0	SE
2MASS J20284361−1128307	CC9	2013 Aug 17	2013.6254	NIRC2/W	K_S	. . . [c]	19.537 ± 0.077	327.34 ± 0.20	. . .	. . .	273.5	SE
GJ 4186 B	CC1	2010 Aug 17	2010.6255	NIRC2/N	H	14.32 ± 0.85	3.251 ± 0.003	231.45 ± 0.20	. . .	. . .	62.8	. . .
GJ 4186 B	CC1	2011 Jun 21	2011.4695	NIRC2/N	H	14.53 ± 1.00	3.451 ± 0.003	233.43 ± 0.20	3.455 ± 0.004	233.35 ± 0.19	66.6	BG
GJ 4185 Aab	CC1	2011 Jun 21	2011.4696	NIRC2/N	H	12.27 ± 0.76	3.586 ± 0.003	76.42 ± 0.20	. . .	. . .	69.9	. . .
GJ 4185 Aab	CC1	2012 May 21	2012.3876	NIRC2/N	K_S	11.31 ± 0.76	3.355 ± 0.003	76.59 ± 0.20	3.387 ± 0.004	75.92 ± 0.21	65.4	BG
GJ 4185 Aab	CC2	2011 Jun 21	2011.4696	NIRC2/N	H	10.58 ± 0.31	2.449 ± 0.003	195.69 ± 0.20	. . .	. . .	47.8	. . .
GJ 4185 Aab	CC2	2012 May 21	2012.3876	NIRC2/N	K_S	9.56 ± 0.22	2.590 ± 0.003	199.51 ± 0.20	2.528 ± 0.004	199.95 ± 0.20	50.5	BG
GJ 4185 Aab	CC3	2011 Jun 21	2011.4696	NIRC2/N	H	11.51 ± 0.28	4.192 ± 0.003	225.30 ± 0.20	. . .	. . .	81.7	. . .
GJ 4185 Aab	CC3	2012 May 21	2012.3876	NIRC2/N	K_S	11.08 ± 0.48	4.402 ± 0.003	226.19 ± 0.20	4.350 ± 0.004	226.99 ± 0.21	85.8	BG
NLTT 54873	CC1	2010 Aug 18	2010.6279	NIRC2/N	H	7.07 ± 0.16	3.616 ± 0.003	292.70 ± 0.20	. . .	. . .	79.6	. . .
NLTT 54873	CC1	2011 Aug 20	2011.6337	NIRC2/N	H	7.45 ± 0.19	3.747 ± 0.003	290.29 ± 0.20	3.738 ± 0.009	290.33 ± 0.24	82.4	BG
GJ 4337 A	CC1	2010 Aug 18	2010.6281	NIRC2/N	H	13.62 ± 0.34	4.174 ± 0.003	242.55 ± 0.20	. . .	. . .	62.2	. . .
GJ 4337 A	CC1	2011 Aug 20	2011.6338	NIRC2/N	H	13.78 ± 0.29	4.515 ± 0.003	245.27 ± 0.20	4.530 ± 0.009	245.44 ± 0.21	67.3	BG
GJ 1290	CC1	2011 Nov 15	2011.8713	NIRC2/N	H	14.12 ± 0.50	3.772 ± 0.003	132.26 ± 0.20	. . .	. . .	83.0	. . .
GJ 1290	CC1	2012 Oct 8	2012.7701	NIRC2/N	H	13.24 ± 1.13	3.527 ± 0.003	138.01 ± 0.20	3.530 ± 0.008	137.87 ± 0.25	77.6	BG
G 68-46	CC1	2012 Aug 23	2012.6447	NIRC2/N	K_S	12.46 ± 0.60	2.246 ± 0.003	27.62 ± 0.20	. . .	. . .	47.2	. . .
G 68-46	CC1	2013 Aug 17	2013.6255	NIRC2/N	K_S	12.58 ± 0.34	2.205 ± 0.003	20.29 ± 0.20	2.204 ± 0.009	20.63 ± 0.28	46.3	BG
G 68-46	CC2	2012 Aug 23	2012.6447	NIRC2/N	K_S	13.50 ± 1.07	3.090 ± 0.003	100.93 ± 0.20	. . .	. . .	64.9	. . .
G 68-46	CC2	2013 Aug 17	2013.6255	NIRC2/N	K_S	13.92 ± 1.05	2.827 ± 0.003	99.89 ± 0.20	2.816 ± 0.008	100.54 ± 0.27	59.4	BG
G 68-46	CC3	2012 Aug 23	2012.6447	NIRC2/N	K_S	13.56 ± 1.15	4.261 ± 0.003	41.82 ± 0.20	. . .	. . .	89.5	. . .
G 68-46	CC3	2013 Aug 17	2013.6255	NIRC2/N	K_S	13.48 ± 0.86	4.148 ± 0.003	38.54 ± 0.20	4.145 ± 0.009	38.43 ± 0.24	87.1	BG
G 68-46	CC4	2012 Aug 23	2012.6447	NIRC2/N	K_S	12.95 ± 0.91	4.332 ± 0.003	51.67 ± 0.20	. . .	. . .	91.0	BG[e]
G 68-46	CC4	2013 Aug 17	2013.6255	NIRC2/N	K_S	13.58 ± 0.90	4.195 ± 0.003	48.12 ± 0.20	4.175 ± 0.009	48.66 ± 0.23	88.1	BG
1RXS J235452.2+383129	CC1	2011 Aug 20	2011.6337	NIRC2/N	H	13.80 ± 0.41	5.304 ± 0.003	236.79 ± 0.20	. . .	. . .	84.3	. . .
1RXS J235452.2+383129	CC1	2012 Aug 23	2012.6448	NIRC2/N	H	13.93 ± 1.04	5.145 ± 0.003	236.58 ± 0.20	5.143 ± 0.009	236.76 ± 0.22	81.8	BG

Notes.

[a] NIRC2/N refers to the narrow (≈10″ × 10″) camera mode; NIRC2/W refers to the wide (≈40″ × 40″) camera.

[b] BG=background object; SE=single epoch detection; AMB=ambiguous whether comoving or background.

[c] The primary and/or companion is saturated or in the nonlinear regime of the infrared array, so no relative photometry is listed.

[d] Colors and/or astrometry are inconsistent with a late-type common proper motion companion based on visual inspection of the field from one or more of the following archival sky surveys: 2MASS (Skrutskie et al. 2006), SDSS (Abazajian et al. 2009), DSS1, or DSS2.

[e] Source appears spatially extended and is probably a background galaxy.

[f] Source is near the edge of the array so no relative photometry is given.

(This table is also available in a machine-readable form)
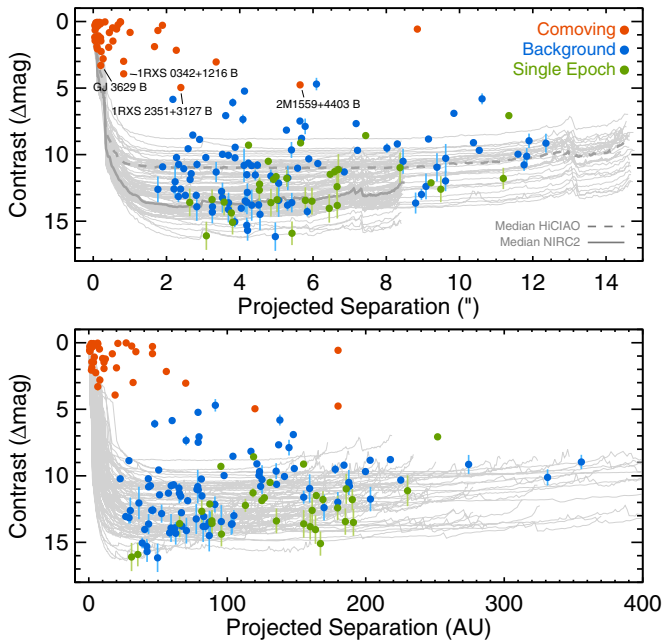
Figure 19. Point sources detected in our survey. Comoving stellar and substellar companions are shown in red, background objects are plotted in blue, and objects with only a single epoch of astrometry are in green. The individual and median NIRC2 and HiCIAO contrasts are overplotted in gray. In the top panel the measured angular separations and contrasts are displayed, while the projected separation is used in the bottom panel. For clarity we have excluded several dozen single epoch candidates in the single crowded field surrounding GJ 9652 A.

where θ, ρ, and σ are the measured and predicted P.A., separation, and their associated uncertainties at epoch i for N epochs of astrometry. ν is the number of degrees of freedom, equal to $2 \times N - 1$. For the background case, the predicted measurements incorporate the proper motion and distance to the target as listed in Table 3. For the co-moving scenario, the predicted P.A. and separation assume no orbital motion as expected for companions on wide orbits.

Table 9 summarizes our tests for common proper motion for candidates with at least two epochs of astrometry. 93 candidates are consistent with background stars. The status of one candidate, 1RXS J124147.5+564506-CC1, is ambiguous. The remaining 73 only have a single epoch of astrometry. We do not identify any planets in our sample.

6. STATISTICAL ANALYSIS

Our null detection of planets provides powerful constraints on the outer architecture of planetary systems around low-mass stars. Likewise, our four brown dwarf discoveries allow us to measure the frequency of brown dwarf companions to M dwarfs over a variety of separations. Since we are not uniformly sensitive to companions in mass and separation, a sensitivity map for each target must be considered. Similarly, our brown dwarf discoveries were made in projected separation and their distributions in semi-major axis space must be inferred to derive accurate statistical constraints. In the following analysis, we assume two forms of eccentricity distributions to test their influence on our results: circular orbits ($e = 0$) and eccentricities following a $1-e$ distribution, in which most planets have small or modest eccentricities (see Section 6.3). The latter case is motivated by the distribution of radial velocity detected planets (Kipping 2013) and M dwarf binaries (Duchêne & Kraus

2013). Below we describe two approaches to derive statistical constraints over a range of companion masses and separations.

6.1. Contrast Curve Selection Guidelines

A common complication of large direct imaging surveys is that not all faint planet candidates can be followed up with second-epoch astrometry. Finite telescope time, different seeing conditions and AO correction, and varying FOV rotation can both prevent candidates found in first-epoch imaging from being recovered and reveal new fainter or wider point sources. In this survey we found that 93 out of 167 faint point sources are stationary background stars. Care must therefore be taken in our statistical treatment of the remaining 74 candidates with unclear status. Note, however, that only 8 of these are within projected separations of 100 AU around single stars in our sample and most of them (42) come from a single low-galactic latitude target.

Following the recipe of Nielsen et al. (2013), we define selection guidelines for choosing contrast curves to use in our statistical analysis. These are considered on a case-by-case basis for each target in our survey.

1. If no candidates are identified in a first-epoch observation and no subsequent deeper imaging is obtained, then the contrast curve is used for our statistical analysis.

   (a) If a later, deeper epoch of imaging uncovers candidates that are shown to be background, this deeper contrast curve is used.

   (b) If a later, deeper epoch uncovers candidates that are *not* shown to be background, then the initial candidate-free first epoch contrast curve is used.

2. If one or more candidates are identified at the first epoch and are shown to be background objects from subsequent imaging, and no other candidates are identified in the follow-up observation, then the deeper of the two contrasts is used.

   (a) If a second epoch reveals additional candidates that only have a single epoch of astrometry, then the first epoch contrast curve is used.

   (b) If a second epoch fails to recover one or more candidates then this second epoch contrast curve is used. This is analogous to (1b) but in reverse order.

3. If only a single first-epoch observation is obtained and one or more candidates are identified then the floor of the contrast curve is defined to be 2σ above the brightest candidate with unknown status, where σ is the uncertainty in the relative contrast of that candidate. Since we have no information about whether single-epoch candidates are background or comoving, the raw contrast curve cannot be included in the statistical analysis. Instead, we homogeneously remove all information about companions below the threshold of the brightest single-epoch candidate in the image.

6.2. Wide Stellar Binaries

Wide stellar binaries beyond $\sim$100 AU can dramatically influence the outer regions of planetary systems by creating dynamically unstable zones where planets cannot exist on long timescales. These wide binaries must therefore be taken into account in the statistical analysis of the survey. Table 10 lists the multiplicity properties of the sample. Altogether, 25 of our targets have companions beyond 100 AU.

Table 9
Common Proper Motion Tests

Name	Cand.	No. of Epochs	Δt (yr)	χ_ν^2 (BG)	χ_ν^2 (CPM)	ν	Comp.?
GJ 3030 AB	CC1	2	1.64	0.57	17.08	3	BG
GJ 3030 AB	CC2	2	1.64	2.31	434960	3	BG
NLTT 1875	CC1	2	1.01	2.74	203.5	3	BG
NLTT 1875	CC2	2	1.01	2.28	344.2	3	BG
NLTT 1875	CC3	2	1.01	0.49	866.9	3	BG
NLTT 1875	CC4	2	1.01	1.62	279.5	3	BG
NLTT 1875	CC5	2	1.01	2.30	63.77	3	BG
NLTT 1875	CC6	2	1.01	3.14	72.03	3	BG
LP 247-13	CC1	5	0.97	1.47	30.24	9	BG
NLTT 13844	CC1	2	0.27	0.66	668.6	3	BG
NLTT 13844	CC2	2	0.27	0.07	634.3	3	BG
1RXS J045101.0+312734	CC1	3	0.93	0.11	6.07	5	BG
1RXS J045101.0+312734	CC2	2	0.93	0.07	6.93	3	BG
AP Col	CC1	3	0.78	2.09	26.90	5	BG
G 108-36	CC1	2	0.93	0.01	7.33	3	BG
G 108-36	CC2	2	0.93	0.02	563613	3	BG
G 108-36	CC3	2	0.93	0.04	11.17	3	BG
G 108-36	CC4	2	0.93	0.25	5.88	3	BG
G 108-36	CC5	2	0.93	0.21	4.41	3	BG
1RXS J073829.3+240014	CC1	2	2.14	1.88	3274.7	3	BG
NLTT 26359	CC1	2	1.35	0.23	19.98	3	BG
NLTT 26359	CC2	2	1.35	0.20	8.98	3	BG
G 13-33 AB	CC1	2	1.10	3.14	49.05	3	BG
G 13-33 AB	CC2	2	0.71	3.49	128.1	3	BG
GJ 3729 AB	CC1	2	0.94	0.94	9.01	3	BG
GJ 3729 AB	CC2	2	0.54	1.08	19.17	3	BG
1RXS J124147.5+564506	CC1	2	0.98	2.35	0.11	3	AMB
2MASS J14124864−1629561	CC1	2	0.94	0.20	308.4	3	BG
G 166-49	CC1	2	0.71	0.53	523.4	3	BG
G 166-49	CC2	2	0.71	0.23	1140	3	BG
G 166-49	CC3	2	0.71	1.13	951.7	3	BG
2MASS J15323737+4653048	CC1	2	1.23	1.47	420.82	3	BG
GJ 3966 AB	CC1	2	0.81	8.27	104.3	3	BG
G 669 A	CC1	2	0.98	2.52	56.39	3	BG
G 669 A	CC2	2	0.98	0.68	29.51	3	BG
G 669 A	CC3	2	0.98	2.38	8.60	3	BG
G 669 A	CC4	2	0.98	2.87	8.44	3	BG
G 669 A	CC5	2	0.98	2.13	11.55	3	BG
LHS 3321	CC1	2	0.89	2.24	178.4	3	BG
GJ 9652 A	CC1	2	1.01	0.03	6587	3	BG
GJ 9652 A	CC2	2	1.01	0.00	1921	3	BG
GJ 9652 A	CC3	2	1.01	0.01	1387	3	BG
GJ 9652 A	CC4	2	1.01	0.35	1820	3	BG
GJ 9652 A	CC5	2	1.01	0.08	3431	3	BG
GJ 9652 A	CC6	2	1.01	0.03	3733	3	BG
GJ 9652 A	CC7	2	1.01	0.60	2834	3	BG
GJ 9652 A	CC10	2	1.01	0.49	1321	3	BG
GJ 9652 A	CC13	2	1.01	0.07	8967	3	BG
GJ 9652 A	CC18	2	1.01	0.00	7737	3	BG
GJ 9652 A	CC19	2	1.01	0.13	6736	3	BG
GJ 9652 A	CC20	2	1.01	0.04	4129	3	BG
GJ 9652 A	CC21	2	1.01	0.00	10728	3	BG
GJ 9652 A	CC22	2	1.01	0.03	10139	3	BG
2MASS J19303829−1335083	CC1	2	0.87	0.37	1387	3	BG
2MASS J19303829−1335083	CC2	2	0.87	0.56	846.6	3	BG
2MASS J19303829−1335083	CC3	2	0.87	3.97	2091	3	BG
2MASS J19303829−1335083	CC4	2	0.87	1.08	2242	3	BG
1RXS J193528.9+374605	CC1	2	1.01	1.20	53.81	3	BG
1RXS J193528.9+374605	CC2	2	1.01	0.58	393.9	3	BG
1RXS J193528.9+374605	CC3	2	1.01	0.60	362.3	3	BG
1RXS J193528.9+374605	CC4	2	1.01	0.58	382.7	3	BG
1RXS J193528.9+374605	CC5	2	1.01	1.74	382.0	3	BG
1RXS J193528.9+374605	CC6	2	1.01	0.56	492.5	3	BG
1RXS J193528.9+374605	CC7	2	1.01	0.97	358.2	3	BG

Table 9
(Continued)

Name	Cand.	No. of Epochs	Δt (yr)	χ_ν^2 (BG)	χ_ν^2 (CPM)	ν	Comp.?
1RXS J193528.9+374605	CC8	2	1.01	0.01	257.2	3	BG
2MASS J19435432−0546363	CC1	2	0.95	5.47	136.9	3	BG
2MASS J19435432−0546363	CC3	2	0.95	0.69	80.83	3	BG
2MASS J19435432−0546363	CC4	2	0.95	0.91	73.78	3	BG
NLTT 48651	CC1	2	0.92	0.19	370.9	3	BG
NLTT 48651	CC2	2	0.92	0.02	538371	3	BG
2MASS J20284361−1128307	CC1	2	1.27	0.06	12.27	3	BG
2MASS J20284361−1128307	CC2	2	1.27	0.20	3.80	3	BG
2MASS J20284361−1128307	CC3	2	1.27	3.33	28.68	3	BG
GJ 4186 B	CC1	2	0.84	0.24	757.1	3	BG
GJ 4185 Aab	CC1	2	0.92	15.43	988.3	3	BG
GJ 4185 Aab	CC2	2	0.92	52.06	429.0	3	BG
GJ 4185 Aab	CC3	2	0.92	38.59	820.0	3	BG
NLTT 54873	CC1	2	1.01	0.31	342.0	3	BG
GJ 4337 A	CC1	2	1.01	0.95	2184	3	BG
GJ 1290	CC1	2	0.90	0.10	1249	3	BG
G 68-46	CC1	2	0.98	0.33	255.0	3	BG
G 68-46	CC2	2	0.98	1.80	1285	3	BG
G 68-46	CC3	2	0.98	0.07	281.2	3	BG
G 68-46	CC4	2	0.98	2.53	400.1	3	BG
1RXS J235452.2+383129	CC1	2	1.01	0.14	468.35	3	BG

Our treatment of wide binaries follows that of Nielsen et al. (2013) and is based on simulations by Holman & Wiegert (1999) of stability zones surrounding close-in planets with a wide stellar companion (S-type orbits) and wide-separation circumbinary planets (P-type orbits). Holmam & Wiegert show that the region of stable orbits is a strong function of both binary eccentricity and mass ratio. The eccentricity distribution of these (very) wide-separation binaries is unknown because of their long orbital periods. However, Abt (2006) showed that eccentricities become increasingly uniform (i.e., random) at long periods (10^5–10^6 days), with a mean eccentricity tending to 0.5. We therefore adopt eccentricities of 0.5 for wide binary companions in our sample. Assuming equal mass stars, the critical semi-major axis for stable S-type orbits from Holman & Wiegert (1999) is $\approx$10% of the stellar semi-major axis. For P-type orbits, the inner stability limit is ~4 times the binary semi-major axis.

Wide binaries in our sample are complicated by projection effects and their unknown current orbital phase. We therefore adopt a median conversion factor of 1.14 from Dupuy & Liu (2011) for the case of no discovery bias to transform projected separations into semi-major axes. For our statistical analysis, we then assume that the region between 10% and 400% of the binary semi-major axis is devoid of planets and does not contribute any information to our statistical analysis. These allowable regions are listed in Table 10. As described above, these are conservative stability limits assuming a star-wide binary companion eccentricity of 0.5 and coplanar binary and planetary orbits. Relaxing these constraints would provide more room for dynamically stable planets to reside. Indeed, Tokovinin et al. (2006) found the empirical limit for dynamical stability of triple star systems is near period ratios of 5 (that is, $P_3/P_1 > 5$), which may be a more realistic boundary. Note that we do not exclude regions surrounding our brown dwarf discoveries for dynamical reasons since we had no *a priori* knowledge of their existence. In this way our sensitivity maps for these targets

contribute to the number of trials and the discoveries contribute to the number of detections in these regions (see Section 6.4).

6.3. Mass Sensitivity

Converting contrast curves into sensitivity limits in planet mass and separation requires the use of substellar evolutionary models. These cooling curves in turn depend on assumptions about the way in which planets form. "Hot-start" models (e.g., Burrows et al. 1997; Saumon & Marley 2008) slowly radiate their initial gravitational potential energy over time and therefore best represent formation via disk instability (e.g., Boss 1997; Mayer 2002). On the other hand, "cold-start" and "warm-start" models (e.g., Marley et al. 2007; Spiegel & Burrows 2012; Mollière & Mordasini 2012; Bodenheimer et al. 2013) follow a core accretion prescription, which assumes significant loss of initial entropy at formation through punctuated energy dissipation associated with accretion events. In addition to differences in initial conditions, though to a lesser degree, assumptions about the atmospheric properties of giant planets can also influence both the rate at which planets cool and the evolution of their spectra (e.g., Chabrier et al. 2000).

We adopt four sets of evolutionary models for this survey to reflect uncertainties in the formation and atmospheric properties of giant planets. Our choices are based on the accuracy of the models in reproducing the observed colors of brown dwarfs and giant planets and on the sampling of the various publicly available grids in mass and age. The properties of all four grids are summarized in Figure 20. We selected solar-metallicity hot-start models incorporating three general prescriptions of photospheric dust: (1) the Cond models of Baraffe et al. (2003), in which dust is modeled as having already formed and settled below the photosphere; (2) the Dusty models of Chabrier et al. (2000), which present an extreme view of photospheric dust formation and retention at all temperatures; and (3) the BT-Settl isochrones from Allard et al. (2011), which simulate the growth and sedimentation of dust across the M/L/T transitions. The Cond models are well sampled from ages of 1 Myr to 10 Gyr and

Table 10
Sample Multiplicity Properties

Name	Type[a]	Wide Comp. Name	ρ ('')	Proj. Sep. (AU)	Orbital Period (yrs)	Allowable Planet a (AU)	Discovery Reference
G 217-32 AB	CVB	. . .	0.5	7.7	48	>35	B14
1RXS J001557.5−163659 AB	CVB	. . .	0.1	1.8	4.5	>8	B14
GJ 3030	MVB	. . .	2.2	56	1000	<6, >260	M01
G 132-50 Aab	PMB+CVB; WVB	G132-51 Bab	0.3; 26	8; 770	32; 25000	36–88, >3500	M05, B14; G63
G 271-110	WVB	EX Cet	610	14600	2500000	<1700, >67000	AF11
G 272-115	SB2	. . .	. . .	. . .	. . .	. . .	Sh15
NLTT 6549 AB	CVB	. . .	0.05	2.2	4.2	>10	B14
2MASS J03033668−2535329 AB	PMB+CVB	. . .	0.8	32	210	>150	M05, J12
1RXS J034231.8+121622 AB	CVB	. . .	0.8	19	76	. . .	J12, B14
G 160-54 ABC	CVB+SB3; MVB	. . .	0.2; 3.3	4; 70	17; 1300	>320	B14, Sh15
2MASS J04220833−2849053 AB	CVB	. . .	0.8	21	120	>100	B14
2MASS J04472312−2750358	MVB	2MASS J04472266−2750295	8.8	180	3200	<21, >820	M01
G 81-34 AB	CVB	. . .	0.6	14	95	>64	B14
L 449-1 AB	CVB	. . .	0.05	0.6	2.5[d]	>0.3	Ri14
GJ 3371 A	WVB	GJ 3372 B	160	2170	140000	<250, >9900	G66a
GJ 3372 B	WVB	GJ 3371 A	160	2170	140000	<250, >9900	G66a
2MASS J06131330−2742054 AB	CVB+SB2	. . .	0.09	2.7	8.3	>12	Ri14, Sh15
LHS 1864 AB	MVB+SB2	. . .	1.8	34	320	<27, >1100	M01, Sh15
1RXS J091744.5+461229 AB	CVB	. . .	0.2	6.5	20	>30	J12
GJ 354.1 B	WVB	DX Leo	65	1160	52000	<130, >5300	G98
PYC J09362+3731 AB	SB2	. . .	. . .	. . .	. . .	. . .	Sc12c
NLTT 22741 A	WVB	2MASS J09510549+3558021	13	400	20000	<46, >1800	Re06
GJ 3577 A	WVB	GJ 3578 B	23	570	23000	<65, >2600	G63
GJ 3578 B	WVB	GJ 3577 A	23	570	23000	<65, >2600	G63
G 196-3 A	WVB	G 196-3 B	16	180	4000	<20, >820	Re98
GJ 2079 AB	PMB+CVB+SB1	. . .	0.1	2.3	4.8	>10	M05, B14, Sh12
GJ 3629 AB	CVB	. . .	0.2	6.5	30	. . .	B12a
PYC J10571+0544 AB	MVB	. . .	1.0	46	780	>210	B14
2MASS J11240434+3808108	MVB	2MASS J11240487+3808054	8.3	170	5100	<19, >780	Cr03
TWA 30 A	WVB	TWA 30 B	80	3370	560000	<380, >15000	Lo10
2MASS J12062214−1314559 AB	CVB	. . .	0.4	11	55	>50	J12
G 13-33 AB	CVB	. . .	0.1	1.5	4.7	>7	B14
LP 735-48 AB	MVB	. . .	1.9	46	470	>210	B14
GJ 3729 AB	CVB	. . .	0.05	0.9	2.4	>4	B14
2MASS J12383713−2703348 AB	CVB	. . .	0.2	5	19	>23	B14
GJ 490 Bab	CVB; WVB	GJ 490 Aab	0.2; 16	3.3; 310	16; 13000	13–35, >1400	B14; G64
GJ 490 Aab	CVB; WVB	GJ 490 Bab	0.1; 16	1.9; 310	7.3; 13000	8–35, >1400	B14; G64
NLTT 34410 AB	CVB[c]	. . .	0.1	3	11	>14	B14
2MASS J14215503−3125537 AB	CVB	. . .	0.07	2.8	8.4	>13	B14
1RXS J150907.2+590422 A	MVB	2MASS J15090696+5904282	9.0	300	8500	<34, >1400	M01
LHS 3122 AB	CVB	. . .	0.2	3.4	12	>16	B14
2MASS J15594729+4403595 AB	MVB	. . .	5.6	180	3800	<21, >820	J12
2MASS J16074132−1103073 AB	CVB	. . .	0.7	27	240	>120	M14
GJ 3966 AB	CVB	. . .	0.09	1.5	3.4	>7	B14
GJ 3997 AB	MVB	. . .	1.7	20	150	>91	B14
LP 447-38 AB	CVB	. . .	0.4	10	52	>46	B14
GJ 669 B	WVB	GJ 669 A	17	200	4100	<23, >910	G64
GJ 669 A	WVB	GJ 669 B	17	200	4100	<23, >910	G64
GJ 9652 A	SB1; WVB	GJ 9652 B	40	780	30000	<89, >3600	Sh12; G66a
1RXS J193528.9+374605	SB1	. . .	. . .	. . .	. . .	. . .	Sh12
2MASS J19560294−3207186 AB	CVB; WVB	TYC 7443-1102-1	0.2; 26	12; 1530	66; 72000	55–170, >7000	B14; L09
TYC 7443-1102-1	WVB	2MASS J19560294−3207186 AB	26	1530	72000	<170, >7000	L09
2MASS J20003177+5921289 AB	CVB	. . .	0.3	6.4	34	>29	J12
2MASS J20100002−2801410 AB	CVB	. . .	0.7	31	290	>140	B10
NLTT 50066 AB	CVB	. . .	0.14	5.3	17	>24	J12
NLTT 50710	SB2	. . .	. . .	. . .	. . .	. . .	Sh15
GJ 4186 B	WVB	GJ 4185 Aab	26	510	18000	<58, >2300	P94
GJ 4185 Aab	CVB; WVB	GJ 4186 B	0.05; 26	1.0; 510	1.6; 18000	<58, >2300	B14; P94
PYC J21376+0137 AB	CVB	. . .	0.4	17	140	>78	B14
1RXS J221419.3+253411 AB	CVB	. . .	0.1	4	23	>18	B14

Table 10
(Continued)

Name	Type[a]	Wide Comp. Name	ρ ('')	Proj. Sep. (AU)	Orbital Period (yrs)	Allowable Planet a (AU)	Discovery Reference
GJ 4338 Bab	CVB; WVB	GJ 4337 A	0.05; 17.6	0.7; 260	1.0; 6200	<30, >1200	B14; G66b
GJ 4337 A	WVB	GJ 4338 Bab	17.6	260	6200	<30, >1200	G66b
1RXS J235133.3+312720 AB	MVB; WVB	2MASS J23514340+3127045	2.4; 126	120; 6300	2200; 630000	<14, 550–720, >29000	B12b; Sk14
GJ 4381 AB	CVB	. . .	0.5	60	11	>50	MZB01

Notes.

[a] CVB = close visual binary (<1''); MVB = moderate visual binary (1–10''); WVB = wide visual binary (>10''); SB1 = single-line spectroscopic binary; SB2 = double-line spectroscopic binary; SB3 = triple-line spectroscopic binary; PMB = proper motion binary.

[b] Dynamically stable regions from Holman & Wiegert (1999) assuming an equal-mass binary with an eccentricity of 0.5. Stable zones within 5 AU are excluded because we lack the sensitivity to detect planets in this region.

[c] The Washington Double Star Catalog lists LP 232-169 as a wide companion to NLTT 34410 AB at 172''. However, Scholz et al. (2005b) find LP 232-169 is a K2 subdwarf at a distance of ∼400–800 pc; they also find that the proper motions significantly disagree. These stars appear to be unrelated.

[d] See Riedel et al. (2014).

References. (AF11) Alonso-Floriano et al. 2011; (B12a) Bowler et al. 2012a; (B12b) Bowler et al. 2012b; (B14) this work; (Cr03) Cruz et al. 2003; (G63) Giclas et al. 1963; (G64) Giclas et al. 1964; (G66a) Giclas et al. 1966a; (G66b) Giclas et al. 1966b; (G98) Gaidos 1998; (J12) Janson et al. 2012; (M01) Mason et al. 2001; (M05) Makarov & Kaplan 2005; (M14) Malo et al. 2014a; (MZB01) McCarthy et al. 2001; (Lo10) Looper et al. 2010a; (L09) Lépine & Simon 2009; (P94) Poveda et al. 1994; (Re98) Rebolo et al. 1998; (Ri14) Riedel et al. 2014; (Sc12b) Schlieder et al. 2012c; (Sh12) Shkolnik et al. 2012; (Sh15) E. L. Shkolnik et al. (in preparation); (Sk14) B. Skiff (2013, private communication).
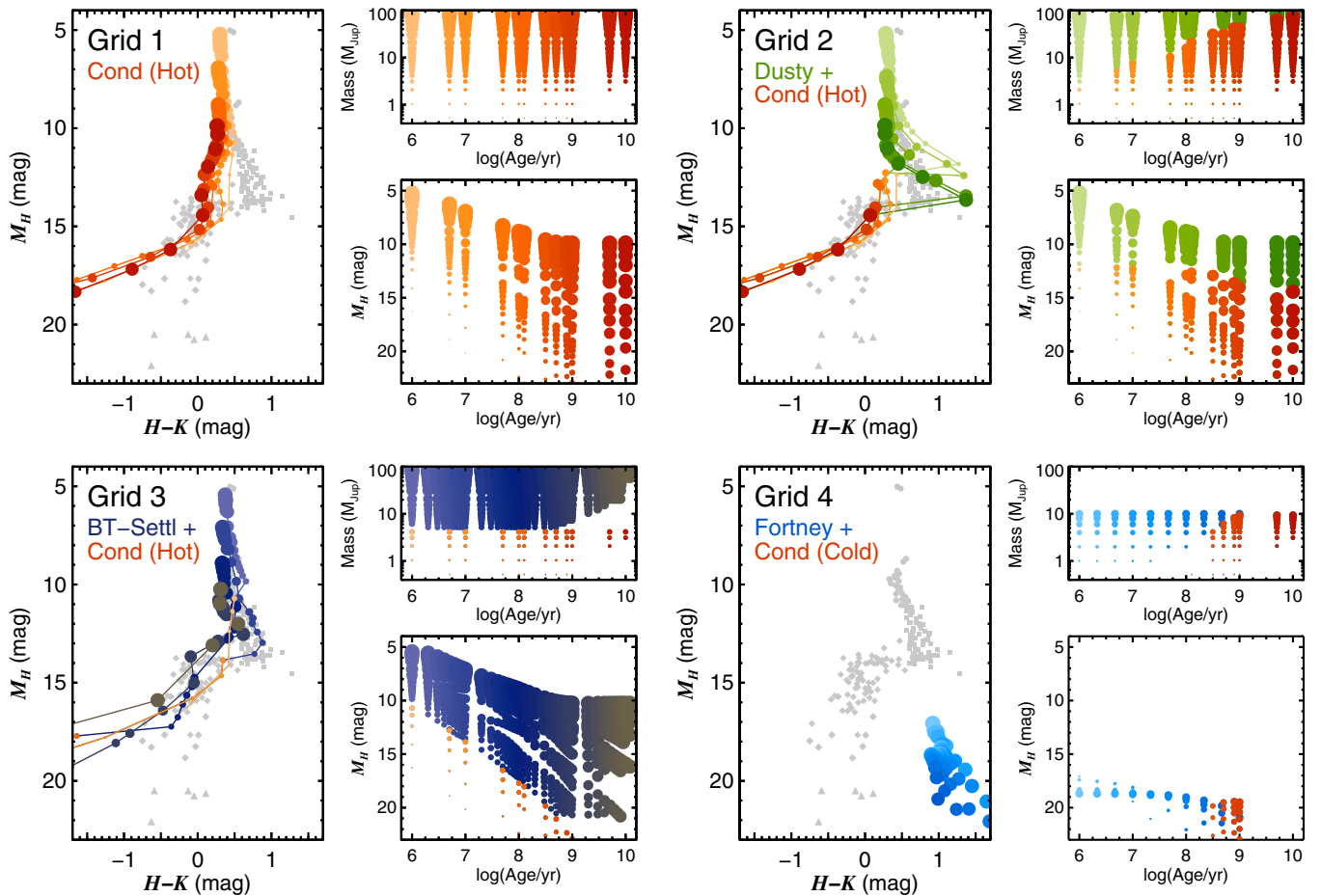
Figure 20. Evolutionary model grids used in this work. Three of the cases (Grids 1–3) are based on a hot-start formation scenario, while the fourth (Grid 4) follows a cold-start prescription. Each three-panel set shows the predicted color–magnitude sequence in M_H vs. H–K compared to the observed sequence of MLTY dwarfs (gray; from Dupuy & Liu 2012 and Dupuy & Kraus 2013), the grid sampling in age and mass, and the evolution of M_H with time. Mass ranges of 0.5–100 M_{Jup} (0.5–10 M_{Jup}) are shown for hot-start (cold-start) cases with symbol sizes scaling with mass. Grid 1 shows the Cond models of Baraffe et al. (2003), which poorly reproduce dusty L dwarfs and mid-to late-T dwarfs in color. Grid 2 is a hybrid of Dusty models from Chabrier et al. (2000) above 1500 K and Cond models at lower temperatures. Grid 3 shows the BT-Settl models from Allard et al. (2011) above 5 M_{Jup} and the Cond grid at lower masses, producing the best fit to the M, L, and early T sequence. The cold-start scenario with slight (5× solar) metal-enrichment from Fortney et al. (2008) is shown in Grid 4 and is supplemented with Cond models at older ages. The three hot-start cases predict similar evolution of absolute magnitude with planet mass and, overall, produce very similar statistical results in this study.

masses of 0.5 $M_{\rm Jup}$–to 0.1 $M_\odot$. Dusty models produce better fits to the L dwarf color-magnitude sequence, but are too red below about 1500 K (Figure 20); we therefore supplement the Dusty grid with Cond models below that temperature, resulting in a "Dusty+Cond" combination. The BT-Settl models do a better job reproducing the M, L, and T sequence, but are not uniformly sampled at very low masses; we therefore supplement that grid with Cond models below 5 $M_{\rm Jup}$. For the cold-start models we adopt the grid from Fortney et al. (2008), which assumes slight metal enrichment (five times solar abundances), includes masses below 13 $M_{\rm Jup}$, and focuses on relatively young ages ($\lesssim$1 Gyr). At older ages, all planetary-mass objects should have temperatures below ~600 K, so we supplement the Fortney grid with Cond models in that region.

Our strategy to infer planet detectability for each target in the {planet mass, semi-major axis} plane is based on Monte Carlo realizations of simulated planets on random orbits. For a given target and semi-major axis a we generate 10^4 orbits projected onto the sky with random ascending node position angles, arguments of periastron, orbital inclinations (drawn from a sin i distribution), and periastron passage times. We consider two possible eccentricity distributions, $e = 0$ and $P(e) \propto 1-e$, to test whether adding modest eccentricities affects the results. This choice of the eccentricity distribution is motivated by observations of intermediate-period (100–10,000 day) M dwarf binaries and extrasolar giant planets measured from radial velocity surveys, which have similar distribution shapes that peak at small eccentricities and diminish roughly linearly to high values (Duchêne & Kraus 2013; Kipping 2013).

For a given companion mass m we use the star's distance and age together with evolutionary models to assign an apparent magnitude to each simulated companion. Gaussian age distributions are adopted for stars that belong to YMGs, while linearly uniform distributions are used for the rest (see Table 2). The uncertainty in the distance is also incorporated as a Gaussian distribution. This allows us to then compare the apparent magnitudes and sky-projected separations of all orbits for a given {m, a} to our contrast curves. The fraction of simulated companions that fall above the curve (the "detections") is the overall sensitivity at that grid point. Fractional FOV coverage is also incorporated by randomly assigning "non-detections" to planets with a probability equal to 1 minus the azimuthal coverage at that separation.

These simulations are repeated for all grid steps in mass (from 0.5–100 $M_{\rm Jup}$) and physical separation (1–1000 AU), all four sets of evolutionary models, both circular orbits and eccentricity distributions following $P(e) \propto 1-e$, and our three methods of PSF subtraction. For our statistical analysis we adopt contrast curves from the aggressive version of the LOCI reduction because overall they produce the best contrasts, but the resulting mass sensitivities are similar for all cases. Figure 21 shows the distribution of contrasts for our three PSF subtraction methods. At 1″, the aggressive implementation of LOCI outperforms the scaled median subtraction and our conservative version of LOCI by $0.5^{+0.7}_{-0.3}$ mag and $0.12^{+0.20}_{-0.17}$ mag, respectively. However, this gain in contrast is only marginal in planet mass: for the typical age of our sample ($\approx$125 Myr), the Cond models of Baraffe et al. (2003) predict an H-band brightness difference between a 9 and 10 $M_{\rm Jup}$ (4 and 5 $M_{\rm Jup}$) planet of 0.50 mag (0.71 mag). Our three hot-start model prescriptions (Cond, Dusty+Cond, BT-Settl+Cond) produce similar sensitivity maps, so for the rest of this work we show representative results with Cond models.
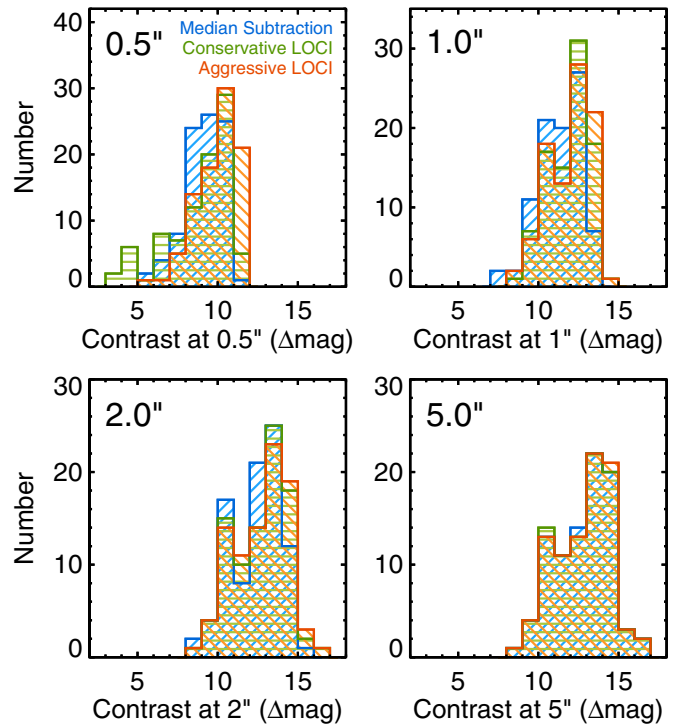
Figure 21. Comparison of three methods of PSF subtraction between 0.″5–5″. Scaled median subtraction (blue) systematically produces slightly worse (7σ) contrasts compared to conservative (green) and aggressive (red) applications of LOCI. At separations of 0.″5 near the IWA, the median subtraction outperforms conservative LOCI when sky rotation is small. Beyond 3″ where the data are no longer contrast-limited, the median scaled subtraction method is used for all contrasts and the distributions are virtually identical.

As an example, Figure 22 shows Cond and Fortney sensitivity maps for G 271-110 based on the contrasts for this target. As expected, our data are not sensitive to planetary companions within ~10 AU nor any companions beyond a few hundred AU because of the limited FOV coverage. In this case most planets in the 10–100 AU range would have been detected. In general, introducing non-zero eccentricities tends to slightly "smear out" the sensitivity plots, but the overall impact is small.

Finally, we note that our sensitivity maps are necessarily dependent on substellar cooling models, which remain poorly constrained by observations. In the few instances where they have been tested through precise dynamical mass measurements of the benchmark brown dwarf systems HD 130948 BC and Gl 417 BC, Dupuy et al. (2009, 2014) found that low-mass evolutionary models systematically overpredict brown dwarf masses by $\approx$15%–25%. A similar result was found by Crepp et al. (2012) with the older HR 7672 AB system. This potential (and worrisome) uncalibrated systematic error in cooling models is much larger than any effects caused by our choice of eccentricity distribution or PSF subtraction method.

6.4. Giant Planet Frequency at a Given Planet Mass

Our first approach focuses on the following question: for a given planet mass and semi-major axis, what planet frequency is consistent with the non-detection from our survey? Since we did not detect any planets, this analysis is concerned with the (95% confidence) upper limits on planet frequencies. We use the sensitivity maps for each target (Section 6.3) to compute the overall 95% confidence upper limit at each {m, a} grid point. For a given m and a, the number of detections $N_{\rm det}$ is
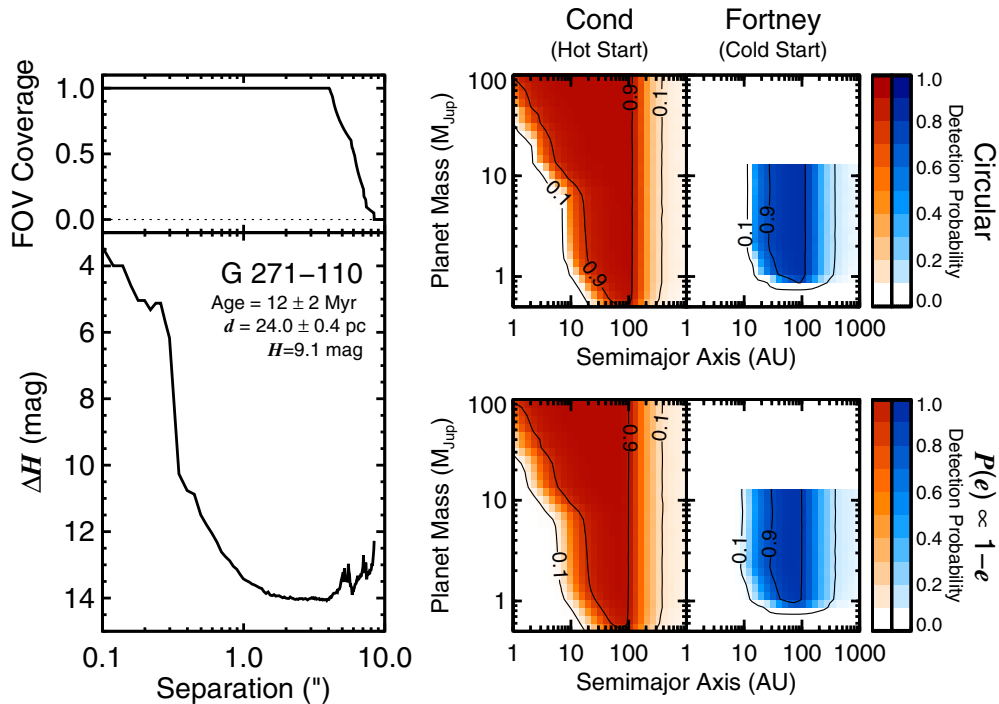
Figure 22. Example of a sensitivity map for G 271-110. Colors correspond to the fraction of simulated random orbits recovered for each {mass, semi-major axis} grid point based on two different evolutionary models: Cond (hot-start) and Fortney (cold-start). The top panels show results for circular orbits, while the bottom panel follows a 1−e eccentricity distribution.

uniformly zero and the effective number of trials N_{trials} is simply the sum of the sensitivities at that grid point ($s(m, a)$) over all targets N_{tar}:

$$N_{trials} = \sum_{i=1}^{N_{tar}} s_i(m, a), \qquad (6)$$

where s is a number from 0 to 1 derived by the methods in Section 6.3. Since these constitute Bernoulli trials we can compute the probability distribution of the occurrence rate f using the binomial distribution. In a region 100% sensitive to companions for all of our targets, the number of trials would simply be equal to the number of targets, and the commonly used binomial distribution applies. On the other hand, for non-integer trials and successes the binomial coefficient can be generalized using Gamma functions. The binomial distribution then becomes

$$P(f \mid n, k) = \frac{\Gamma(n+1)}{\Gamma(k+1)\Gamma(n-k+1)} f^k (1-f)^{n-k}(n+1), \quad (7)$$

where n is the number of trials and k is the number of successes. The final $(n + 1)$ factor is a normalization constant.[11] This is similar to the widely used method from Nielsen et al. (2008), but here we use the more general binomial distribution instead of the Poisson distribution, which is only applicable for cases when N_{trials} is large and f is small. For regions in {m,a} where the sensitivity to planets is low (small separations, large separations, and low masses), N_{trials} is small so the binomial distribution must be used to accurately measure upper limits.

Figure 23 shows the results for the Cond and Fortney models with two assumptions about the planet eccentricity distributions.
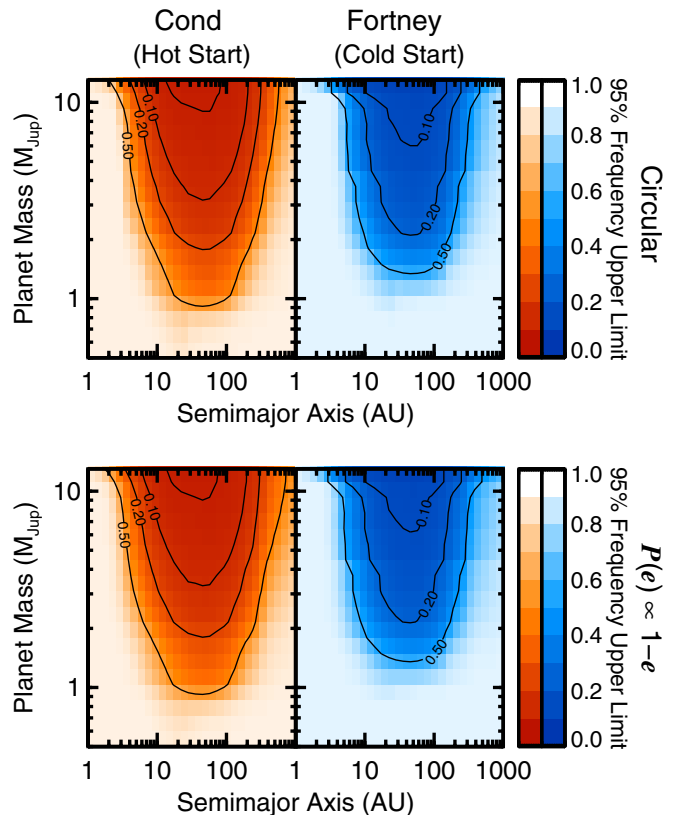
Figure 23. Upper limits on the frequency of gas giant planets. Each grid point represents the 95% confidence upper limit on the planet frequency. The strongest constraints from our survey are for massive giant planets (5–13 M_{Jup}) between 10–100 AU. Contours show the 5%, 10%, 20%, and 50% upper limits.

---

[11] The meaning of a "trial" and "success" becomes less intuitive with continuous rather than integer values. However, noting that $\Gamma(x + 1) = x!$ for integer values of x, Equation (7) reduces to its usual form when k and n are natural numbers.

Table 11
Giant Planet Frequency Upper Limits for a Given
Planet Mass (95% Confidence)

Mass (M_{Jup})	⩽5%	⩽10%	⩽20%	⩽50%
Cond (Circular Orbits)				
13.0	13–85 AU	6.1–200 AU	3.6–320 AU	1.8–570 AU
10.0	36–61 AU	8.5–190 AU	5.6–300 AU	3.3–540 AU
7.0	. . .	11–160 AU	6.6–260 AU	3.9–470 AU
5.0	. . .	13–140 AU	7.3–240 AU	4.0–440 AU
3.0	. . .	. . .	11–170 AU	5.0–330 AU
2.0	. . .	. . .	18–120 AU	7.0–260 AU
1.0	. . .	. . .	. . .	18–110 AU
Cond ($P(e) \propto 1-e$)				
13.0	13–77 AU	5.7–200 AU	3.3–300 AU	1.6–730 AU
10.0	36–57 AU	8.1–180 AU	5.0–290 AU	3.0–660 AU
7.0	. . .	11–150 AU	6.2–260 AU	3.4–520 AU
5.0	. . .	13–130 AU	6.7–240 AU	3.6–460 AU
3.0	. . .	. . .	10–160 AU	4.6–320 AU
2.0	. . .	. . .	17–110 AU	6.3–260 AU
1.0	. . .	. . .	. . .	17–100 AU
Fortney (Circular Orbits)				
13.0	. . .	10–150 AU	5.6–240 AU	3.3–450 AU
10.0	. . .	21–96 AU	9.7–180 AU	5.2–340 AU
7.0	. . .	33–67 AU	11–160 AU	5.4–300 AU
5.0	. . .	. . .	12–150 AU	5.7–290 AU
3.0	. . .	. . .	17–110 AU	7.4–220 AU
2.0	. . .	. . .	33–63 AU	9.6–180 AU
1.0	. . .	. . .	. . .	. . .
Fortney ($P(e) \propto 1-e$)				
13.0	. . .	10–140 AU	5.3–250 AU	2.9–490 AU
10.0	. . .	20–85 AU	9.0–180 AU	4.8–330 AU
7.0	. . .	36–60 AU	10–150 AU	5.0–300 AU
5.0	. . .	. . .	11–140 AU	5.2–290 AU
3.0	. . .	. . .	17–98 AU	6.7–220 AU
2.0	. . .	. . .	35–54 AU	8.7–170 AU
1.0	. . .	. . .	. . .	. . .

Each colored grid point reflects the 95% confidence upper limit on the planet frequency, and contours show the 50%, 20%, 10%, and 5% upper limits on planet frequency. Table 11 summarizes the semi-major axes corresponding to these upper limits for each planet mass. The best constraints are for high-mass planets between 10–100 AU, while the worst constraints are for small separations below ∼5 AU, large separations beyond ∼500 AU, and planet masses below ∼1 M_{Jup}. Assuming circular orbits and hot-start cooling models, we find that fewer than 10% of single M dwarfs harbor 10 M_{Jup} (5 M_{Jup}) planets between 8.1–180 AU (13–130 AU). These results are insensitive to the choice of the hot-start model grid. Naturally, cold-start models produce poorer constraints; fewer than 10% (20%) of M dwarfs harbor 10 M_{Jup} (5 M_{Jup}) planets between 21–96 AU (12–150 AU) using the Fortney models.

6.5. Giant Planet Frequency Over a Range of Planet Masses and Semi-major Axes

Our second approach focuses on a related but slightly different question: what is the frequency of giant planets over a *range* of planet masses and semi-major axes? This can be addressed with our sensitivity maps and assumptions about the form of the underlying distributions of planet masses and semi-major axes. For the following analysis we adopt logarithmically

flat distributions in mass from 0.5–100 M_{Jup} and semi-major axis from 1–1000 AU: $dN/(d \log a \, d \log m) \propto m^{\alpha} \, a^{\beta}$, where $\alpha = 0.0$ and $\beta = 0.0$. The choice of power-law representations is partly motivated (but not defined) by planet populations at smaller separations (<10 AU), which have mass and period distributions that are well-reproduced with this functional form (e.g., Cumming et al. 2008; Howard et al. 2010). Moreover, the logarithmically flat forms are broadly consistent with the projected separation distribution and mass distribution for planets around M dwarfs found in microlensing surveys (Gould et al. 2010; Cassan et al. 2012). This particular case of a logarithmically flat distribution in semi-major axis corresponds to "Öpik's law" (Öpik 1924) which is a good representation of visual binaries in some circumstances (see Duchêne & Kraus 2013 for a summary).[12]

In this case the number of trials for a given target is the average value over a and m:

$$N_{\text{trials}} = \frac{\sum_{i=1}^{N_{\text{tar}}} \sum_{j=1}^{N_a} \sum_{k=1}^{N_m} s_i(m_k, a_j)}{N_a N_m}, \qquad (8)$$

where N_a and N_m are the number of grid points in a and m in the region of interest. The number of detections is zero and, once again, the binomial distribution can be used to compute an upper limit on the planet fraction at the desired level.

Table 12 summarizes the results for a various ranges of mass and semi-major axis for the Cond and Fortney models with circular and eccentric distributions. Overall our survey is most sensitive to the 10–100 M_{Jup} range (Figures 24 and 25), so we would expect the tightest constraints in this region. For masses between 1 and 13 M_{Jup}, semi-major axes between 10–100 AU, circular orbits, and a hot-start formation, $N_{\text{trials}} = 26.6$, which translates into a 95% frequency upper limit of <10.3%. That is, fewer than 10.3% of M dwarfs harbor giant planets between 10–100 AU at the 95% confidence level. For the cold-start models, N_{trials} is reduced to 16.1, and the upper limit is weakened to <16.0%. If we instead isolate the high-mass planet population of 5–13 M_{Jup}, N_{trials} grows to 47.0 (27.7) and the upper limits tighten to <6.0% (<9.9%) for the Cond (Fortney) cooling models.

As expected, exploring broader ranges of physical separation lowers N_{trials} and the constraints weaken since we begin to sample regions with poor sensitivity, diluting each target's average sensitivity. For the Cond case with circular orbits between 1–10 AU, the upper limit over the entire planetary-mass range is <51% and from 100–1000 AU it is <29%. Likewise, for the entire 1–1000 AU, 1–13 M_{Jup} range, the planet frequency is <20.0%. Adding modest eccentricities tends to dilute these statistics, but overall the effect is small.

6.6. The Frequency of Brown Dwarf Companions to M Dwarfs

Measuring the frequency of brown dwarfs over various ranges of a involves the additional step of de-projecting the observed (sky-projected) separations onto the semi-major axis plane. Like

---

[12] Although it is a common practice in the analysis of direct imaging surveys to extrapolate power-law distributions from radial velocity-detected planets, it is not clear that extending the population of giant planets from within a few AU out to hundreds of AU is any more informative than the logarithmically uniform, scale-invariant Jeffrey's prior we have adopted. In fact, it is conceivable that giant planets are better represented by other more complex functional forms, like a power-law distribution in semi-major axis at small separations and a log-normal form at wide separations, especially if there are two modes of planet formation (e.g., Boley 2009).
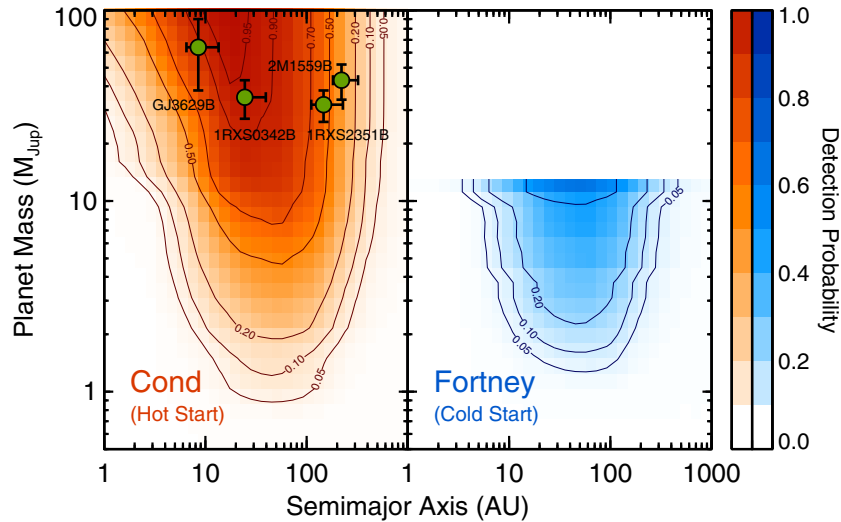
Figure 24. Survey sensitivity map showing the fraction of targets sensitive to companions between semi-major axes of 1–1000 AU and masses of 0.5–100 M_{Jup}. Our four brown dwarf discoveries are shown as green circles. Contours show the 5%, 10%, 20%, 50%, 90%, and 95% levels for the Cond (left) and Fortney (right) evolutionary models.
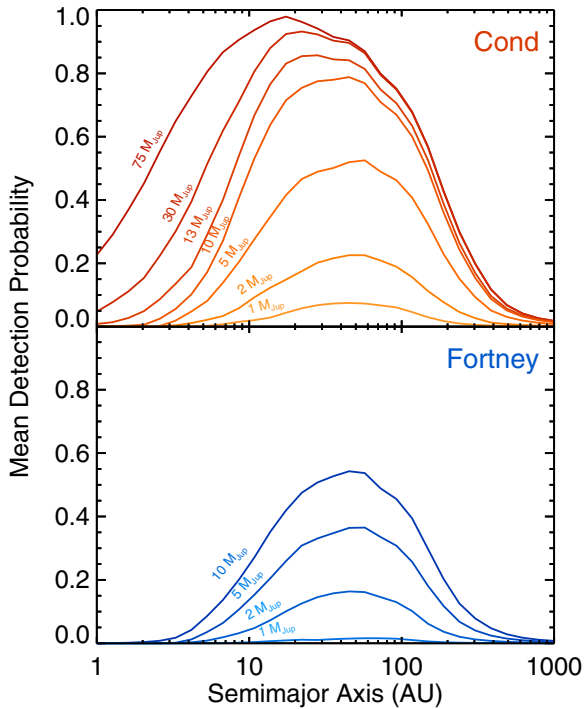
Figure 25. Survey sensitivity map showing the mean detection probability as a function of semi-major axis for varying planet masses.

the above analysis, this involves assumptions about the form of the semi-major axis distribution of substellar companions and their eccentricities (which can be defined or parameterized and freely fit). Here we adopt the same logarithmically flat distribution in a assuming both circular and mildly eccentric orbits (following 1–e). Our approach is to simulate random sky-projected orbits at each step in a grid of semi-major axes, here 1–1000 AU. The number of planets at each grid point is scaled according to the power-law index used, resulting in a distribution of projected separations at each step in a. The cumulative distribution of projected separations over the entire range of a is then used to infer the original semi-major axis distribution based

on the location a companion has been observed. Uncertainties in the measured projected separation due to errors in the target's distance and angular separation measurement are incorporated in a Monte Carlo fashion.

The results of these simulations for our four brown dwarf discoveries are shown in Figure 26. In general the eccentricity distributions "smear out" to smaller physical separations, which is expected since planets can reach larger projected separations when they are on eccentric orbits. The inferred median a and 68.3% confidence range about the median for GJ 3629 B, 1RXS J034231.8+121622 B, 1RXS J235133.3+312720 B, and 2MASS J15594729+4403595 B is 8.5 (6.5–13.5) AU, 24.5 (21.5, 39.5) AU, 145 (105–235) AU, and 225 (182–345) AU, respectively (for circular orbits). These a priori semi-major axis distributions can then be used to compute the fraction that fall within a given range of a, or N_{det}.

If the mass of a brown dwarf companion is near the hydrogen-burning limit, or if its mass uncertainty is large enough, then it is possible to overestimate the inferred substellar occurrence rate since there is a chance that object might be a low-mass star. To take this into account we weigh each of our four discoveries by the probability they are substellar using the mass distributions we derived from their age and luminosity. This mostly affects GJ 3629 B, which has a probability of 62% of falling below the hydrogen-burning limit. The corresponding probability for 2MASS J15594729+4403595 B is 99.1%, and is 100% for both 1RXS J034231.8+121622 B or 1RXS J235133.3+312720 B. Once properly weighted by their substellar probabilities, the fractional detections within some range of semi-major axis can be summed to determine N_{det}. Figure 26 exemplifies this for the 10–100 AU region; for circular orbits, the total contribution from each companion is 0.17, 0.988, 0.079, and 0.000, which sums to 1.23 "detections."

Applying the same analysis as in Section 6.4 to compute N_{trials} between {13–75 M_{Jup}, 10–100 AU} yields 66.8 "trials," implying a substellar companion frequency of $2.8^{+2.4}_{-1.5}$%. Similarly, we measure a frequency of $3.9^{+4.8}_{-2.6}$% for brown dwarfs between 1–10 AU. Over the entire range of 1–1000 AU (encompassing all four weighted detections), we find a frequency of $11.1^{+5.7}_{-4.3}$%. Results for all permutations of a are listed in Table 12.
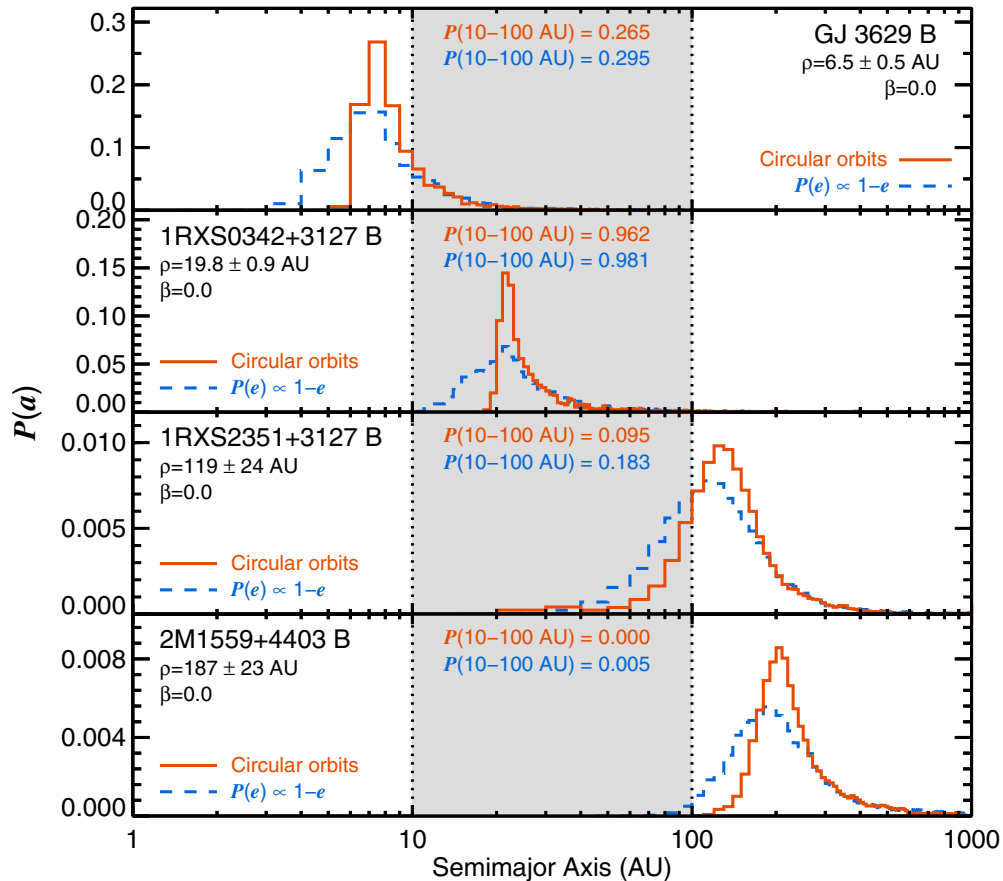
Figure 26. Semi-major axis probability distributions for the four brown dwarfs discovered in our survey based on their observed sky-projected separations. Two underlying eccentricity distributions are assumed: circular orbits and $P(e) \propto 1-e$. The latter creates a broader shape since smaller semi-major axes can reproduce the observed projected separations. The gray shaded region shows our method for computing N_{det}, the number of detected companions. In this example, N_{det} between 10–100 AU is the sum of all four probability distributions falling in that region (weighted by their likelihood of being substellar). Here the semi-major axis power-law index β is flat (equal to 0.0) in log space.

7. DISCUSSION

The well-established correlation between stellar host mass and giant planet frequency offers one of the strongest cases for core accretion at small separations ($\lesssim 2.5$ AU; Johnson et al. 2007, 2010). Since orbital period scales as $M_*^{-1/2}$, the timescale associated with planetesimal coagulation (a few Myr) is faster for high-mass stars so more cores are able to form and accrete gaseous envelopes before protoplanetary disks disperse (e.g., Laughlin et al. 2004; Kennedy & Kenyon 2008). In addition, there is now ample observational evidence that protoplanetary disk masses scale with stellar host mass, resulting in increased raw material for giant planet formation around high-mass stars compared to low-mass stars (Andrews et al. 2013; Mohanty et al. 2013).

Much less is known about the dependence of *wide-separation* (>10 AU) giant planet frequency on stellar host mass. Like core accretion at small separations, disk instability predicts a positive trend with primary mass assuming protoplanetary disk masses scale with protostellar mass (Boss 2011). A total of seven gas-giant planets have been directly imaged to date around three high-mass (1.2–1.9 $M_\odot$) young A-type stars and one G star (HR 8799, β Pic, HD 95086, GJ 504; Marois et al. 2008, 2010b; Rameau et al. 2013b; Kuzuhara et al. 2013). Around low-mass stars, companions near the deuterium-burning limit ($\approx 13 \, M_{Jup}$) have been found at close separations within 100 AU (e.g.,

2MASS J01033563–5515561 C, Delorme et al. 2013; 2MASS J01225093–2439505 B, Bowler et al. 2013), and a growing population of planetary-mass objects on extreme orbits beyond 100 AU has been identified (e.g., GU Psc b, Naud et al. 2014). However, no companions below 10 M_{Jup} have been imaged at <100 AU around stars between 0.1–1.0 $M_\odot$,[13] perhaps pointing to a correlation between stellar mass and giant planet occurrence rate (Crepp & Johnson 2011).

On the other hand, this apparent trend can also be explained by a selection bias since nearly all large direct imaging planet searches are focusing on high-mass stars. For example, the NICI Planet-Finding Campaign (Liu et al. 2010a), Gemini Planet Imager Exoplanet Survey (Macintosh et al. 2014), SEEDS (Tamura et al. 2006), LBTI Exozodi Exoplanet Common Hunt (Skemer et al. 2014), and the International Deep Planet Search (Vigan et al. 2012) concentrate on AFGK stars ($\approx$0.6–2 $M_\odot$), so a paucity of imaged planets around low-mass stars is not surprising.

The only way to test whether giant planet frequency correlates with stellar host mass is to compare the statistical properties of long-period planets in different stellar mass regimes. The largest imaging program targeting high-mass stars is the NICI

---

[13] Interestingly, several planetary-mass companions are known around brown dwarfs (Chauvin et al. 2004; Todorov et al. 2010; Liu et al. 2012; Han et al. 2013), indicating an alternative formation mechanism of planetary-mass companions around very low host masses.

Table 12
The Frequency of Brown Dwarfs and Giant Planets Around Low-mass Stars

Mass (M_{Jup})	a (AU)	Eccentricity Distribution	N_{det}	N_{trials}	Frequency
Brown Dwarf Frequency (Cond)					
13–75	1–10	Circ	0.41	26.6	4^{+5}_{-3}%
13–75	1–10	1–e	0.41	28.0	4^{+4}_{-2}%
13–75	1–20	Circ	0.59	36.0	3^{+4}_{-2}%
13–75	1–20	1–e	0.59	37.0	3^{+4}_{-2}%
13–75	1–100	Circ	1.68	46.7	5^{+4}_{-3}%
13–75	1–100	1–e	1.68	47.0	5^{+4}_{-3}%
13–75	1–1000	Circ	3.61	37.4	11^{+6}_{-4}%
13–75	1–1000	1–e	3.61	37.4	11^{+6}_{-4}%
13–75	10–100	Circ	1.23	66.8	3^{+2}_{-2}%
13–75	10–100	1–e	1.23	66.0	3^{+3}_{-2}%
13–75	10–200	Circ	2.18	61.4	5^{+3}_{-2}%
13–75	10–200	1–e	2.18	60.1	5^{+3}_{-2}%
13–75	10–1000	Circ	3.17	42.7	9^{+5}_{-4}%
13–75	10–1000	1–e	3.17	42.0	9^{+5}_{-4}%
13–75	100–1000	Circ	1.88	18.7	13^{+9}_{-6}%
13–75	100–1000	1–e	1.88	18.0	13^{+9}_{-6}%
Giant Planet Frequency (95% Confidence; Cond)					
1–13	1–10	Circ	0.00	3.1	<51%
1–13	1–10	1–e	0.00	3.7	<47%
1–13	1–20	Circ	0.00	7.3	<30%
1–13	1–20	1–e	0.00	7.8	<29%
1–13	1–100	Circ	0.00	14.9	<17%
1–13	1–100	1–e	0.00	15.1	<17%
1–13	1–1000	Circ	0.00	12.4	<20%
1–13	1–1000	1–e	0.00	12.5	<20%
1–13	10–100	Circ	0.00	26.6	<10%
1–13	10–100	1–e	0.00	26.4	<10%
1–13	10–200	Circ	0.00	24.8	<11%
1–13	10–200	1–e	0.00	24.3	<11%
1–13	10–1000	Circ	0.00	17.2	<15%
1–13	10–1000	1–e	0.00	16.9	<15%
1–13	100–1000	Circ	0.00	7.7	<29%
1–13	100–1000	1–e	0.00	7.4	<30%
5–13	1–10	Circ	0.00	6.2	<34%
5–13	1–10	1–e	0.00	7.3	<30%
5–13	1–20	Circ	0.00	13.9	<18%
5–13	1–20	1–e	0.00	14.9	<17%
5–13	1–100	Circ	0.00	26.6	<10%
5–13	1–100	1–e	0.00	26.9	<10%
5–13	1–1000	Circ	0.00	22.5	<12%
5–13	1–1000	1–e	0.00	22.6	<12%
5–13	10–100	Circ	0.00	47.0	<6.0%
5–13	10–100	1–e	0.00	46.6	<6.1%
5–13	10–200	Circ	0.00	43.9	<6.4%
5–13	10–200	1–e	0.00	43.0	<6.6%
5–13	10–1000	Circ	0.00	30.6	<9.0%
5–13	10–1000	1–e	0.00	30.2	<9.1%
5–13	100–1000	Circ	0.00	14.3	<18%
5–13	100–1000	1–e	0.00	13.8	<18%
Giant Planet Frequency (95% Confidence; Fortney)					
1–13	1–10	Circ	0.00	1.4	<71%
1–13	1–10	1–e	0.00	1.7	<67%
1–13	1–20	Circ	0.00	3.7	<47%
1–13	1–20	1–e	0.00	4.1	<45%
1–13	1–100	Circ	0.00	8.7	<26%
1–13	1–100	1–e	0.00	8.8	<26%
1–13	1–1000	Circ	0.00	7.1	<31%
1–13	1–1000	1–e	0.00	7.1	<31%

Table 12
(Continued)

Mass (M_{Jup})	a (AU)	Eccentricity Distribution	N_{det}	N_{trials}	Frequency
1–13	10–100	Circ	0.00	16.1	<16%
1–13	10–100	1–e	0.00	15.9	<16%
1–13	10–200	Circ	0.00	14.6	<17%
1–13	10–200	1–e	0.00	14.3	<18%
1–13	10–1000	Circ	0.00	9.9	<24%
1–13	10–1000	1–e	0.00	9.8	<24%
1–13	100–1000	Circ	0.00	3.8	<46%
1–13	100–1000	1–e	0.00	3.7	<47%
5–13	1–10	Circ	0.00	2.8	<54%
5–13	1–10	1–e	0.00	3.3	<50%
5–13	1–20	Circ	0.00	7.0	<31%
5–13	1–20	1–e	0.00	7.6	<30%
5–13	1–100	Circ	0.00	15.3	<17%
5–13	1–100	1–e	0.00	15.4	<17%
5–13	1–1000	Circ	0.00	12.5	<20%
5–13	1–1000	1–e	0.00	12.6	<20%
5–13	10–100	Circ	0.00	27.7	<9.9%
5–13	10–100	1–e	0.00	27.5	<10%
5–13	10–200	Circ	0.00	25.4	<11%
5–13	10–200	1–e	0.00	24.9	<11%
5–13	10–1000	Circ	0.00	17.4	<15%
5–13	10–1000	1–e	0.00	17.7	<15%
5–13	100–1000	Circ	0.00	7.1	<31%
5–13	100–1000	1–e	0.00	6.8	<32%

Planet-Finding Campaign (Liu 2010a)Liu Wahhaj). From their subsample of 70 young B- and A-type stars, Nielsen et al. (2013) find that fewer than 20% of 1.5–2.5 $M_\odot$ stars harbor >4 M_{Jup} planets between 59–460 AU. Other smaller surveys have mostly resulted in upper limits or, in some cases, weak constraints if the HR 8799 and/or β Pic systems are included (Ehrenreich et al. 2010; Janson et al. 2011; Rameau et al. 2013a). For example, Vigan et al. (2012) targeted 38 A stars and 4 F stars and arrived at a frequency of $4.3^{+9.1}_{-1.3}$% when β Pic b is excluded (*a priori* knowledge of its existence can strongly bias the way the observations are conducted).

Several large ($N > 50$) direct imaging surveys have focused on young Sun-like stars. The analysis of 100 FGK stars by Nielsen & Close (2010), which combined the surveys of Masciadri et al. (2005), Biller et al. (2007), and Lafrenière et al. (2007a), is the largest study of wide-period planets around 0.6–1.2 $M_\odot$ host stars to date. No planets were detected, yielding an upper limit of <20% (at the 95% confidence level) for the frequency of >4 M_{Jup} planets between ≈40–470 AU. More recently, Chauvin et al. (2014) measured similar constraints of <15% for >5M_{Jup} planets between 100–300 AU in their sample of 51 Sun-like stars.

We find an upper limit of <6.0% in this survey of 78 single young M dwarfs, which is by far the most substantial program to date in the low-mass regime. Taken together with similarly large surveys targeting A and FGK stars, there is currently no statistical evidence for a dependency of giant planet frequency with stellar host mass. In the future, larger sample sizes will be needed to distinguish between small differences in the relative occurrence rates of long-period giant planets around A stars and M dwarfs.

7.1. A Constant Substellar Companion Fraction with Host Mass

The relative occurrence rates of brown dwarf companions as a function of stellar host mass also provides clues about their formation. Large-scale hydrodynamical simulations of fragmenting molecular clouds by Bate (2009, 2012) produced brown dwarf companion frequencies with no discernible dependency on the primary host star mass. This seems to be consistent with observations: Vigan et al. (2012) find a frequency of $2.8^{+6.0}_{-0.9}\%$ between 5–320 AU for massive A and F stars, Metchev & Hillenbrand (2009) find a frequency of $3.2^{+3.1}_{-2.7}\%$ (2σ limits) between 28–1590 AU around FGK stars, and we infer a rate of $2.8^{+2.4}_{-1.5}\%$ ($4.5^{+3.1}_{-2.1}\%$) between 10–100 AU (10–200 AU) for M dwarfs. Although the ranges of semi-major axes being considered are different in these studies, they all point to comparable rates of a few percent across all separations.

Metchev & Hillenbrand (2009) compared all published direct imaging searches for brown dwarf companions as of 2009 and found a tentative trend between the frequency of brown dwarf companions and both stellar host mass and separation. Surveys targeting low-mass stars (≈ 0.2–0.6 $M_\odot$) at small separations ($\lesssim 150$ AU) found a paucity of brown dwarfs compared to those focusing on more massive stars ($\gtrsim 0.7$ $M_\odot$) and wide separations ($\gtrsim 150$ AU). However, our results do not support this correlation; our brown dwarf companion frequency of a few percent is similar to the higher-mass, wide-separation surveys. As emphasized by Metchev & Hillenbrand, most of these previous surveys did not correct for incompleteness in their observations, so the inferred substellar frequencies should be treated with caution. On the other hand, our deep observations probe the *entire* substellar regime and we correct for incompleteness in the regions in which we are not sensitive. Incidentally, two *additional* brown dwarfs were previously known at separations of ≈ 350–400 AU around single stars in our sample (G 196-3 and NLTT 22741; Rebolo et al. 1998; Reid & Walkowicz 2006). Neither were detected in our data so they were not included in our statistical results, but together they imply that at least six out of 78 single M dwarfs in our sample host substellar companions, a rate much higher than inferred from previous, less sensitive surveys targeting low-mass stars listed in Metchev & Hillenbrand. Our results are supported by the *HST* multiplicity survey by Dieterich et al. (2012), which found a multiplicity rate of $2.3^{+5.0}_{-0.7}\%$ for L0–T9 companions to field M dwarfs.[14]

An ongoing debate over whether gas giants can form via direct gravitational collapse of a massive protoplanetary disk has consumed much of the discussion about planet formation for the past decade, especially after the discovery of the HR 8799 planets (e.g., Boss 2007; Durisen et al. 2007; Boley 2009; Dodson-Robinson et al. 2009; Nero & Bjorkman 2009; Kratter et al. 2010). Simulations show that protoplanetary disks can collapse when conditions are both cool enough and disk surface densities are high enough. The region between a few tens to a few hundreds of AU occupies this "sweet spot" and is the most likely place for giant planets to form from this mechanism (e.g., Stamatellos & Whitworth 2009; Vorobyov & Basu 2010; Boss 2011). Our constraints on the frequency of giant planets in this region for the most common type of star imply that, overall, disk instability is not an efficient mechanism for producing gas giants around low-mass stars.

8. SUMMARY AND CONCLUSIONS

We have carried out a deep direct imaging search for giant planets around nearby ($\lesssim 40$ pc) young ($\lesssim 300$ Myr) low-mass stars with Keck and Subaru. Out of 122 targets, 44 are resolved into close visual binaries with separations ranging from $\approx 0\rlap{.}''05$–$2''$; 27 of these are new or spatially resolved for the first time. Because known binaries were removed prior to the start of this survey, we infer a minimum stellar companion frequency of $>35.4 \pm 4.3\%$ within 100 AU. 38% of our sample are confirmed or likely members of YMGs spanning ages of 8–620 Myr and 57% of our targets have measured parallaxes. Below we summarize results of our deep imaging search for planets around the 78 single M dwarfs in our sample:

1. Four comoving brown dwarfs with masses between 30–70 $M_{\rm Jup}$ and projected separations of 6–190 AU were discovered in our survey: 1RXS J235133.3+312720 B (Bowler et al. 2012b), GJ 3629 B (Bowler et al. 2012a), 1RXS J034231.8+121622 B, and 2MASS J15594729+4403595 B. 1RXS J235133.3+312720 is likely a member of the ≈ 120 Myr AB Dor moving group.

2. Taking into account our detection limits, we measure a brown dwarf companion fraction of $2.8^{+2.4}_{-1.5}\%$ ($4.5^{+3.1}_{-2.1}\%$) between 10–100 AU (10–200 AU) around single M dwarfs. These results are consistent with the brown dwarf occurrence rate found around high- and intermediate-mass primaries, which is also in general agreement with hydrodynamical simulations of turbulent fragmentation by Bate (2009).

3. No planets were confirmed in our survey. Among 102 candidates detected around 38 single stars in our deep imaging, 60 are shown to be stationary background stars. The status of the remaining 42 candidates with only a single epoch of astrometry is unclear, but only 8 of these are located at projected separations less than 100 AU.

4. Our null detection of planets implies that $<10.3\%$ ($<6.0\%$) of single M dwarfs harbor 1–13 $M_{\rm Jup}$ (5–13 $M_{\rm Jup}$) planets between 10–100 AU assuming hot-start evolutionary models and logarithmically uniform distributions in planet mass and semi-major axis.

5. The dearth of massive planets at tens to hundreds of AU around the most common type of star in our galaxy implies that, overall, disk instability is not a common mechanism of giant plant formation.

6. Finally, comparing the largest direct imaging planet searches in three mass regimes (A, FGK, and M stars), there is currently no statistical evidence for a correlation between stellar host mass and giant planet frequency at large separations (>10 AU).

In the future, much larger samples of several hundred stars in each stellar mass bin will be needed to discriminate differences in the relative frequencies of giant planets at $\gtrsim 10$ AU. We caution that for large homogeneous analyses incorporating our contrast curves and those of any other surveys, not all planet candidates have been rejected as background stars and so targets and contrast curves must be carefully selected on a case-by-case basis. Ultimately, large statistical comparisons with the current generation of instruments on 8–10 meter class telescopes will set the stage—and statistical baseline—for the next generation

---

[14] Note that old low-mass stars have effective temperatures reaching early L spectral types, so this frequency is slightly different from the substellar companion fraction.

of 30 meter telescopes to image true Jupiter analogs in the 3–10 AU region.

APPENDIX A

HICIAO DISTORTION CORRECTION

The HiCIAO optical distortion, plate scale, and orientation were measured using *H*-band images of the globular cluster M5 obtained on the nights of 2011 January 27 UT and 2012 May 10 UT. We targeted a $\approx 20''$ × $20''$ region near the center of the cluster covering the same dense stellar field as in Cameron et al. (2009). The HiCIAO camera lens was changed in 2011 April, so we generated two distortion maps: one for our 2011 January observing run, and one for our 2011 December/2012 January and 2012 May runs. NIRC2 images of the same field obtained on 2006 February 7 UT using the wide camera (A. Kraus 2013, private communication) were used as an absolute reference frame. We first corrected the NIRC2 optical distortions using the solution created by B. Cameron (2007, private communication). Stars were then identified in the images from both instruments with the DAOPHOT photometry package (Stetson 1987). Finally, the AMOEBA downhill simplex algorithm was used to fit for relative x/y offsets (in pixel coordinates) between the two systems, a relative magnification scale for HiCIAO, an overall rotation of HiCIAO, and 18 coefficients comprising a 2D, third-order polynomial fit following Anderson & King (2003). A total of 297 and 344 stars are used for our 2011 and 2012 calibration measurements, respectively.

The best-fit distortion solutions are shown in Figures 27 and 28. The upgraded camera lens created a significant qualitative difference in the optical distortion, with most of the optical aberrations occurring in the *y*-direction along the detector columns with the new lens in place. The uncorrected optical distortion produces significant positional offsets of up to 30 pixels near the edges of the detector at both epochs. After applying our solution, the average total residual displacement between the HiCIAO and NIRC2 positions is 0.8 pixel and 1.2 pixel for the 2011 and 2012 calibration data sets, respectively, showing little dependence on spatial position across the entire 2048 × 2048 pixel array. We therefore adopt 1 pixel as a typical systematic positional uncertainty caused by optical distortions (σ_d) for our HiCIAO observations. The best-fit solutions give magnification scales of 4.103 and 4.100 times smaller than the NIRC2 wide camera for the 2011 and 2012 data. We also solved for HiCIAO distortion solutions at each epoch using the same field and instrument setup, except with the coronagraph slide in place to test its influence on the astrometry. The results are virtually identical to the solutions without the coronagraph in place, giving magnification scales of 4.104 and 4.101 at each epoch. Because of these similarities, we assume identical magnification factors of 4.102 ± 0.002. Based on the NIRC2 wide camera plate scale of 39.884 ± 0.039 mas pixel^{-1} measured by Pravdo et al. (2006), this implies a HiCIAO *H*-band plate scale of 9.723 ± 0.011 mas pixel^{-1}. The HiCIAO detector appears to be aligned very closely with celestial north; the best-fit solutions imply rotations of $-0°.01$ (–$0°.09$) and +$0°.03$ (+$0°.03$) for the 2011 and 2012 data sets without (with) the coronagraph (positive is east from north). We conservatively adopt a detector orientation of $0°.0 ± 0°.1$.

Our observations of the $5''.6$ pair 2MASS J15594729+4403595 AB in the *Y*, *J*, *H*, and K_S filters at the same position on the detector show that the HiCIAO plate scale varies significantly with wavelength. The separation in *H* band is 580.8 ± 1.4 pixel, or 5647 ± 15 mas using our plate scale measurement, which is in excellent agreement with the value of 5638 ± $0''.004$ measured by Janson et al. (2012, no orbital motion is expected given the system's ∼190 AU separation). On the other hand, the separations in *Y*, *J*, and K_S bands are 575.5 ± 1.4 pixel, 579.2 ± 1.4 pixel, and 583.7 ± 1.4 pixel, respectively, implying plate scales of 9.81 ± 0.04 mas pixel^{-1}, 9.75 ± 0.04 mas pixel^{-1}, 9.67 ± 0.03 mas pixel^{-1}. We adopt these wavelength-dependent plate scales for our astrometry. On the other hand, the P.A.s are consistent within $0°.01$, so we do not make any corrections to that.

APPENDIX B

NIRC2 600 MAS CORONAGRAPH ATTENUATION

NIRC2 has several circular, partly transmissive occulting spots located on a clear slide in its first focal plane. We made use the 600 mas diameter spot for our survey. To calibrate the transmission, we observed the young, $2''.9$ separation M1.5+M4.0 binary NLTT 32659 (Shkolnik et al. 2009) on 2012 May 21 UT with and without the primary under the spot. The observations and resulting flux ratios are listed in Table 13. Aperture photometry using an extraction radius of 5 pixel yields a transmission of 7.51 ± 0.14 mag (0.099 ± 0.013%) in *H* and 6.65 ± 0.10 mag (0.22 ± 0.02%) in K_S. Incidentally, our P.A. and separation measurements are in excellent agreement with Shkolnik et al. (2012).

APPENDIX C

NOTES ON INDIVIDUAL OBJECTS

GJ 3030 AB (2MASS J00215781+4912379). GJ 3030 AB was first identified as a visual binary in the Washington
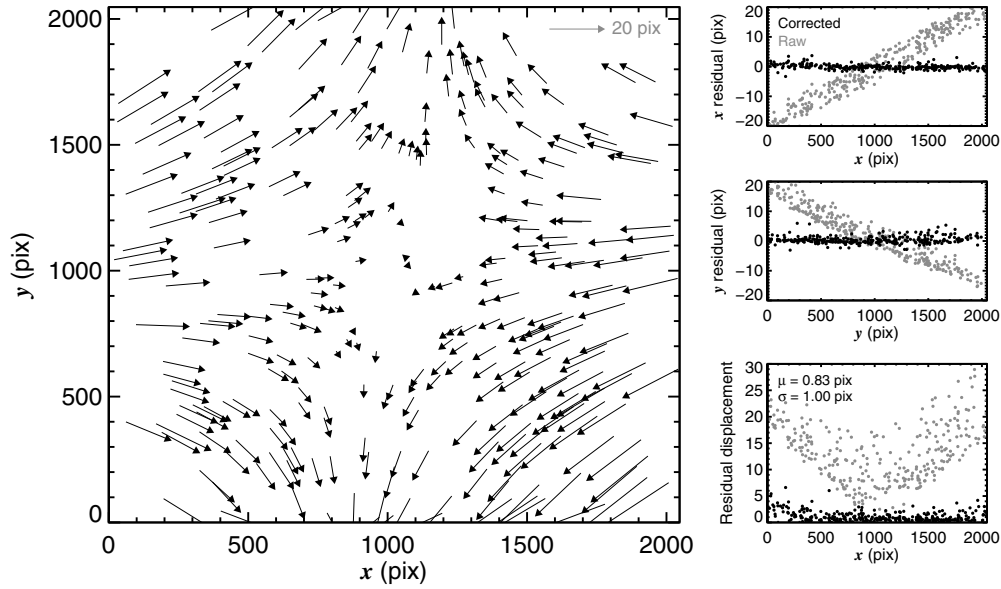
Figure 27. Our HiCIAO distortion solution from 2011 January. Arrow bases and heads indicate the measured and corrected stellar positions, respectively, in our images of M5 after applying third-order polynomial polynomial fit in *x* and *y*. For visual purposes all arrow lengths have been increased by a factor of 10. The average residual displacement after correction is 0.8 pixel (7.8 mas in *H* band).
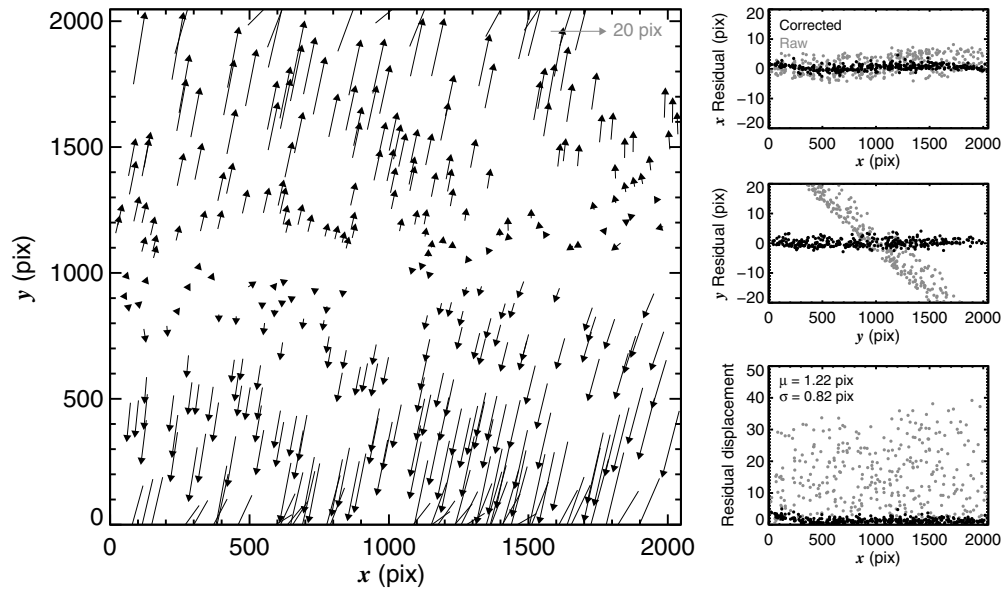
Figure 28. Our HiCIAO distortion solution from 2012 May. In 2011 April the HiCIAO camera lens was replaced, creating a substantially different distortion map compared to the 2011 January one shown in Figure 27. After correction, the typical residual displacement is 1.2 pixel (11.7 mas in *H* band). Arrow lengths have been increased by a factor of 10 for visual purposes.

Table 13
NIRC2 Coronagraph Calibration Measurements of NLTT 32659 AB

Date (UT)	Coronagraph	Filter	$N \times$ Coadds $\times$ Exp. Time (s)	FWHM (mas)	Strehl	Separation ($''$)	P.A. ($°$)	Δmag
2012 May 21	None	K_S	$28 \times 10 \times 0.15$	61 ± 7	0.16 ± 0.08	2.899 ± 0.002	88.54 ± 0.03	2.03 ± 0.04
2012 May 21	600 mas	K_S	$13 \times 1 \times 3.0$	62 ± 4	0.11 ± 0.03	2.898 ± 0.002	88.64 ± 0.03	4.60 ± 0.09
2012 May 21	None	H	$17 \times 1 \times 0.15$	50 ± 4	0.10 ± 0.04	2.897 ± 0.003	88.59 ± 0.06	2.18 ± 0.07
2012 May 21	600 mas	H	$12 \times 1 \times 2.5$	53 ± 4	0.08 ± 0.02	2.902 ± 0.004	88.59 ± 0.07	5.30 ± 0.11

Double Star Catalog (WDS; Mason et al. 2001) and later by McCarthy & Zuckerman (2004) in their coronagraphic search for brown dwarf companions, although no astrometry is provided in the latter. The WDS catalog lists a companion to the M2.4 primary with a contrast of 2.9 mag in the optical at a separation of 2″5–2″9 and a position angle of 290°–291° from two epochs in 1995 and 1998. We confirm the physical separation of the pair and detect modest orbital motion. Unresolved light curves of GJ 3030 AB from the HATNet survey (Hartman et al. 2011) reveal a photometric period of 6.166 ±

0.014 days likely corresponding to the rotation period of the primary.

NLTT 1875 (2MASS J00350487+5953079). Shkolnik et al. (2012) proposed this M4.3e star as a candidate kinematic member of IC 2391 based on their measured radial velocity (-1.0 ± 0.1 km s^{-1}) and its photometric distance of 26 ± 6 pc. Recently, Dittmann et al. (2013) presented a trigonometric parallax of 38.3 ± 2.2 pc to NLTT 1875. At this revised distance, the star's *U*, *V*, and *W* space velocities are $\{-34 \pm 2, -21.8 \pm 1.2, -3.1 \pm 0.3$ km s$^{-1}\}$, respectively, which do not correspond to any known YMGs. Moreover, it does not appear overluminous compared to normal main-sequence stars on the M_V vs. V–K_S diagram. We therefore adopt a wider age range of 100–500 Myr for this star.

G 271-110 (2MASS J01365529–0647363). This active M4 star is a very wide (14,600 AU) companion to EX Cet (Alonso-Floriano et al. 2011), a young G5 star with an *Hipparcos* distance of 24.0 ± 0.4 pc. One faint ($\Delta K = 13.8 \pm 1.0$ mag) point source was identified at a separation of $6\rlap{.}''662 \pm 0\rlap{.}''003$ (160 AU) and a P.A. of $23.18 \pm 0\rlap{.}''20$ from this star in our first epoch of imaging, but we were unable to recover it in several follow-up attempts because conditions were worse or integration times were insufficient.

1RXS J022735.8+471021 (2MASS J02273726+4710045). Based on the radial velocity of -6.0 ± 0.7 from Shkolnik et al. (2012) and the parallactic distance of 27.4 ± 1.7 km s^{-1} from Dittmann et al. (2013), the *UVW* space velocities for the M4.6 star 1RXS J022735.8+471021 are $\{-7.9 \pm 1.2, -23.9 \pm 1.6, -14.7 \pm 1.4$ km s$^{-1}\}$. These agree well with the AB Dor moving group (e.g., Torres et al. 2008), so we assign 1RXS J022735.8+471021 as a probable member of this moving group.

2MASS J03033668–2535329 AB. Makarov & Kaplan (2005) first noted this M0 star as a likely binary from significant differences between *Hipparcos* and Tycho proper motions. This $0\rlap{.}''83$ binary ($\Delta K_S = 2.99 \pm 0.06$ mag) was later resolved as part of the Astralux Lucky imaging survey by Bergfors et al. (2010) and Janson et al. (2012). Their astrometry from 2008.88 ($\rho = 0\rlap{.}''834 \pm 0\rlap{.}''005$, $\theta = 7.6 \pm 0\rlap{.}°3$) and 2010.08 ($\rho = 0\rlap{.}''834 \pm 0\rlap{.}''005$, $\theta = 3.5 \pm 0\rlap{.}°3$) together with our measurements from 2011 reveal a constant separation but a P.A. changing by $\approx 3°$ yr^{-1}.

2MASS J04220833–2849053 AB. This star is a $0\rlap{.}''74$ equal-flux K7Ve binary system. Torres et al. (2006) found strong Hα emission (EW = 12 Å) and Liλ6708 absorption ($EW = 70$ mÅ). Based on the stars' V–I color of 1.2 mag from UCAC4, the Li depletion implies an age consistent with the Pleiades (Torres et al. 2008). We therefore adopt a conservative age range of 50–200 Myr for this system.

2MASS J04472312–2750358 and 2MASS J04472266–2750295. 2MASS J04472312–2750358 is the M2Ve secondary companion to the bright M0V star 2MASS J04472266–2750295 separated by $8\rlap{.}''8$. The stars share similar radial velocities and proper motions (Torres et al. 2006), and imaging dating to the early twentieth century shows some orbital motion (Mason et al. 2001). The system was detected by *ROSAT* and both components are detected in *GALEX*. The primary shows no Hα emission but Torres et al. (2006) found the companion is in emission, suggesting an upper age limit of $\sim$1.2 Gyr. We therefore adopt the lower limit of 400 Myr from Shkolnik et al. (2009) and an upper limit of 1.2 Gyr for the system.

L 449-1 AB (2MASS J05172292–3521545). This nearby (11.9 pc; Riedel et al. 2014) active pair of mid-M dwarfs

was first noted by Scholz et al. (2005a). Riedel et al. (2014) identify a close stellar companion to the M4.0e primary at a separation of 47 mas from *HST* Fine Guidance Sensor interferometry from 2008. We did not resolve the companion in our HiCIAO observations from 2011. Interestingly, deep VLT/SINFONI observations from 1.4–2.5 μm by Janson et al. (2008) revealed a candidate marginally resolved ($\approx$50 mas) low-contrast companion, though they attribute it to a PSF artifact. Riedel et al. (2014) find no evidence the system is particularly young and tentatively associate it with the UMa moving group based on its kinematics.

AP Col (2MASS J06045215–3433360). Scholz et al. (2005a) first drew attention to this active, optically variable M4.5 star because of its strong X-ray emission and proximity to the Sun. Riedel et al. (2011) measured a parallactic distance of 8.4 pc and kinematically associate it with the young ($\sim$40–50 Myr) Argus or IC 2391 moving groups. The origin and relationship of these two groups remains ambiguous (see Section 4.1 of Riedel et al. 2011 for a detailed discussion), but because of its proximity to Earth compared to typical IC 2391 members ($\sim$150 pc), we adopt Argus as the physical association. Deep AO imaging of AP Col by Quanz et al. (2012) did not reveal any planetary companions down to contrasts of $\Delta L' \sim 11$ mag at $0\rlap{.}''5$, corresponding to planetary masses near 1 $M_{\rm Jup}$. Our HiCIAO observations in *H* band reach a sensitivity of 13.5 mag at $1''$ and we identify a single wide candidate companion at $7\rlap{.}''1$ (60 AU). Our follow-up astrometry at Keck shows it is a background star.

1RXS J091744.5+461229 AB (2MASS J09174473+4612246). This M2.5 star was resolved into a $0\rlap{.}''25$ binary by Janson et al. (2012), who also confirmed the physical nature of the pair from two epochs of astrometry in 2008 and 2009. We detect modest orbital motion with our new astrometry. A rotational period of 0.562 days for the unresolved system was measured in the HATNet survey (Hartman et al. 2011).

GJ 354.1 B (2MASS J09324827+2659443). This star is a widely separated ($72''$, $\approx$1300 AU) M5.5 companion to the young K0 star DX Leo (Gaidos 1998; Montes et al. 2001; Lowrance et al. 2005). The primary has a long history of potential kinematic matches to YMGs: Gaidos et al. (2000) list it as a candidate member of the Pleiades; Montes et al. (2001) and Maldonado et al. (2010) broadly associate it with the Local Association; Gaidos (1998) and Fuhrmann (2004) link it with the Her-Lyr group (though this is refuted by López-Santiago et al. 2006); Nakajima & Morino (2012) find Tuc-Hor to be the best match; and Brandt et al. (2014) link it with Columba. While the *UVW* kinematics of DX Leo are in good agreement with members of the Carina, Tuc-Hor, and Columba YMGs, its XYZ space positions do not entirely agree with a single group. Because of its close kinematic agreement with Carina members, we adopt that association and age ($\approx$30 Myr) for GJ 354.1 B, though a complete kinematic traceback analysis is needed to confirm this.

PYC J09362+3731 AB (2MASS J09361593+3731456; HIP 47133). This star is an equal-mass M0.5 SB2 system identified by Schlieder et al. (2012b) and Schlieder et al. (2012c) as a likely member of the β Pic moving group based on its *UVW* kinematics. However, Malo et al. (2013) note that the spatial position of PYC J09362+3731 AB disagrees with established members by $\sim$40 pc. This casts doubt on the membership of PYC J09362+3731 AB, especially since the activity detected by *ROSAT* and *GALEX* could be a result of tidal interactions rather than youth. We therefore assume it is a member of

the field for this study and adopt a conservative age range of 10 Myr–10 Gyr.

NLTT 22741 A (2MASS J09510459+3558098). LP 261-75 A is an active M4.5e star with an L6.5 companion separated by 12″ (Reid & Walkowicz 2006). At a distance of 33 pc (Bowler et al. 2013; Dittmann et al. 2013; F. Vrba, in preparation), this corresponds to ≈360 AU in projected separation. Combining its distance and radial velocity from Shkolnik et al. (2012) gives *UVW* space velocities of {−14.1 ± 0.7, −24.3 ± 1.5, −1.1 ± 0.7} km s^{-1}. The *U* and *V* velocities are consistent with the Columba association, but differ by ≈5 km s^{-1} in *W*. Note, however, that the NIR spectrum of NLTT 22741 B (L4.5 ± 1.0 spectral type) from Bowler et al. (2013) does not have the angular *H*-band features expected for a young (≲100 Myr) brown dwarf. Lacking a likely YMG match, we therefore adopt the age estimate of 100–200 Myr from Reid & Walkowicz (2006) for this system.

GJ 2079 AB (2MASS J10141918+2104297). This active M0.5 ± 0.5 star (also known as DK Leo, HIP 50156) has a parallactic distance of 23.1 ± 0.1 pc (Perryman et al. 1997; van Leeuwen 2007). Makarov & Kaplan (2005) and Frankowski et al. (2007) found evidence for a close astrometric companion based on differences between *Hipparcos* and *Tycho*-2 proper motions. Similarly, Shkolnik et al. (2012) identified GJ 2079 as an SB1 from variable radial velocity measurements spanning a decade. We resolved the likely culprit with AO imaging at Keck: a tight (∼90 mas) companion with a K_S-band contrast of 1.8 mag. The system is unresolved in our 2011 December 28 UT Subaru data, but two epochs at Keck (obtained before and after our HiCIAO data on 2011 March 25 UT and 2013 February 4 UT) separated by ∼2 yr show substantial orbital motion. GJ 2079 was also imaged by the Subaru SEEDS program on 2011 December 24 UT—just a week before our own non-detection with HiCIAO reported here—and the companion was not resolved; Brandt et al. (2014) report an upper limit of ∼20 mas, suggesting GJ 2079 B had moved too close to the primary to resolve at that epoch.

Schlieder et al. (2012b) identify GJ 2079 as a probable member of the *β* Pic YMG, but Shkolnik et al. (2012) suggest the Carina YMG is more likely based on their more recent radial velocity measurement, the lack of Li absorption, and weak Hα emission (see note *k* in their Table 6). Similarly, Malo et al. (2013) propose GJ 2079 is a member of the Columba group regardless of its (varying) radial velocities. Since GJ 2079 is a close binary, continued monitoring is clearly needed to derive a systemic radial velocity before reassessing its kinematic membership to YMGs. For this work we follow Shkolnik et al. in adopting GJ 2079 AB as a member of the Carina YMG with an age of ∼30 Myr.

2MASS J11240434+3808108. This M4.5 star has a known M8.5 companion located at 8″3 (≈170 AU given its photometric distance of ≈20 pc), 2MASS J11240487+3808054 (Close et al. 2003; Cruz et al. 2003). In addition to their common proper motion, the radial velocity of the companion (−14 ± 3 km s^{-1}) measured by Reiners & Basri (2009) agrees with that of the primary (−11.5 ± 0.5 km s^{-1}) from Shkolnik et al. (2012). Shkolnik et al. (2009) assign an age range of 40–300 Myr for the primary from its high X-ray emission and lack of spectroscopic indicators of youth, while Shkolnik et al. (2012) tentatively assign it to the Ursa Major moving group (∼500 ± 100 Myr; King et al. 2003) from its kinematics. Burgasser et al. (2004) obtained a low-resolution near-infrared spectrum of the companion, which does not show obvious signs of low gravity in the form of an angular *H*-band shape, supporting an age ≳100 Myr (e.g., Allers & Liu 2013). The HATNet survey measured a fast rotation period of 0.475 days for the primary (Hartman et al. 2011); unfortunately, rotation periods become unreliable age indicators for stars that are fully convective (Irwin et al. 2011).

The 2MASS *H*-band spectrophotometric distance to the companion 2MASS J11240487+3808054 B is 20.3 ± 1.3 pc using the relations from Dupuy & Liu (2012). (This error incorporates the rms spread from Dupuy & Liu, a spectral type uncertainty of 0.5 subclasses, and the photometric uncertainty.) At this distance, the *UVW* space velocities of the system ({14.8 ± 0.7, 2.8 ± 0.3, −6.7 ± 0.5} km s^{-1}) are an excellent kinematic match with Ursa Major (see Table 2 of Eiff & Guenther 2009). We therefore adopt an age of 500 ± 100 Myr for this system. The corresponding luminosity of the companion is log $L_{Bol}/L_\odot$ = −3.35 ± 0.06 dex, which translates into a mass of 81 ± 5 M_{Jup} using evolutionary models from Burrows et al. (1997). This is very near the substellar boundary; however, the probability that the mass is below 75 M_{Jup} is only 15%. Regardless, it was not detected in our high-contrast imaging due to its large angular separation so does not enter into our statistical analysis.

TWA 30 A (2MASS J11321831–3019518). This young M5 star was identified as a new member of the TWA moving group by Looper et al. (2010b). It exhibits Li I λ6708 absorption and forbidden optical line emission, probably a result of outflow activity. Looper et al. (2010a) identified a very wide (∼3400 AU) companion, which shows similar forbidden lines emission. Although TWA 30 B is much fainter (5 mag in *K* band), its earlier spectral type (M4) and variable reddening suggests it harbors an edge-on disk. Our NIRC2 data show that TWA 30 A is single down to ≈0″06 (2.5 AU), and deep imaging did not reveal any substellar candidates. Note that TWA 30 A is strongly variable in the NIR (Looper et al. 2010a). This affects the conversion of relative contrast curves to absolute contrasts and companion mass sensitivities. For this work we have adopted the 2MASS K_S-band magnitude for the primary, which may not accurately represent the apparent brightness of TWA 30 A during our deep ADI observation.

2MASS J12062214–1314559 AB. This M3.5 system was first resolved from a single epoch of imaging by Janson et al. (2012) into a ≈0″4 binary with a *z*-band contrast of 2.2 mag. We confirm the physical nature of the pair and detect orbital motion relative to the astrometry from Janson et al. at epoch 2010.11 (*ρ* = 0″420 ± 0″003, *θ* = 65.9 ± 0°3). Riaz et al. (2006) identified 2MASS J12062214–1314559 AB as a chromospherically active star (EW(Hα) = −4.9 Å).

LHS 2613 (2MASS J12424996+4153469). This single, X-ray active M4.0 dwarf has been identified by E. L. Shkolnik et al. (in preparation) as a possible nearby young star. Its parallactic distance of 10.6 ± 1.3 pc (van Altena et al. 1995) combined with its measured radial velocity of −4.0 ± 0.2 km s^{-1} (E. L. Shkolnik et al., in preparation) imply *UVW* kinematics of {−23 ± 3, −13.7 ± 1.6, −5.2 ± 0.3} km s^{-1}, which agree well with the Argus YMG. The large uncertainty in *U* is mostly influenced by the error in the distance to the system. Association with the ∼40 Myr Argus group agrees with the star's placement on the color-magnitude diagram; with *V* = 12.4 mag (Zacharias et al. 2013) and M_V = 12.3 mag, LHS 2613 lies ∼0.5–1 mag above the main sequence given its *V*–K_S color of 5.16 (see, e.g., Figure 4 from Riedel et al. 2014). This is further bolstered by an 86% membership probability by the BANYAN II web tool from

Gagné et al. (2014).[15] If confirmed with a more precise distance, LHS 2613 will be among the nearest pre-main-sequence stars.

GJ 1167 A (2MASS J13093495+2859065). A 194″ companion to the M3.5 star GJ 1167 A at a P.A. of 23° (LP 322-835; GJ 1167 B) is listed in the Washington Double Star catalog (Mason et al. 2001). However, the proper motion of GJ 1167 B ($\mu_\alpha\cos\delta = -232 \pm 7$ mas yr^{-1}, $\mu_\delta = -160 \pm 5$ mas yr^{-1}; Monet et al. 2003) disagrees with GJ 1167 A ($\mu_\alpha\cos\delta = -338 \pm 8$ mas yr^{-1}, $\mu_\delta = -211 \pm 8$ mas yr^{-1}; Zacharias et al. 2013), so the pair are unlikely to be physically related.

G 227-22 (2MASS J18021660+6415445). The parallactic distance of 8.5 ± 0.3 pc to G 227-22 from Dittmann et al. (2013) combined with the radial velocity measurement of -1.2 ± 0.2 km s^{-1} from Shkolnik et al. (2012) yield *UVW* space velocities of $\{15.0 \pm 0.6, 4.2 \pm 0.3, -8.3 \pm 0.4\}$ km s^{-1}. These are in excellent agreement with the Ursa Major moving group (Eiff & Guenther 2009), so we assign G 227-22 as a likely member of that association and adopt the group age of 500 ± 100 Myr for this star.

2MASS J20003177+5921289 AB. This near equal-flux M4.1-type 0″.3 binary was first identified by Janson et al. (2012) from imaging in 2008 and 2009. Our 2010 data show continued outward orbital motion by ≈20 mas in separation and ≈5° in P.A.

NLTT 48651 (2MASS J20043077–2342018). NLTT 48651 is a single M4.5 dwarf detected by *ROSAT* and *GALEX* and identified by E. L. Shkolnik et al. (in preparation) as a possible nearby young star. The radial velocity of -7.5 ± 0.7 km s^{-1} measured by Shkolnik et al. enable partial constraints on the star's kinematics, which agree well with AB Dor moving group members at a distance of ~18 pc. Indeed, the BANYAN II web tool suggests an AB Dor membership probability of 93%, so we adopt the AB Dor age of 120 ± 10 Myr for this star. A parallax will be needed for unambiguous confirmation of group membership.

2MASS J20284361–1128307. This X-ray active M3.5 dwarf has mostly gone unnoticed in the literature. Riaz et al. (2006) measured moderately strong Hα emission (6.3 Å) and, more recently, Riedel et al. (2014) presented a trigonometric distance of 18.8 ± 0.6 pc. Although lacking a radial velocity, Riedel et al. argue that this star is a probable member of the Argus association based on its position on the HR diagram and partially constrained kinematics. Assuming membership to Argus, they predict a radial velocity of –25.4 km s^{-1}. E. L. Shkolnik et al. (in preparation) measure a radial velocity of -25.2 ± 0.3 km s^{-1} implying *UVW* kinematics of $\{-24.4 \pm 0.4, -17.7 \pm 0.5, -3.8 \pm 0.7\}$ km s^{-1}. These are in good agreement with the Argus moving group, so we consider 2MASS J20284361–1128307 a likely member.

NLTT 50066 AB (2MASS J20531465–0221218). This M3.0 equal flux binary ($\Delta H = 0.1$ mag) was first resolved by Janson et al. (2012). The pair has undergone significant orbital evolution since the Janson et al. first epoch in 2008. Its parallactic distance of 37.9 ± 5.7 pc (Shkolnik et al. 2012) implies a physical separation of ~3–5 AU. With an expected orbital period of ~10–20 yr, astrometric monitoring should continue in order to yield a dynamical mass.

G 68-46 (2MASS J23512227+2344207). Lacking a parallax for G 68-46, previous studies have tentatively associated this active M4.0e star with the β Pic (Malo et al. 2013) and Cha-Near (Shkolnik et al. 2012) moving groups. However, based on the trigonometric distance of 21.0 ± 1.3 pc from Dittmann et al. (2013) and radial velocity of -2.1 ± 0.5 km s^{-1} from Shkolnik et al. (2012), we find that the *UVW* kinematics of G 68-46 ($\{-19.4 \pm 1.5, -16.4 \pm 1.1, -10.5 \pm 1.0\}$ km s^{-1}) do not match those of any nearby YMGs. We therefore adopt the age estimate of 35–300 Myr from Shkolnik et al. (2009).

REFERENCES

Abazajian, K. N., Adelman-McCarthy, J. K., Agüeros, M. A., et al. 2009, ApJSS, 182, 543
Abt, H. A. 2006, ApJ, 651, 1151
Alibert, Y., Mordasini, C., Benz, W., & Winisdoerffer, C. 2005, A&A, 434, 343
Allard, F., Homeier, D., & Freytag, B. 2011, in ASP Conf Ser. 448, 16th Cambridge Workshop on Cool Stars, Stellar Systems, and the Sun, ed. C. Johns-Krull, M. K. Browning, & A. A. West (San Francisco, CA: ASP), 91
Allen, P. R., & Reid, I. N. 2008, AJ, 135, 2024
Allers, K. N., Jaffe, D. T., Luhman, K. L., et al. 2007, ApJ, 657, 511
Allers, K. N., & Liu, M. C. 2013, ApJ, 772, 79
Alonso-Floriano, F. J., Caballero, J. A., & Montes, D. 2011, in Stellar Clusters & Associations: A RIA Workshop on Gaia, ed. E. J. Alfaro Navarro, A. T. Gallego Calvente, & M. R. Zapatero Osorio, 344
Anderson, J., & King, I. R. 2003, PASP, 115, 113
Andrews, S. M., Rosenfeld, K. A., Kraus, A. L., & Wilner, D. J. 2013, ApJ, 771, 129
Baraffe, I., Chabrier, G., Allard, F., & Hauschildt, P. H. 1998, A&A, 337, 403
Baraffe, I., Chabrier, G., Barman, T. S., Allard, F., & Hauschildt, P. H. 2003, A&A, 402, 701
Barenfeld, S. A., Bubar, E. J., Mamajek, E. E., & Young, P. A. 2013, ApJ, 766, 6
Barrado y Navascués, D. 1998, A&A, 339, 831
Bate, M. R. 2009, MNRAS, 392, 590
Bate, M. R. 2012, MNRAS, 419, 3115
Bergfors, C., Brandner, W., Janson, M., et al. 2010, A&A, 520, A54
Berta, Z. K., Irwin, J., & Charbonneau, D. 2013, ApJ, 775, 91
Biller, B., Artigau, E., Wahhaj, Z., et al. 2008, Proc. SPIE, 7015, 70156Q
Biller, B. A., Close, L. M., Masciadri, E., et al. 2007, ApJSS, 173, 143
Biller, B. A., Liu, M. C., Wahhaj, Z., et al. 2013, ApJ, 777, 160
Binks, A. S., & Jeffries, R. D. 2014, MNRAS, 438, L11
Bochanski, J. J., Hawley, S. L., Covey, K. R., et al. 2010, AJ, 139, 2679
Bodenheimer, P., D'angelo, G., Lissauer, J. J., Fortney, J. J., & Saumon, D. 2013, ApJ, 770, 120
Boley, A. C. 2009, ApJL, 695, L53
Bonfils, X., Delfosse, X., Udry, S., et al. 2013, A&A, 549, 109
Boss, A. P. 1997, Sci, 276, 1836
Boss, A. P. 2007, ApJL, 661, L73
Boss, A. P. 2011, ApJ, 731, 74
Bowler, B. P., Johnson, J. A., Marcy, G. W., et al. 2010, ApJ, 709, 396
Bowler, B. P., Liu, M. C., Shkolnik, E. L., & Dupuy, T. J. 2013, ApJ, 774, 55
Bowler, B. P., Liu, M. C., Shkolnik, E. L., & Tamura, M. 2012a, ApJ, 756, 69
Bowler, B. P., Liu, M. C., Shkolnik, E. L., et al. 2012b, ApJ, 753, 142
Brandt, T. D., Kuzuhara, M., McElwain, M. W., et al. 2014, ApJ, 786, 1
Brandt, T. D., McElwain, M. W., Turner, E. L., et al. 2013, ApJ, 764, 183
Burgasser, A. J., McElwain, M. W., Kirkpatrick, J. D., et al. 2004, AJ, 127, 2856
Burrows, A., Marley, M., Hubbard, W. B., et al. 1997, ApJ, 491, 856
Buscombe, W. 1998, yCat (Evanston, IL: Northwestern Univ.)
Butler, R. P., Johnson, J. A., Marcy, G. W., et al. 2006, PASP, 118, 1685
Butler, R. P., Vogt, S. S., Marcy, G. W., et al. 2004, ApJ, 617, 580
Cameron, P. B., Britton, M. C., & Kulkarni, S. R. 2009, AJ, 137, 83
Cantrell, J. R., Henry, T. J., & White, R. J. 2013, AJ, 146, 99
Cassan, A., Kubas, D., Beaulieu, J.-P., et al. 2012, Natur, 481, 167
Chabrier, G., Baraffe, I., Allard, F., & Hauschildt, P. 2000, ApJ, 542, 464
Charbonneau, D., Berta, Z. K., Irwin, J., et al. 2009, Natur, 462, 891
Chauvin, G., Lagrange, A.-M., Bonavita, M., et al. 2010, A&A, 509, A52
Chauvin, G., Lagrange, A.-M., Dumas, C., et al. 2004, A&A, 425, L29
Chauvin, G., Vigan, A., Bonnefoy, M., et al. 2014, arXiv:1405.1560
Clanton, C., & Gaudi, B. S. 2014, ApJ, 791, 91
Close, L. M., Siegler, N., Freed, M., & Biller, B. 2003, ApJ, 587, 407
Conroy, C., & van Dokkum, P. G. 2012, ApJ, 760, 71
Crepp, J. R., & Johnson, J. A. 2011, ApJ, 733, 126
Crepp, J. R., Johnson, J. A., Fischer, D. A., et al. 2012, ApJ, 751, 97
Crepp, J. R., Pueyo, L., Brenner, D., et al. 2011, ApJ, 729, 132
Cruz, K. L., Reid, I. N., Liebert, J., Kirkpatrick, J. D., & Lowrance, P. J. 2003, AJ, 126, 2421
Cumming, A., Butler, R. P., Marcy, G. W., et al. 2008, PASP, 120, 531

---

15 http://www.astro.umontreal.ca/~gagne/banyanII.php

Cushing, M. C., Rayner, J. T., & Vacca, W. D. 2005, ApJ, 623, 1115
Cushing, M. C., Vacca, W. D., & Rayner, J. T. 2004, PASP, 116, 362
Daemgen, S., Siegler, N., Reid, I. N., & Close, L. M. 2007, ApJ, 654, 558
Degennaro, S., Hippel, T. V., Jefferys, W. H., et al. 2009, ApJ, 696, 12
Delfosse, X., Beuzit, J.-L., Marchal, L., et al. 2004, in ASP Conf. Ser. 318,
    Spectroscopically and Spatially Resolving the Components of Close Binary
    Stars, ed. R. W. Hilditch, H. Hensberge, & K. Pavlovski (San Francisco, CA:
    ASP), 166
Delorme, P., Gagné, J., Girard, J. H., et al. 2013, A&A, 553, L5
Delorme, P., Lagrange, A. M., Chauvin, G., et al. 2012, A&A, 539, A72
Dieterich, S. B., Henry, T. J., Golimowski, D. A., Krist, J. E., & Tanner, A. M.
    2012, AJ, 144, 64
Diolaiti, E., Bendinelli, O., Bonaccini, D., et al. 2000, A&AS, 147, 335
Dittmann, J. A., Irwin, J. M., Charbonneau, D., & Berta-Thompson, Z. K.
    2014, ApJ, 784, 156
Dodson-Robinson, S. E., Veras, D., Ford, E. B., & Beichman, C. A. 2009, ApJ,
    707, 79
Dressing, C. D., & Charbonneau, D. 2013, ApJ, 767, 95
Duchêne, G. 2010, ApJL, 709, L114
Duchêne, G., & Kraus, A. 2013, ARA&A, 51, 269
Dupuy, T. J., & Kraus, A. L. 2013, Sci, 341, 1492
Dupuy, T. J., & Liu, M. C. 2011, ApJ, 733, 122
Dupuy, T. J., & Liu, M. C. 2012, ApJSS, 201, 19
Dupuy, T. J., Liu, M. C., & Ireland, M. J. 2009, ApJ, 692, 729
Dupuy, T. J., Liu, M. C., & Ireland, M. J. 2014, ApJ, 790, 133
Durisen, R. H., Boss, A. P., Mayer, L., et al. 2007, in Protostars and Planets V,
    ed. e. B. Reipurth, D. Jewitt, & K. Keil (Tucson, AZ: Univ. Arizona Press),
    607
Eggen, O. J. 1958, MNRAS, 118, 65
Eggen, O. J. 1983, AJ, 88, 642
Eggen, O. J. 1998, AJ, 116, 284
Egner, S., Ikeda, Y., Watanabe, M., et al. 2010, Proc. SPIE, 7736, 77364V
Ehrenreich, D., Lagrange, A.-M., Montagnier, G., et al. 2010, A&A, 523, A73
Eiff, M. A.-V., & Guenther, E. W. 2009, A&A, 508, 677
Endl, M., Cochran, W. D., Kürster, M., et al. 2006, ApJ, 649, 436
Famaey, B., Jorissen, A., Luri, X., et al. 2005, A&A, 430, 165
Fischer, D. A., & Marcy, G. W. 1992, ApJ, 396, 178
Fortney, J. J., Marley, M. S., Saumon, D., & Lodders, K. 2008, ApJ, 683, 1104
Frankowski, A., Jancart, S., & Jorissen, A. 2007, A&A, 464, 377
Fu, H., Cooray, A., Feruglio, C., et al. 2014, Natur, 498, 338
Fuhrmann, K. 2004, AN, 325, 3
Gagné, J., LaFreniere, D., Doyon, R., Malo, L., & Artigau, E. 2014, ApJ,
    783, 121
Gaidos, E., Fischer, D. A., Mann, A. W., & Howard, A. W. 2013, ApJ, 771, 18
Gaidos, E. J. 1998, PASP, 110, 1259
Gaidos, E. J., Henry, G. W., & Henry, S. M. 2000, AJ, 120, 1006
Giclas, H. L., Burnham, R., & Thomas, N. G. 1963, LowOB, 6, 1
Giclas, H. L., Burnham, R., & Thomas, N. G. 1964, LowOB, 6, 135
Giclas, H. L., Burnham, R., & Thomas, N. G. 1966a, LowOB, 6, 271
Giclas, H. L., Burnham, R., & Thomas, N. G. 1966b, LowOB, 6, 233
Golimowski, D. A., Leggett, S. K., Marley, M. S., et al. 2004, AJ, 127, 3516
Gould, A., Dong, S., Gaudi, B. S., et al. 2010, ApJ, 720, 1073
Gould, A., & Loeb, A. 1992, ApJ, 396, 104
Han, C. 2006, ApJ, 644, 1232
Han, C. 2009, ApJ, 700, 945
Han, C., Jung, Y. K., Udalski, A., et al. 2013, ApJ, 778, 38
Hartman, J. D., Bakos, G. Á., Noyes, R. W., et al. 2011, AJ, 141, 166
Hawley, S. L., Gizis, J. E., & Reid, I. N. 1996, AJ, 112, 2799
Hayano, Y., Takami, H., Oya, S., et al. 2010, Proc. SPIE, 7736, 77360N
Henry, T. J., Jao, W.-C., Subasavage, J. P., et al. 2006, AJ, 132, 2360
Hinkley, S., Oppenheimer, B. R., Soummer, R., et al. 2007, ApJ, 654, 633
Hodapp, K. W., Suzuki, R., Tamura, M., et al. 2008, Proc. SPIE, 7014, 701419
Holman, M. J., & Wiegert, P. A. 1999, AJ, 117, 621
Howard, A. W., Marcy, G. W., Johnson, J. A., et al. 2010, Sci, 330, 653
Ida, S., & Lin, D. N. C. 2005, ApJ, 626, 1045
Irwin, J., Berta, Z. K., Burke, C. J., et al. 2011, ApJ, 727, 56
Janson, M., Bonavita, M., Klahr, H., et al. 2011, ApJ, 736, 89
Janson, M., Brandner, W., & Henning, T. 2008, A&A, 478, 597
Janson, M., Hormuth, F., Bergfors, C., et al. 2012, ApJ, 754, 44
Johnson, J. A., Aller, K. M., Howard, A. W., & Crepp, J. R. 2010, PASP,
    122, 905
Johnson, J. A., Butler, R. P., Marcy, G. W., et al. 2007, ApJ, 670, 833
Joshi, M. M., Haberle, R. M., & Reynolds, R. T. 1997, Icar, 129, 450
Kalas, P., Graham, J. R., Chiang, E., et al. 2008, Sci, 322, 1345
Kennedy, G. M., & Kenyon, S. J. 2008, ApJ, 673, 502
King, J. R., Villarreal, A. R., Soderblom, D. R., Gulliver, A. F., & Adelman, S.
    J. 2003, AJ, 125, 1980

Kipping, D. M. 2013, MNRAS, 434, L51
Kirkpatrick, J. D., Cruz, K. L., Barman, T. S., et al. 2008, ApJ, 689, 1295
Kirkpatrick, J. D., Gelino, C. R., Cushing, M. C., et al. 2012, ApJ, 753, 156
Kiss, L. L., Moór, A., Szalai, T., et al. 2010, MNRAS, 411, 117
Kratter, K. M., Murray-Clay, R. A., & Youdin, A. N. 2010, ApJ, 710, 1375
Kraus, A. L., Ireland, M. J., Hillenbrand, L. A., & Martinache, F. 2012, ApJ,
    745, 19
Kraus, A. L., Shkolnik, E. L., Allers, K. N., & Liu, M. C. 2014, AJ, 147, 146
Kraus, A. L., Tucker, R. A., Thompson, M. I., Craine, E. R., & Hillenbrand, L.
    A. 2011, ApJ, 728, 48
Kuzuhara, M., Tamura, M., Kudo, T., et al. 2013, ApJ, 774, 11
Lada, C. J. 2006, ApJL, 640, L63
Lafrenière, D., Doyon, R., Marois, C., et al. 2007a, ApJ, 670, 1367
Lafrenière, D., Marois, C., Doyon, R., Nadeau, D., & Artigau, É. 2007b, ApJ,
    660, 770
Lagrange, A.-M., Bonnefoy, M., Chauvin, G., et al. 2010, Sci, 329, 57
Larkin, J., Barczys, M., Krabbe, A., et al. 2006, Proc. SPIE, 6269, 42
Laughlin, G., Bodenheimer, P., & Adams, F. C. 2004, ApJL, 612, L73
Law, N. M., Hodgkin, S. T., & Mackay, C. D. 2008, MNRAS, 384, 150
Lebreton, Y., Fernandes, J., & Lejeune, T. 2001, A&A, 374, 540
Leggett, S. K., Currie, M. J., Varricatt, W. P., et al. 2006, MNRAS, 373, 781
Lépine, S., & Gaidos, E. 2011, AJ, 142, 138
Lépine, S., Hilton, E. J., Mann, A. W., et al. 2013, AJ, 145, 102
Lépine, S., & Simon, M. 2009, AJ, 137, 3632
Liu, M. C. 2004, Sci, 305, 1442
Liu, M. C. 2010a, Proc. SPIE, 7736, 77361K
Liu, M. C., Dupuy, T. J., Bowler, B. P., Leggett, S. K., & Best, W. M. J. 2012, ApJ,
    758, 57
Liu, M. C., Dupuy, T. J., & Ireland, M. J. 2008, ApJ, 689, 436
Liu, M. C., Dupuy, T. J., & Leggett, S. K. 2010b, ApJ, 722, 311
Looper, D. L., Bochanski, J. J., Burgasser, A. J., et al. 2010a, AJ, 140, 1486
Looper, D. L., Burgasser, A. J., Kirkpatrick, J. D., & Swift, B. J. 2007, ApJL,
    669, L97
Looper, D. L., Mohanty, S., Bochanski, J. J., et al. 2010b, ApJ, 714, 45
López-Santiago, J., Montes, D., Crespo-Chacón, I., & Fernández-Figueroa, M.
    J. 2006, ApJ, 643, 1160
Lovis, C., & Mayor, M. 2007, A&A, 472, 657
Lowrance, P. J., Becklin, E. E., Schneider, G., et al. 2005, AJ, 130, 1845
Luhman, K. L., Stauffer, J. R., & Mamajek, E. E. 2005, ApJL, 628, L69
Macintosh, B., Graham, J. R., Ingraham, P., et al. 2014, PNAS, 111, 12661
Macintosh, B., Poyneer, L., Sivaramakrishnan, A., & Marois, C. 2005, Proc.
    SPIE, 5903, 170
Makarov, V. V., & Kaplan, G. H. 2005, AJ, 129, 2420
Maldonado, J., Martínez-Arnáiz, R. M., Eiroa, C., Montes, D., & Montesinos,
    B. 2010, A&A, 521, A12
Malo, L., Artigau, E., Doyon, R., et al. 2014a, ApJ, 788, 81
Malo, L., Doyon, R., Feiden, G., et al. 2014b, ApJ, 792, 37
Malo, L., Doyon, R., Lafrenière, D., et al. 2013, ApJ, 762, 88
Mamajek, E. E. 2005, ApJ, 634, 1385
Mamajek, E. E. 2012, ApJL, 754, L20
Mamajek, E. E., & Bell, C. P. M. 2014, MNRAS, 445, 2169
Marley, M. S., Fortney, J. J., Hubickyj, O., Bodenheimer, P., & Lissauer, J. J.
    2007, ApJ, 655, 541
Marois, C., Doyon, R., Nadeau, D., et al. 2005, PASP, 117, 745
Marois, C., Doyon, R., Racine, R., & Nadeau, D. 2000, PASP, 112, 91
Marois, C., Lafrenière, D., Doyon, R., Macintosh, B., & Nadeau, D. 2006, ApJ,
    641, 556
Marois, C., Macintosh, B., Barman, T., et al. 2008, Sci, 322, 1348
Marois, C., Macintosh, B., & Véran, J.-P. 2010a, Proc. SPIE, 7736, 77361J
Marois, C., Zuckerman, B., Konopacky, Q. M., Macintosh, B., & Barman, T.
    2010b, Natur, 468, 1080
Masciadri, E., Mundt, R., Henning, T., Alvarez, C., & Navascués, D. B. Y.
    2005, ApJ, 625, 1004
Mason, B. D., Wycoff, G. L., Hartkopf, W. I., Douglass, G. G., & Worley, C. E.
    2001, AJ, 122, 3466
Mayer, L. 2002, Sci, 298, 1756
Mayor, M., Bonfils, X., Forveille, T., et al. 2009, A&A, 507, 487
McCarthy, C., & Zuckerman, B. 2004, AJ, 127, 2871
McCarthy, C., Zuckerman, B., & Becklin, E. E. 2001, AJ, 121, 3259
McLean, I. S., Wilcox, M. K., Becklin, E. E., et al. 2000, ApJL, 533, L45
Metchev, S. A., & Hillenbrand, L. A. 2009, ApJSS, 181, 62
Mieda, E., Wright, S. A., Larkin, J. E., et al. 2014, PASP, 126, 250
Mohanty, S., Ercolano, B., & Turner, N. J. 2013, ApJ, 764, 65
Mollière, P., & Mordasini, C. 2012, A&A, 547, A105
Monet, D. G., Levine, S. E., Canzian, B., et al. 2003, AJ, 125, 984
Montes, D., López-Santiago, J., Fernández-Figueroa, M. J., & Gálvez, M. C.
    2001, A&A, 379, 976

52

Montet, B. T., Crepp, J. R., Johnson, J. A., Howard, A. W., & Marcy, G. W. 2014, ApJ, 781, 28
Morton, T. D., & Swift, J. 2014, ApJ, 791, 10
Muirhead, P. S., Johnson, J. A., Apps, K., et al. 2012, ApJ, 747, 144
Nakajima, T., & Morino, J.-I. 2012, AJ, 143, 2
Naud, M.-E., Artigau, É., Malo, L., et al. 2014, ApJ, 787, 5
Navascués, D. B. Y. 2006, A&A, 459, 511
Nero, D., & Bjorkman, J. E. 2009, ApJL, 702, L163
Nielsen, E. L., & Close, L. M. 2010, ApJ, 717, 878
Nielsen, E. L., Close, L. M., Biller, B. A., Masciadri, E., & Lenzen, R. 2008, ApJ, 674, 466
Nielsen, E. L., Liu, M. C., Wahhaj, Z., et al. 2013, ApJ, 776, 4
Öpik, E. 1924, in Publications de L'Observatoire Astronomique de l'Universite de Tartu, Vol. 25, No. 6
Oppenheimer, B. R., & Hinkley, S. 2009, ARA&A, 47, 253
Ortega, V. G., Jilinski, E., Reza, R. D. L., & Bazzanella, B. 2007, MNRAS, 377, 441
Perryman, M. A. C., Brown, A. G. A., Lebreton, Y., et al. 1998, A&A, 331, 81
Perryman, M. A. C., Lindegren, L., Kovalevsky, J., et al. 1997, A&A, 323, L49
Pollack, J. B., Hubickyj, O., Bodenheimer, P., et al. 1996, Icar, 124, 62
Poveda, A., Herrera, M. A., Allen, C., Cordero, G., & Lavalley, C. 1994, RMxAA, 28, 43
Pravdo, S. H., Shaklan, S. B., Wiktorowicz, S. J., et al. 2006, ApJ, 649, 389
Pueyo, L., Crepp, J. R., Vasisht, G., et al. 2012, ApJSS, 199, 6
Quanz, S. P., Crepp, J. R., Janson, M., et al. 2012, ApJ, 754, 127
Quintana, E. V., Barclay, T., Raymond, S. N., et al. 2014, Sci, 344, 277
Racine, R., Walker, G. A. H., Nadeau, D., Doyon, R., & Marois, C. 1999, PASP, 111, 587
Rameau, J., Chauvin, G., Lagrange, A.-M., et al. 2013a, A&A, 553, A60
Rameau, J., Chauvin, G., Lagrange, A.-M., et al. 2013b, ApJL, 779, L26
Rayner, J. T., Cushing, M. C., & Vacca, W. D. 2009, ApJSS, 185, 289
Rayner, J., Toomey, D. W., Onaka, P. M., et al. 2003, PASP, 115, 362
Rebolo, R., Osorio, M. R. Z., Madruga, S., et al. 1998, Sci, 282, 1309
Reid, I. N., Cruz, K. L., & Allen, P. R. 2007, AJ, 133, 2825
Reid, I. N., Hawley, S. L., & Gizis, J. E. 1995, AJ, 110, 1838
Reid, I. N., & Walkowicz, L. M. 2006, PASP, 118, 671
Reiners, A., & Basri, G. 2009, ApJ, 705, 1416
Riaz, B., Gizis, J. E., & Harvin, J. 2006, AJ, 132, 866
Ribas, I. 2003, A&A, 400, 297
Riedel, A. R., Finch, C. T., Henry, T. J., et al. 2014, AJ, 147, 85
Riedel, A. R., Murphy, S. J., Henry, T. J., et al. 2011, AJ, 142, 104
Riedel, A. R., Subasavage, J. P., Finch, C. T., et al. 2010, AJ, 140, 897
Rodriguez, D. R., Zuckerman, B., Kastner, J. H., et al. 2013, ApJ, 774, 101
Roeser, S., Demleitner, M., & Schilbach, E. 2010, AJ, 139, 2440
Röser, S., Schilbach, E., Piskunov, A. E., Kharchenko, N. V., & Scholz, R.-D. 2011, A&A, 531, A92
Röser, S., Schilbach, E., Schwan, H., et al. 2008, A&A, 488, 401
Saumon, D., & Marley, M. S. 2008, ApJ, 689, 1327
Schlieder, J. E., Lépine, S., Rice, E., et al. 2012a, AJ, 143, 114
Schlieder, J. E., Lépine, S., & Simon, M. 2010, AJ, 140, 119
Schlieder, J. E., Lépine, S., & Simon, M. 2012b, AJ, 143, 80
Schlieder, J. E., Lépine, S., & Simon, M. 2012c, AJ, 144, 109
Scholz, R.-D., Curto, G. L., Méndez, R. A., et al. 2005a, A&A, 439, 1127
Scholz, R.-D., Meusinger, H., & Jahreiß, H. 2005b, A&A, 442, 211
Shkolnik, E., Liu, M. C., & Reid, I. N. 2009, ApJ, 699, 649
Shkolnik, E. L., Anglada-Escudé, G., Liu, M. C., et al. 2012, ApJ, 758, 56
Shkolnik, E. L., Hebb, L., Liu, M. C., Reid, I. N., & Cameron, A. C. 2010, ApJ, 716, 1522

Shkolnik, E. L., Liu, M. C., Reid, I. N., Dupuy, T., & Weinberger, A. J. 2011, ApJ, 727, 6
Silva, G. M. D., D'Orazi, V., Melo, C., et al. 2013, MNRAS, 431, 1005
Simons, D. A., & Tokunaga, A. 2002, PASP, 114, 169
Skemer, A. J., Hinz, P., Esposito, S., et al. 2014, Proc. SPIE, 9148, 91480L
Skrutskie, M. F., Cutri, R. M., Stiening, R., et al. 2006, AJ, 131, 1163
Slesnick, C. L., Hillenbrand, L. A., & Carpenter, J. M. 2004, ApJ, 610, 1045
Soderblom, D. R., & Mayor, M. 1993, AJ, 105, 226
Soummer, R., Hagan, J. B., Pueyo, L., et al. 2011, ApJ, 741, 55
Sparks, W. B., & Ford, H. C. 2002, ApJ, 578, 543
Spiegel, D. S., & Burrows, A. 2012, ApJ, 745, 174
Stamatellos, D., & Whitworth, A. P. 2009, MNRAS, 392, 413
Stephenson, C. B. 1986, AJ, 92, 139
Stetson, P. B. 1987, PASP, 99, 191
Sumi, T., Kamiya, K., Bennett, D. P., et al. 2011, Natur, 473, 349
Suzuki, R., Kudo, T., Hashimoto, J., et al. 2010, Proc. SPIE, 7735, 773530
Swift, J. J., Johnson, J. A., Morton, T. D., et al. 2013, ApJ, 764, 105
Tamura, M., Hodapp, K., Takami, H., et al. 2006, Proc. SPIE, 6269, 62690V
Thatte, N., Abuter, R., Tecza, M., et al. 2007, MNRAS, 378, 1229
Todorov, K., Luhman, K. L., & Mcleod, K. K. 2010, ApJL, 714, L84
Tokovinin, A., Thomas, S., Sterzik, M., & Udry, S. 2006, A&A, 450, 681
Tokunaga, A. T., & Vacca, W. D. 2005, PASP, 117, 421
Torres, C. A. O., da Silva, L., Quast, G. R., de la Reza, R., & Jilinski, E. 2000, AJ, 120, 1410
Torres, C. A. O., Quast, G. R., da Silva, L., et al. 2006, A&A, 460, 695
Torres, C. A. O., Quast, G. R., de la Reza, R., et al. 2003, in Open Issues in Local Star Formation, ed. J. Lepine & J. Gregorio-Hetem (Astrophysics and Space Science Library, Vol. 299; Dordrecht: Kluwer), 83
Torres, C. A. O., Quast, G. R., Melo, C. H. F., & Sterzik, M. F. 2008, in Young Nearby Loose Associations, ed. B. Reipurth (San Francisco, CA: ASP), 757
Torres, G., Neuhäuser, R., & Guenther, E. W. 2002, AJ, 123, 1701
Torres, G., & Ribas, I. 2002, ApJ, 567, 1140
Udry, S., Bonfils, X., Delfosse, X., et al. 2007, A&A, 469, L43
Vacca, W. D., Cushing, M. C., & Rayner, J. T. 2003, PASP, 115, 389
van Altena, W. F., Lee, J. T., & Hoffleit, E. D. 1995, The General Catalogue of Trigonometric Stellar Parallaxes (New Haven, CT: Yale University Observatory)
van Dam, M. A., Bouchez, A. H., Le Mignant, D., et al. 2006, PASP, 118, 310
van Dokkum, P. G., & Conroy, C. 2010, Natur, 468, 940
van Leeuwen, F. 2007, A&A, 474, 653
Vigan, A., Patience, J., Marois, C., et al. 2012, A&A, 544, 9
Vorobyov, E. I., & Basu, S. 2010, ApJL, 714, L133
Wahhaj, Z., Liu, M. C., Biller, B. A., et al. 2013a, ApJ, 779, 80
Wahhaj, Z., Liu, M. C., Nielsen, E. L., et al. 2013b, ApJ, 773, 179
Webb, R. A., Zuckerman, B., Platais, I., et al. 1999, ApJL, 512, L63
Weinberger, A. J., Anglada-Escudé, G., & Boss, A. P. 2013, ApJ, 762, 118
West, A. A., Hawley, S. L., Bochanski, J. J., et al. 2008, AJ, 135, 785
Wizinowich, P., Acton, D. S., Shelton, C., et al. 2000, PASP, 112, 315
Wizinowich, P. L., Le Mignant, D., Bouchez, A. H., et al. 2006, PASP, 118, 297
Yee, J. C., & Jensen, E. L. N. 2010, ApJ, 711, 303
Yelda, S., Lu, J. R., Ghez, A. M., et al. 2010, ApJ, 725, 331
Zacharias, N., Finch, C. T., Girard, T. M., et al. 2013, AJ, 145, 44
Zacharias, N., Monet, D. G., Levine, S. E., et al. 2005, yCat, 1297, 0
Zapatero Osorio, M. R., Bejar, V. J. S., Miles-Páez, P., et al. 2014, A&A, 568, A6
Zuckerman, B., Song, I., & Bessell, M. S. 2004, ApJL, 613, L65
Zuckerman, B., Song, I., & Webb, R. A. 2001, ApJ, 559, 388